Neuromuscular Disorders

Proteomic characterisation of human LMNA-related congenital muscular dystrophy muscle cells

--Manuscript Draft--

Manuscript Number:	NMD-D-24-00022R1
Article Type:	Research paper
Keywords:	L-CMD; lamin A; LMNA; congenital muscular dystrophy; emerin; SUN2; proteome; proteomics
Corresponding Author:	Heidi R Fuller Keele University Oswestry, Shropshire UNITED KINGDOM
First Author:	Emily C Storey
Order of Authors:	Emily C Storey
	Ian Holt
	Silvia Synowsky
	Sally Shirran
	Sharon Brown
	Heidi R Fuller
Abstract:	LMNA-related congenital muscular dystrophy (L-CMD) is caused by mutations in the LMNA gene, encoding lamin A/C. To further understand the molecular mechanisms of L-CMD, proteomic profiling using DIA mass spectrometry was conducted on immortalized myoblasts and myotubes from controls and L-CMD donors each harbouring a different LMNA mutation (R249W, del.32K and L380S). Compared to controls, 124 and 228 differentially abundant proteins were detected in L-CMD myoblasts and myotubes, respectively, and were associated with enriched canonical pathways including synaptogenesis and necroptosis in myoblasts, and Huntington's disease and insulin secretion in myotubes. Abnormal nuclear morphology and reduced lamin A/C and emerin abundance was evident in all L-CMD cell lines compared to controls, while nucleoplasmic aggregation of lamin A/C was restricted to del.32K cells, and mislocalisation of emerin was restricted to R249W cells. Abnormal nuclear morphology indicates loss of nuclear lamina integrity as a common feature of L-CMD, likely rendering muscle cells vulnerable to mechanically induced stress, while differences between L-CMD cell lines in emerin and lamin A localisation suggests that some molecular alterations in L-CMD are mutation specific. Nonetheless, identifying common proteomic alterations and molecular pathways across all three L-CMD lines has highlighted potential targets for the development of non-mutation specific therapies.
Suggested Reviewers:	Ignacio Perez de Castro Insua iperez@isciii.es
	Peter Meinke Peter.Meinke@med.uni-muenchen.de
	Quiping Zhang qp.zhang@kcl.ac.uk
Response to Reviewers:	

Figure 1

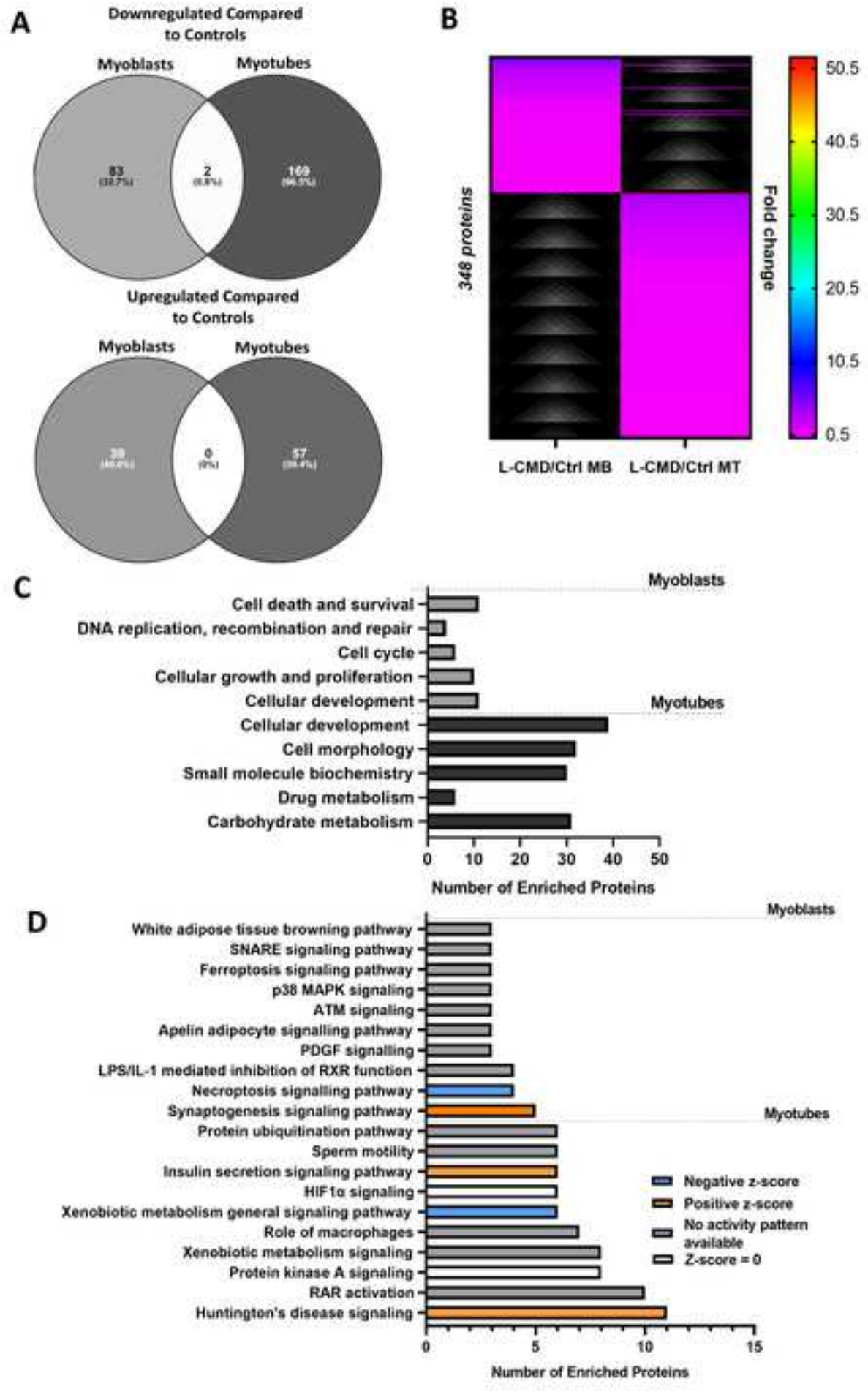

Figure 2

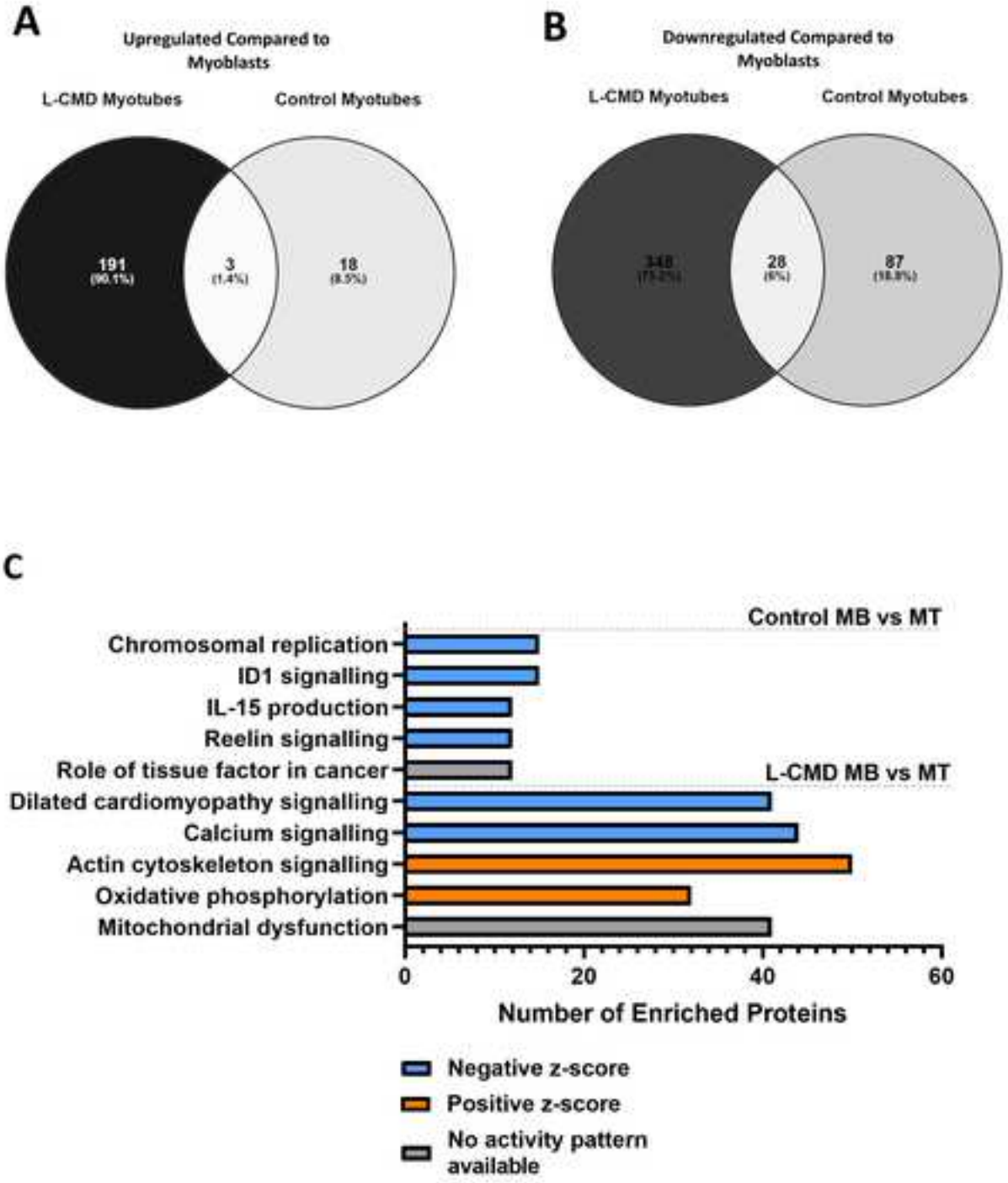

SUBMISSION CHECKLIST for Neuromuscular Disorders

Please ensure that your paper conforms to the following guidelines. Once you have completed the checks, please upload this file as a separate document using the file type "Checklist".

x **Title**: No abbreviations are to appear in the title

x **Authors' names**

x **Authors' affiliations/addresses**

x **Address** (including fax number and e-mail address) **of the corresponding author**

x **Abstract:**
x max. 200 words (150 for Case Reports)
x No abbreviations to appear in the abstract
x Continuous text with no sub-headings

x **Pages:** numbered

x **Keywords**

x **Highlights**: 3-5 bullet points (each to be no more than 85 characters including spaces)

x **Font size 12pt**

x **Single-column printout**

x **Double-spaced text**

x **Language**:
x Spelling checked
x Grammar checked

x **Figures**:
x Acceptable line quality and must fit on a portrait page
x Uploaded as separate files not embedded in the text
x Colour figures must clearly marked as being intended for colour reproduction

N/A **Consent for recognisable figures provided** (if applicable) and uploaded with the manuscript files

x **Figure and Table legends**: Separate list provided

x **Tables**:
x Should be in portrait format, but if landscape they must fit across a portrait page
x Uploaded as separate files and not embedded in the text

x **References**: For six or more authors, please list the first six names followed by "et al."

x **Author Agreement:**
It is the corresponding author's responsibility to ensure all co-authors have read and agreed the contents of the paper (on initial submission and on any revisions or subsequent resubmissions). Please prepare a statement confirming that all authors have agreed the contents of the submission. Please include the title and date, and signature. The corresponding author may sign on behalf of all co-authors.

19 January 2024

Declaration of interest

The authors hereby confirm that they have nothing to declare in respect of the following manuscript:

"Proteomic characterisation of human LMNA-related congenital muscular dystrophy muscle cells"

Signed by Heidi Fuller on behalf of all authors

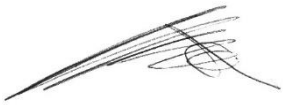

Dr Heidi Fuller (corresponding author)

Laboratory research lead, Wolfson Centre for Inherited Neuromuscular Disease
TORCH Building, RJAH Orthopaedic Hospital, Oswestry, UK, SY10 7AG |
https://www.keele.ac.uk/pharmacy-bioengineering/ourpeople/heidifuller/

Dean of Education, Faculty of Medicine and Health Sciences
Senior Lecturer in Medical Science
Keele University, Keele, Staffordshire, UK ST5 5BG

Highlights

- L-CMD myoblasts and myotubes have differentially abundant proteins vs controls
- L-CMD cells have abnormal nuclear morphology and reduced lamin A/C and emerin
- Some molecular alterations in L-CMD may be mutation specific
- Common proteomic alterations represent potential targets for therapy development

19 January 2024

Author agreement

We hereby confirm that all authors contributed to the preparation of the following written manuscript and have given approval to the final version:

"Proteomic characterisation of human LMNA-related congenital muscular dystrophy muscle cells"

Signed by Heidi Fuller on behalf of both authors

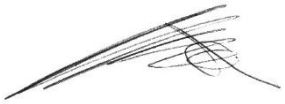

Dr Heidi Fuller (corresponding author)

Laboratory research lead, Wolfson Centre for Inherited Neuromuscular Disease
TORCH Building, RJAH Orthopaedic Hospital, Oswestry, UK, SY10 7AG |
https://www.keele.ac.uk/pharmacy-bioengineering/ourpeople/heidifuller/

Dean of Education, Faculty of Medicine and Health Sciences
Senior Lecturer in Medical Science
Keele University, Keele, Staffordshire, UK ST5 5BG

Supplementary File 1

Click here to access/download

e-Component

Storey et al 2024_NMD_Supplementary File 1.docx

Supplementary File 2

Click here to access/download

e-Component

Storey et al 2024_NMD-Supplementary File 2.xlsx

Proteomic characterisation of human *LMNA*-related congenital muscular dystrophy muscle cells

Emily C Storey[1,2], Ian Holt[1,2], Sharon Brown[1,2], Silvia Synowsky[3], Sally Shirran[3], Heidi R Fuller[1,2]*

[1]Wolfson Centre for Inherited Neuromuscular Disease, RJAH Orthopaedic Hospital, Oswestry, SY10 7AG, UK. [2]The School of Pharmacy and Bioengineering, Keele University, ST5 5BG, UK. [3]BSRC Mass Spectrometry and Proteomics Facility, University of St Andrews, KY16 9ST, UK

* Correspondence to h.r.fuller@keele.ac.uk

Abstract

LMNA-related congenital muscular dystrophy (L-CMD) is caused by mutations in the *LMNA* gene, encoding lamin A/C. To further understand the molecular mechanisms of L-CMD, proteomic profiling using DIA mass spectrometry was conducted on immortalized myoblasts and myotubes from controls and L-CMD donors each harbouring a different *LMNA* mutation (R249W, del.32K and L380S). Compared to controls, 124 and 228 differentially abundant proteins were detected in L-CMD myoblasts and myotubes, respectively, and were associated with enriched canonical pathways including synaptogenesis and necroptosis in myoblasts, and Huntington's disease and insulin secretion in myotubes. Abnormal nuclear morphology and reduced lamin A/C and emerin abundance was evident in all L-CMD cell lines compared to controls, while nucleoplasmic aggregation of lamin A/C was restricted to del.32K cells, and mislocalisation of emerin was restricted to R249W cells. Abnormal nuclear morphology indicates loss of nuclear lamina integrity as a common feature of L-CMD, likely rendering muscle cells vulnerable to mechanically induced stress, while differences between L-CMD cell lines in emerin and lamin A localisation suggests that some molecular alterations in L-CMD are mutation specific. Nonetheless, identifying common proteomic alterations and

molecular pathways across all three L-CMD lines has highlighted potential targets for the development of non-mutation specific therapies.

Key words

L-CMD; lamin A; LMNA; congenital muscular dystrophy; emerin; SUN2; proteome; proteomics

1. Introduction

LMNA-related congenital muscular dystrophy (L-CMD, ORPHA:157973) is an extremely rare genetic condition, with an estimated incidence of <1/1,000,000 [1]~~[1]~~ caused by mutations in the *LMNA* gene that encodes the type V intermediate filament proteins, lamins A and C [2,3]~~[2,3]~~. L-CMD has been described as the most severe of the striated muscle laminopathies and is characterized by onset before the age of 2 years old [3,4]~~[3]~~. Distinct features include major muscle atrophy and weakness, mainly affecting the axial muscles, leading to a complete absence of or limited motor achievements [3,4]~~[3]~~. A hallmark of L-CMD is a "dropped head" due to weakness of muscles in the neck [2,5–7]~~[2,4–6]~~, and other characteristics include the presence of multiple joint contractures, and life-threatening severe respiratory insufficiency, requiring mechanical ventilation [3,4]~~[3]~~. Cardiac arrhythmias have been identified in L-CMD patients, suggesting there is some cardiac involvement in this disease [3,4]~~[3]~~. Current treatment options are limited to physiotherapy, surgery to treat contractures, as well as managing the risk of respiratory and cardiac manifestations which are common causes of premature death.

Lamins A and C, along with B-type lamins, are the major components of the nuclear lamina (NL) [8–10]~~[7–9]~~. Lamin A/C are connected to other nuclear envelope (NE) proteins through their mutual association with the Linker of Nucleoskeleton and Cytoskeleton (LINC) complex, which functions to connect the NL to the cytoskeleton in mammalian cells [11]~~[10]~~. Lamin A/C is known to interact directly with LINC complex proteins Sad1 and UNC84 domain containing SUN proteins 1 and 2 [12]~~[11]~~, and associated protein, emerin [13]~~[12]~~, and is involved with a wide variety of cellular processes including the regulation of cell stability,

cell motility, mechanosensing, gene regulation, chromosome organization, DNA damage repair, telomere protection, and cell differentiation, including myogenesis [14–20][~~13–19~~]. Lamin A/C has been widely studied in many of these contexts, and in recent years, some progress has been made to elucidate the pathophysiological mechanisms of L-CMD, downstream of *LMNA* mutations. It was noted, for example, that fibroblasts from an individual with a severe L-CMD and lipodystrophy phenotype harbouring a heterozygous *LMNA* R388P mutation senesced prematurely, had abnormal cellular morphology and a small percentage of abnormally shaped nuclei [21][~~20~~]. In C2C12 cells transfected with lamin A carrying the same mutation, mutant lamin A mostly accumulated within the nucleoplasm, with less lamin A being correctly localized at the nuclear periphery [22][~~21~~]. Additionally, altered anchorage of the inner nuclear membrane protein and interaction partner of lamin A/C, emerin, and LAP2α, another nuclear envelope protein, was evident [22][~~21~~]. In C2C12 cells in which the R249W *LMNA* mutation, a common cause of L-CMD, was introduced by CRISPR/Cas9 editing, mislocalised emerin was detected at the endoplasmic reticulum, nuclei showed a significant reduction in their circularity index, and there was evidence of DNA damage and impaired myogenic differentiation [23][~~22~~]. Similarly, skin fibroblasts from L-CMD individuals carrying R249W and del.K32 *LMNA* mutations also exhibited mislocalised lamin A/C, which was almost exclusively found in the nucleoplasm [24][~~23~~]. In the del.K32 myoblasts from a mouse model of L-CMD, a strong reduction of lamin A/C was noted, in addition to partially mislocalized emerin. The cells were found to have impaired differentiation, with highly misshapen myonuclei, that were elongated, enlarged, and situated in the middle of myotubes [24][~~23~~]. In addition to emerin, lamin B1 and SUN2 were also mislocalized in del.K32 mouse myotubes, in contrast to the apparent correct localization of lamin B1 and SUN1 in the respective myoblasts, suggesting that the nuclear defects are exacerbated by differentiation [24][~~23~~]. There is evidence too that L-CMD causing mutations interfere with mechanosignalling pathways in skeletal muscle, subsequently affecting muscle growth [25][~~24~~]. Human muscle stem cells carrying either the del.K32, R249W or L380S *LMNA* mutations were each found to have impaired myogenic fusion, due to disorganized cadherin/β catenin adhesion complexes, stretched myotubes and overloaded muscle fibres with aberrant regulation of the yes-associated protein (YAP) [25,26][~~24,25~~]. Skeletal muscle from *Lmna*-CMD mice was also unable to

hypertrophy in response to functional overload, due to defective accretion of activated satellite cells [25,26]~~[24,25]~~.

The wide range of *LMNA* mutations known to cause L-CMD complicates gene therapy development for the condition [27]~~[26]~~, and it may be too late for gene therapy to be fully effective by the time a diagnosis is made. Variable severity and symptom onset time with little obvious relationship to the mutation further complicates matters [3,4]~~[3]~~. Alternatively, therapies tailored towards conserved features of L-CMD might, in combination with gene therapy, offer maximum benefit to patients. This approach is gaining momentum for another inherited neuromuscular disease, spinal muscular atrophy, where gene replacement strategies have shown incomplete efficiency [28,29]~~[27,28]~~. While the studies described above have generated valuable insights into the cellular consequences of L-CMD, identification of targets for therapy development is hindered by limited insights into the molecular pathways downstream from *LMNA* to modulate pathogenesis.

Here, we have conducted targeted and unbiased proteomic analyses on immortalized myoblasts and myotubes from healthy controls compared to three individuals with L-CMD, each harbouring a different *LMNA* mutation (i.e., R249W, del.32K and L380S), with the aim of determining whether the L-CMD cells may share a core molecular signature.

2. Materials and Methods

2.1. Cell culture

Immortalized myoblast cell lines were from three human control donors without neuromuscular disease, and from three individuals with L-CMD (**Supplementary File 1, Table 1**) [3,30]~~[3,29]~~. They were immortalized by transduction with human telomerase reverse transcriptase (hTERT) and cyclin-dependent kinase-4 (Cdk4-R24C mutant) containing retroviral vectors, at the Institut de Myologie, Paris, as described previously [31]~~[30]~~. Myoblasts were cultured in skeletal muscle cell growth medium (Cat No: C-23060; PromoCell GmbH, Heidelberg, Germany) containing supplement mix (Cat No: C-39365; PromoCell) with 10% Fetal Bovine Serum (Cat No: 10270; Gibco; Thermo Fisher Scientific,

Paisley, UK) and Penicillin-Streptomycin (Cat No: 15140122; Gibco; Thermo Fisher Scientific). Differentiation was induced once myoblasts had reached approximately 80-90% confluency by washing adherent myoblasts in serum free medium and then culturing in DMEM (Cat No: 31966-021; Gibco; Thermo Fisher Scientific) supplemented with Insulin-Transferrin-Selenium-Ethanolamine (ITS-X) (Cat No: 51500-056; Gibco; Thermo Fisher Scientific) and Penicillin-Streptomycin (Cat No: 15140122; Gibco; Thermo Fisher Scientific) without the addition of serum. After a further four days of cell culture, approximately 80% of the cells had fused into myotubes.

2.2. Cell proliferation assay

Control (C5d, C25, C41) and L-CMD (L380S, del.K32, R249W) myoblasts were grown in complete medium, as described above, seeded in T25 cell culture flasks at a density of 30,000 cells per flask (approximately 1% of the maximum confluency of a T25 flask). The cells were maintained in a humidified incubator (LEEC, Nottingham, UK) at 37°C and 5% CO_2 for three days during their exponential growth phase. After this point, the media was removed from the flask and cells were trypsinized and counted. Each cell line was grown in three T25 flasks (to provide technical replicates), and each flask was counted four times. Before the final cell count, each of the cell lines were less than 50% confluent, indicating that the myoblasts were still growing exponentially. A total of 12 measurements were performed for each cell line. Doubling time (DT) for each cell was calculated using the following equation: $DT = \ln(2) \times t/(\ln(C2) - (\ln(C1))$. Here, t represents the culture duration in hours, C2 is the number of cells at the end of the culture, and C1 is the number of seeded cells at the beginning of the experiment.

2.3. Western blotting

Myoblast and myotube pellets were resuspended in RIPA buffer (p.25% deoxycholic acid, 1mM ethylenediaminetetracetic acid, 150mM sodium chloride and 50mM TRIS-HCl buffer, pH 7.4), left on ice for 5 min, then sonicated briefly for 10s. Samples were centrifuged for 5 min at 13,000 RPM (MSE, Heathfield, UK; Harrier 18/80R) at 4°C to pellet any insoluble material. Protein extracts were then subject to SDS-PAGE and western blotting. Samples were then briefly heated in 2x Laemmli buffer [32]~~[31]~~ (4% sodium dodecyl sulfate, 10% 2-mercaptoethanol, 20% glycerol, 0.125 M TRIS-HCl) at 95°C for 3 min and subjected to SDS-

PAGE (Biorad, Hercules, CA, USA) using 4-12% Bis-Tris 15-well precast gels (Cat No: NW04125BOX; Life Technologies; Invitrogen). A small section from the top of the gel was excised and stained with Coomassie blue (Cat No: 20278; Thermo Scientific; ThermoFisher Scientific) as an internal loading control for total protein, as previously described [33]~~[32]~~. The proteins in the remaining gel were transferred to nitrocellulose membrane by western blotting overnight [34]~~[33]~~. Membranes were blocked with 4% powdered milk, and then incubated with primary antibodies; mouse anti-lamin A/C (MANLAC1 4A7; 1:100 [35]~~[34]~~), mouse anti-emerin (MANNEM1 5D10; 1:100 [36,37]~~[35,36]~~), rabbit anti-SUN2 (HPA001209; 1:500, Merck Life Science, Gillingham, UK) in western blot buffer (1% BSA, 10% horse serum, 10% fetal calf serum in PBS with 0.05% triton) for 1-2 h, followed by incubation with secondary antibodies; HRP-labelled rabbit anti-mouse immunoglobulins (Cat No: P026002-2; Dako; Agilent; 1:1000) or HRP-labelled goat anti-rabbit immunoglobulins (Cat No: P0448; Dako; Agilent; 1:1000). Membranes were then incubated with West Pico chemiluminescent substrate (Cat No: 34580; Thermo Fisher Scientific; Thermo Fisher Scientific), or SuperSignal™ West Femto chemiluminescent substrate (Cat No: 10391544; Thermo Fisher Scientific; Thermo Fisher Scientific) for low signal detection and visualized using a Gel Image Documentation system (Biorad, Hercules, CA, USA). Densitometry measurements of antibody reactive bands were obtained using ImageJ software (version 1.8.0_112) and were normalized to densitometry measurements of the Coomassie stained gel [38]~~[37]~~.

2.4. Immunofluorescent microscopy

Immortalized myoblasts were fixed in acetone:methanol (50:50) for 5-10 min and incubated with primary antibody, mouse anti-emerin (MANEM1 5D10; 1:4 [36,37]~~[35,36]~~), rabbit anti-lamin A/C (MANLAC1 4A7; 1:4 [35]~~[34]~~), and rabbit anti-SUN2 (HPA001209, 1:100, Merck Life Science, Gillingham, UK) in blocking buffer (1% FBS and 1% HS in PBS) for 1 h. After incubation with secondary antibody, goat anti-mouse immunoglobulins Alexa Fluor® 488 or 546 (Cat No: A11029, Cat no: A11030; Life Technologies; 1:400) or goat anti-rabbit immunoglobulins Alexa Fluor® 546 (Cat No: A11010; Life Technologies; 1:400), coverslips were mounted with ProLong™ Gold Antifade Mountant with DAPI (Cat No: P36941, Thermo Fisher Scientific), and cells were imaged using Leica SP5 confocal microscope with 63x oil immersion objective.

2.5. Quantitative DIA-MS proteomics analysis

2.5.1. Sample preparation

Protein was extracted from myoblast and myotube samples from healthy control donors (n=3) and L-CMD patients harbouring mutations in *LMNA* (n=3) using 250µL of extraction buffer (8M urea (Cat no: U0631; Sigma Aldrich), 100mM ammonium bicarbonate, 2% sodium deoxycholate in sterile dH_2O). Samples were sonicated at 5 microns for 10s and centrifuged at 13000 RPM for 5 min at 4°C to pellet insoluble material. A small aliquot of cell extract from each sample was used to determine protein concentration, whilst the remaining samples were stored at -80°C for downstream analysis. The protein concentration of each sample was determined using the Pierce™ BCA Protein Assay Kit. A minimum of 30µg of protein is needed to perform quantitative DIA MS analysis with a bespoke identification library therefore we ensured each sample contained more than the minimum protein concentration.

Each sample (50µg) was diluted with extraction buffer to obtain equal concentrations and then reduced with 5mM tris(2-carboxyethyl) phosphine (TCEP) at 30°C for 1 h followed by alkylation with 10mM iodoacetamide (IAA) in darkness at room temperature for 30 min. The reaction was quenched with 20mM DTT to deactivate any unreacted reagents. The samples were diluted to 1.5M urea and subsequently digested overnight with sequencing grade trypsin in a ratio of 1µg of protease to 50µg protein.

The peptides were subjected to cleanup using C18 columns, and the cleaned, digested sample was then dried and resuspended to 1µg/µl in loading buffer (100% water, 0.1% formic acid). Data independent acquisition was performed on individual samples (DIA-MS). In addition, a pool of all the samples was prepared, and a portion subjected to nanoLC MS/MS analysis using data dependent acquisition (DDA-MS). The remnant of the pooled sample was then fractionated on high pH C18 Reverse Phase into 12 fractions before analysing the fractions individually in DDA mode.

2.5.2. Data dependent acquisition (DDA)

Peptides (5 µg) were subjected to LCMS/MS using an Ultimate 3000 RSLC (Thermo Fisher Scientific) coupled to an Orbitrap Fusion Lumos mass spectrometer (Thermo Fisher Scientific). The peptides were injected onto a Pepmap100 C18 5µm 0.3 × 5 mm reverse-phase trap for pre-concentration and desalted with loading buffer, at 5 µL/min for 10 min. The trap was then switched in-line with the analytical column (Easy-spray Pepmap RSLC C18 2µm, 50cm x75um ID). Peptides were eluted from the column using a linear solvent gradient using the following gradient: linear 4–40% of buffer B over 120 min, linear 40–60% of buffer B for 30 min, sharp increase to 95% buffer B within 0.1 min, isocratic 95% of buffer B for 15 min, sharp decrease to 2% buffer B within 0.1 min and isocratic 2% buffer B for 15 min. The mass spectrometer was operated in DDA positive ion mode with a cycle time of 1.5 s. The Orbitrap was selected as the MS1 detector at a resolution of 120000 with a scan range of from m/z 375 to 1500. Peptides with charge states 2 to 5 were selected for fragmentation in the ion trap using HCD as collision energy.

The raw data files were converted into mgf using MSconvert (ProteoWizard) and searched using Mascot with trypsin as the cleavage enzyme and carbamidomethylation as a fixed modification of cysteines, against the Swissprot database, restricted only to proteins from humans. Note that the iRT peptides were added to this database. The mass accuracy for the MS scan was set to 20 ppm and for the fragment ion mass to 0.6 Da.

2.5.3. Data independent acquisition (DIA) mode

For quantitative MS, sample (5 µg) was injected onto the same LCMS set up as above with the same gradient, however data acquisition was performed in data independent acquisition (DIA) mode. The DIA MS method alternates between a MS scan and a tMS2 scan containing 24 scan windows. The MS scan has the following parameters: the Orbitrap at 120000 resolution is selected as detector with a m/z range from 400 to 1000. The tMS2 scan uses HCD as activation energy with fragments detected in the Orbitrap at 30000 resolution. The first 20 m/z windows are 20 mass units wide from 410 to 790 followed by a 30m/z window from 790-820, a 40m/z window from 820-860, a 50m/z window from 860-910 and a 60m/z window from 910-970.

All Mascot searches using the DIA data were exported as .dat file and assembled to a spectral library in Skyline by associating each peptide to its respective protein. After the quantitative spectra were imported, peaks were reintegrated using the mProphet peak scoring model [39][~~38~~] To identify differentially expressed proteins, the sum total area value for each protein identified by ≥2 peptides in the L-CMD (n=3) and control samples (n=3) was averaged, and only proteins with an average fold change of <0.8 and >1.25 with a $p < 0.05$ (as determined by a t-test) across the three L-CMD samples compared to controls were considered in further analysis.

2.5.4. QIAGEN Ingenuity Pathway Analysis (IPA®)

Dysregulated pathways were identified downstream of *LMNA* mutations in L-CMD patient myoblasts and myotubes (compared to controls) using QIAGEN Ingenuity Pathway Analysis (IPA®) software (QIAGEN; https://digitalinsights.qiagen.com/products-overview/discovery-insights-portfolio/analysis-and-visualization/qiagen-ipa/). The fold change value for each protein along with the assigned p-value was inputted into IPA® in the form of an Excel spreadsheet. IPA® uses right-tailed Fisher's Exact Test to calculate the p-value determining the probability that each cellular and molecular function or canonical pathway assigned to that dataset is due to chance alone, and the final lists of functions and pathways were ranked accordingly to the resulting p-value. IPA® also produces a Z-score for enriched canonical pathways. The Z-score is a prediction of whether a pathway is activated or inhibited based on the direction of expression change in the input dataset. This is done by comparing the IPA® database, which predicts what to expect when an upstream regulator interacts with its downstream target, to the direction of differential gene/protein expression that was observed in the input dataset. Z-score of ≥2 represents the prediction of activation, while Z-score ≤ -2 represents the prediction of inhibition.

2.6. Statistical analysis

All statistical analysis were carried out using GraphPad Prism Version 9.0.0. for Windows (GraphPad Software, San Diego, CA, USA, www.graphpad.com). Western blot densitometry measurements were assessed using unpaired, two-tailed t-tests, with unequal variance to determine significant differences between L-CMD myoblast and myotube samples and healthy controls. To determine if changes in protein expression in L-CMD myoblasts and

myotubes were significantly different to controls after MS analysis, multiple unpaired two-tailed t-tests were performed assuming unequal variance applying no correction for multiple comparisons. Also following MS analysis, significant protein expression changes were determined between L-CMD myoblasts and L-CMD myotubes, as well as control myoblasts and control myotubes. For this, ~~multiple~~ paired two-tailed t-tests with unequal variance were used.

3. Results

3.1. Quantitative proteomic identification of differentially expressed protein profiles in L-CMD cells compared to healthy controls

To determine whether there is a molecular signature of L-CMD in myoblasts and myotubes that is conserved across each of the three different mutations (R249W, L380S, del.K32) a quantitative proteomic comparison was made with control cells (C5d, C25, C41) using Data Independent Acquisition MS This approach identified a total of 10,977 proteins in total with a Mascot significance threshold for of $p<0.05$ (**Supplementary File 2**). Following the subsequent filtering steps described in the methods section, 124 and 228 proteins met the criteria for differential abundance in the L-CMD myoblasts and myotubes, respectively, compared to control cells (**Figure 1A & B**). Of these, 85 and 171 proteins were downregulated in the L-CMD myoblasts and myotubes, respectively, compared to controls. Two proteins, BCL7B (B-cell CLL/lymphoma 7 protein family member B) and transketolase, were commonly downregulated in both L-CMD myoblasts and myotubes compared to control cells. No commonly upregulated proteins were identified between the 39 and 57 proteins that were significantly increased in L-CMD myoblasts and myotubes, respectively, compared to controls (**Figure 1A & B**), though two proteins, DNA primase large subunit and F-box/LRR-repeat protein 3, were upregulated in L-CMD myoblasts but downregulated in L-CMD myotubes. Lamin A/C itself met the criteria for reduced abundance in the L-CMD myotubes compared to controls (ratio=0.450, p=0.038). Other LINC complex-associated proteins including lamin B1 and B2, emerin, FHL1, SUN1 and SUN2, and nesprin-1 and nesprin 2, were detected but did not meet the criteria for differential abundance. In the case of SUN2 and emerin, this was most likely due to the technical variability in the

detection and measurement of individual peptides within each sample, as confirmed by inspection of the raw proteomics data.

Ingenuity pathway analysis (IPA®) identified enriched molecular and cellular functions with which the dysregulated proteins in the L-CMD cells were associated. The top five terms were cell death and survival (n=11, p=1.18 x 10^{-02}-7.27 x 10^{-04}), cellular growth and proliferation (n=10, p=1.36 x 10^{-02}–3.19 x 10^{-04}), cell cycle (n=6, p=1.03 x 10^{-02}–3.92x 10^{-04}), DNA replication, recombination, and repair (n=4, p=1.03x 10^{-02}-3.92 x 10^{-04}), and cellular development (n=11, p=1.03 x 10^{-02}-3.19 x 10^{-04}) (**Figure 1C**). Differentially expressed proteins in the L-CMD myotubes were also associated with cellular development (n=39, p=9.46 x 10^{-03}-7.13 x 10^{-05}), while other enriched molecular and cellular functions included cell morphology (n=32, p=9.46 x 10^{-03}-7.13 x 10^{-05}), small molecule biochemistry (n=30, p=9.46 x 10^{-03}-1.56 x 10^{-06}), drug metabolism (n=6, p=9.46 x 10^{-03}-1.56 x 10^{-06}) and carbohydrate metabolism (n=31, p=1.18 x 10^{-02}-7.27 x 10^{-04}) (**Figure 1C**).

IPA® also identified significantly enriched canonical pathways among the list of differentially expressed proteins in L-CMD cells compared to controls. In the dataset comparing L-CMD and control myoblasts, top enriched canonical pathways included the white adipose tissue browning pathway (n=3, p=0.035), SNARE signalling pathway (n=3, p=0.034), ferroptosis signalling pathway (n=3, p=0.031), p38MAPK signalling (n=3, p=0.025), ATM signalling (n=3, p=0.015), apelin adipocyte signalling pathway (n=3, p=0.023), PDGF signalling (n=3, p=0.010), and LPS/IL-1 mediated inhibition of RXR function (n=5, p=0.043). For these pathways, it was not possible to predict an activity pattern. The necroptosis pathway, however, had a z-score of -2, indicating a predicted downregulation (n=4, p=0.009), whilst the synaptogenesis signalling pathway was assigned a z-score of 1.342, suggesting the pathway is upregulated (n=5, p=0.025) (**Figure 1D**). In the L-CMD versus control myotube dataset, top enriched canonical pathways included the protein ubiquitination pathway (n=6, p=0.047), sperm motility (n=6, p=0.035), role of macrophages, fibroblasts and endothelial cells in rheumatoid arthritis (n=7, p=0.037), xenobiotic metabolism signalling (n=8, p=0.007), and RAR activation (n=10, p=<0.001), none of which had predicted directionality of activation. HIF1α signaling (n=6, p=0.014454) and protein kinase A signalling (n=8, p=0.042) had z-scores of 0, whilst the insulin secretion signalling pathway (n=6, p=0.046) and

Huntington's disease signalling (n=11, *p*=<0.001) had positive z-scores of 0.816, suggesting activation, and the xenobiotic metabolism general signalling pathway (n=6, *p*=0.002) had a negative z-score of -0.816, predicting inhibition (**Figure 1C**). There were no enriched canonical pathways in common between the differentially expressed proteins that were identified in the L-CMD myoblasts and myotubes.

To gain insights into whether the molecular response associated with myoblast differentiation was similar in the L-CMD cells compared to controls, the differentially expressed proteins identified in L-CMD myoblasts vs their respective myotubes were compared with those that were differentially expressed in the control myotubes vs their respective myoblasts. A total of 136 proteins were differentially expressed in control myoblasts compared to their myotubes, whilst 570 proteins were differentially expressed in L-CMD myoblasts compared to their myotubes. Of these, only 3 proteins were commonly upregulated and 28 commonly downregulated in L-CMD and control myoblasts compared to their respective myotubes (**Figure 2A & B**). The lack of overlap of differentially expressed proteins in the L-CMD and control myoblast vs myotube datasets, therefore implies that proteins that are involved at different points during muscle cell differentiation are dysregulated in L-CMD myoblasts and/or myotubes.

Top canonical pathways identified by IPA® for the differentially expressed proteins in the control myoblasts vs myotubes comparison included cell cycle control of chromosomal replication (n=15, *p*=1.31E-15), ID1 signalling pathway (n-15, *p*=1.87E-07), IL-15 production (n=12, *p*=1.89E-07), and reelin signalling in neurons (n=12, p=7.16E-07), which had negative z-scores of -3.4, -3.4, -3.5, and -2.1, respectively, indicating predicted inhibition, whilst role of tissue factor in cancer (n=12, *p*=9.88E-08) was also an enriched pathway, but had no predicted activity (**Figure 2C**). For the proteins identified in the L-CMD myoblasts vs their myotubes, top enriched canonical pathways were very different and included dilated cardiomyopathy signalling pathway (n=41, *p*=5.18E-24) and calcium signalling (n=44, p=9.92E-20), which had z-scores of -5 and -0.6, suggesting inhibition, actin cytoskeleton signalling (n=50, *p*=1.79E-22) and oxidative phosphorylation (n=32, *p*=1.32E-19) which had z-scores of 2.2 and 5.7, suggesting activation, and mitochondrial dysfunction (n=41, *p*=2.05E-21), for which activity could not be predicted (**Figure 2C**). Whilst top canonical pathways for

the dysregulated proteins in the control myotubes included ID1 signalling and IL-15 production, which are pathways known to be involved in muscle cell differentiation or skeletal muscle hypertrophy [40,41]~~[39,40]~~, the top canonical pathways for the dysregulated proteins in the L-CMD myotubes included pathways associated with disease states including dilated cardiomyopathy signalling and mitochondrial dysfunction [42]~~[41]~~.

3.2. L-CMD myoblasts have a decreased proliferation rate and both myoblasts and myotubes exhibit nuclear morphology abnormalities

Next, we investigated the doubling time of each myoblast cell line, to determine the relevance of the finding described above that ten differentially abundant proteins in the L-CMD myoblast cell lines were associated with cell growth and proliferation canonical pathways. On average, the L-CMD myoblasts had a longer doubling time compared to the control cells during their exponential growth phase (36.24hrs vs 26.72 hrs, p = 0.023), indicating that the L-CMD cells had a decreased proliferation rate (**Figure 3A**). The quantitative proteomics analysis also identified that 32 proteins differentially abundant in the L-CMD myotubes compared to controls were associated with cell morphology. In culture, there were no obvious differences in the gross cellular morphology of L-CMD myoblasts compared to controls (**Supplementary File 1, Figures 1-2**). All L-CMD and control myoblasts appeared small and uniform in shape, except for the C5d control cell line which appeared to have slightly larger cells that were less uniform in shape, with some myoblasts appearing elongated. Across all cell lines, the myotubes also appeared similar in morphology when growing in culture (**Supplementary File 1, Figures 1-2**). Immunofluorescence microscopy analysis using DAPI nuclear staining, however, demonstrated that each of the L-CMD cell line myotubes exhibited disordered nuclei that did not all appear to fuse together properly and their placement within the myotube was more random and irregular compared to control myotube nuclei (**Figure 3B**). In contrast, control myotubes contained consistently fused nuclei that formed elongated, thick structures. In addition, some L-CMD myotubes were shorter, contained less nuclei or formed myotubes with “clumps” of nuclei which were not elongated.

To determine whether the L-CMD myoblasts used in this study also have nuclear morphology abnormalities, a ~~the~~ classification method described previously ~~by Van Tienen et al. (2018)~~ by van Tienen *et al.* (2018) was used to analyse immunofluorescence microscopy images from L-CMD myoblast and myotube cultures [43]. Lamin A/C immunostaining in combination with DAPI allowed the nuclear envelope and nuclear defects to be visualized more clearly than with DAPI alone. A representative example of each type of abnormality that was identified is given in **Figure 3C**. Approximately 49% and 50% of myoblast nuclei were classified as abnormal in the L380S and del.K32 L-CMD myoblasts, while 47% and 54% of the nuclei in the myotubes for the respective cell lines were abnormally shaped (**Figure 3D and E**). The R249W L-CMD cells exhibited an increased amount of abnormally shaped nuclei in myotubes (95%) compared to myoblasts (54%), suggesting that nuclear defects in this L-CMD cell line are exacerbated during differentiation (**Figure 3D and E**). In comparison, only 4% of control myoblasts had nuclear abnormalities, which is comparable to the previous study by van Tienen et al., where 4.8% of healthy cell nuclei were abnormal, and only 2% of control myotube nuclei appeared to have abnormalities (**Figure 3D and E**). Nuclear shape abnormalities (NSA) were the most frequent abnormalities seen across all three L-CMD myoblasts and myotubes, followed by blebs. L-CMD L380S myoblasts also exhibited many nuclei with donut shapes, which was not observed in the other L-CMD cell lines. In comparison to the L-CMD nuclei, the control cell nuclei were spherical or slightly oval, as expected.

3.3. Lamin A/C is reduced in expression in L-CMD myotubes compared to controls and is partially mislocalized in L-CMD del.K32 myoblasts

With lamin A/C having been identified by quantitative proteomics analysis as reduced in abundance in the L-CMD myotubes compared to controls (ratio=0.450, p=0.038), we next determined the relative levels of lamin A/C in myoblast and myotubes extracts using quantitative western blotting analysis. Quantitative western blotting analysis of myoblast cell extracts indicated slight, non-statistically significant reduction in lamin A, but not lamin C levels in the L-CMD cells compared to healthy controls (by 54.55%, p=0.244) (**Figure 4A &E**). The lamin A band exhibited a slightly faster electrophoretic mobility in the L-CMD myoblasts compared to control myoblasts (**Figure 4A & C**) that was not apparent in the

myotube extracts (**Figure 4B**), where lamin A appeared to be of comparable molecular weight in the L-CMD and control samples. The lower molecular weight lamin A band in L-CMD myoblasts may indicate the presence of truncated lamin A in each of the L-CMD cell lines or a degraded form of mature lamin A, potentially due to lamin A being more unstable in the L-CMD myoblasts. It was also observed that there were higher molecular weight lamin A bands that were present in addition to the lamin A bands at the expected molecular weight (70kDa) in C25 and C41 control myoblast samples, as well as in all of the control myotube samples. This could indicate the presence of pre-lamin A, which would have a slightly higher molecular weight than mature lamin A [44], however further experiments are needed to confirm this. In myotube extracts, both lamin A and C were reduced in the L-CMD cells vs controls (by 98.68%, p=0.044, and by 63.29%, p=0.043, respectively) (**Figure 4B & D)**.

With the observations of reduced levels of lamin A/C and differences in its molecular weight in L-CMD cells compared to controls, we next wished to determine whether lamin A/C is correctly localized in the L-CMD cells, which may help to gain insights into the cause and / or consequence of its reduced expression. In the L-CMD myoblasts harbouring the R249W and L380S mutations, lamin A/C was observed at the nuclear envelope, possibly with some diffuse lamin A/C immunoreactivity also in the nucleoplasm, to a greater extent than was evident in the control myoblasts (**Figure 4F & G**). Technically, this was unreliable to quantify, particularly in the R249W cell line, due to the abnormal nuclear morphologies causing wrinkling and invaginations around the nuclei. In the L-CMD del.K32 myoblasts, some lamin A/C was evident at the nuclear envelope, but most appeared to be present in nuclear aggregates within the nucleoplasm in all cells examined (out of 100 cells) (**Figure 4G**). This nuclear aggregation was not apparent in myotubes derived from the del.K32 cell line, and localization of lamin A/C in myotubes from the R249W and L380S cell lines also appeared to be relatively consistent with the distribution seen in healthy controls. To note, *LMNA* protein expression was not quantifiable using immunofluorescence microscopy and could not be compared to western blot analysis of total *LMNA* protein as samples were not imaged using consistent laser intensity.

3.4. Emerin is mislocalized to the cytoplasm in L-CMD R249W myoblasts and is reduced in expression in L-CMD myotubes compared to controls

The lamin A/C binding protein, emerin, was clearly localized at the nuclear envelope in all control myoblast and myotube cell lines examined, though some emerin was found to be mislocalized to the cytoplasm in approximately one third of the L-CMD myoblasts examined that harboured the R249W mutation (**Figure 5A**). On average across the three L-CMD myoblast cell lines, emerin was not significantly different to controls (p=0.097) (**Figure 5B**). In L-CMD myotubes, emerin was, however, significantly reduced compared to controls (by 74.25%, p=0.040) (**Figure 5C**). An incidental finding, prompted by this observation, is that emerin expression generally appeared to be decreased on average by 81.37% in fully formed control myotubes, compared to their respective proliferating and differentiating myoblasts across six different cell lines. The most prominent reduction in emerin expression levels occurred between the second and third day (corresponding to timepoints 4 and 5) following differentiation initiation (timepoint 3) (**Supplementary File 1, Figure 3**). A similar pattern was noted in the L-CMD cell lines, albeit with emerin being less easily detectable at each timepoint examined (**Supplementary File 1, Figure 3**).

3.5. SUN2 was correctly localized at the nuclear envelope in L-CMD cells and reduced in expression in myotubes

SUN2 is a known interaction partner of lamin A at the INM (Crisp, et al., 2006), and is dependent on lamin A for its correct localization at the NE (Haque et al., 2010). SUN2 appeared to be correctly localised at the NE in the control and L-CMD myoblasts and myotubes, suggesting that the *LMNA* mutations harboured in the L-CMD cells do not affect SUN2 localization (**Figure 6A**). The intensity of SUN2 staining appeared reduced in L-CMD myoblasts and myotubes compared to control cells, when imaged using a consistent laser intensity (**Figure 6A**). When measured, it was found that in L-CMD myoblasts, SUN2 staining intensity was reduced by 32.23% compared to controls, but this reduction was not statistically significant (p= 0.439). In L-CMD myotubes, however, SUN2 staining was reduced by 85.35%, which was statistically significant (p= 0.010). Quantitative western blotting analysis confirmed this result, showing that SUN2 was not significantly different in expression in the L-CMD myoblasts compared to controls (p=0.401) (**Figure 6B)**. In the

myotube samples, SUN2 was significantly reduced in L-CMD myotubes compared to controls (by 52.21%, *p*=0.049) (**Figure 6C)**.

4. Discussion

In the past couple of decades, quantitative proteomics has gained popularity as a useful method for identifying and quantifying all the proteins within a biological sample on a large-scale in an unbiased manner. Proteomic studies have advanced our understanding of cellular signalling networks and have improved diagnosis and molecular understanding of disease mechanisms. Comparison of the proteome of L-CMD cells to controls, a total of 124 differentially expressed proteins were identified in the L-CMD myoblasts, and 228 proteins were identified in the L-CMD myotubes, which could be potentially linked to the development of the disease. It was noted that there were more dysregulated proteins in the L-CMD myotubes than the L-CMD myoblasts, compared to controls, indicating that processes are potentially more impaired in L-CMD myotubes. There was also found to be very little cross over between the dysregulated proteins that were identified in the L-CMD myoblasts and myotubes. This implies the processes and signalling pathways that are dysregulated in L-CMD myoblasts and myotubes differ. This was substantiated by the finding that the molecular and cellular pathways and the canonical pathways associated with the dysregulated proteins were different for the L-CMD myoblasts and myotubes.

Several particularly interesting canonical pathways were found to be associated with the dysregulated proteins that were identified in the L-CMD myoblasts and myotubes. A substantial number of the dysregulated proteins in myotubes were linked to carbohydrate metabolism. The two major energy sources for muscle contraction are glycogen and fatty acids, whose metabolic pathways converge into actyl-CoA for final oxidation via the Krebs cycle and the respiratory chain, therefore carbohydrate metabolism is important for muscle function [45]~~[42]~~. Metabolic dysfunction has been observed in Duchenne muscular dystrophy, and is characterised by reduced glycolytic and oxidative enzymes, decreased and abnormal mitochondria, decreased ATP, and increased oxidative stress [46–51]~~[43–48]~~. However, alterations in carbohydrate metabolism are often associated with neuromuscular disorders [52]~~[49]~~, therefore it may not be a direct consequence of *LMNA* mutations in L-

CMD, and instead may be a result of muscle damage or abnormal function. Interestingly the insulin secretion signalling pathway, which is also a component of carbohydrate metabolism, was additionally found to be upregulated in L-CMD myotubes compared to controls.

The synaptogenesis signalling pathway was found to be elevated in L-CMD myoblasts compared to controls. Synaptogenesis is the formation of synapses between neurons in the nervous system. NMJ defects have been previously observed in models of autosomal dominant Emery-Dreifuss muscular dystrophy (AD-EDMD), which, similarly to L-CMD, is caused by *LMNA* mutations [53]~~[50]~~. Two AD-EDMD mouse models *($Lmna^{H222P/H222P}$, $Lmna^{-/-}$)* were found to show innervation defects including misexpression of electrical activity-dependent genes and altered epigenetic chromatin modifications, as well as aberrant NMJ architecture [53]~~[50]~~. Considering these results, it is plausible to infer that NMJ defects contribute to L-CMD pathophysiology, though confirmation would further investigation.

Huntington's disease signalling was upregulated in L-CMD myotubes compared to controls, and upon further examination of the dysregulated proteins involved in this pathway, two proteins that are involved in apoptosis were of particular interest; apoptotic protease-activating factor 1 (Apaf-1) and caspase-7. Apoptosis dysregulation has been identified as a feature of a number of neurodegenerative diseases, including Huntington's disease [54–57]~~[51–54]~~ In L-CMD myoblasts, it was found that the necroptosis pathway, another method of cell death, was significantly downregulated. Necroptosis has been found to be of central pathophysiological relevance in a variety of disease states including myocardial infarction and stroke [58,59]~~[55,56]~~, atherosclerosis [60]~~[57]~~, ischemia-reperfusion injury [61,62]~~[58,59]~~, pancreatitis [63,64]~~[60,61]~~, inflammatory bowel diseases [65]~~[62]~~, as well as neurological disorders [66,67]~~[63,64]~~. More recently, necroptosis has been implicated in neuromuscular diseases including Duchenne muscular dystrophy (DMD) and spinal muscular atrophy (SMA) [68,69]~~[65,66]~~. Considering the necroptosis pathway's emerging role in neuromuscular conditions as well as identification of its dysregulation in L-CMD myoblasts, it merits further verification.

We found that L-CMD myoblasts had a significantly decreased proliferation rate compared to controls. Furthermore, cellular growth and proliferation as well as cell development were enriched canonical terms associated with the differentially expressed proteins that were identified in L-CMD myoblasts using quantitative proteomics. This may suggest that *in-vivo* myoblasts fail to proliferate adequately, which could consequently hinder muscle regeneration and repair, as myoblast proliferation is a key step in this process. This would therefore impact L-CMD patients muscle integrity if it is subject to any damage or injury. For example, in models of other neuromuscular diseases, cell proliferation rate has previously been found to be altered compared to that of healthy controls. Satellite cells cultured from Duchenne muscular dystrophy patients (DMD) have been found to have an increased generation time, ceasing to proliferate beyond 100-1,000 cells, but still were capable of forming myotubes when differentiation was induced [70][~~67~~]. In a study on spinal muscular atrophy (SMA), C2C12 myoblasts with differing levels of survival motor neuron protein (*Smn*) knockdown have reduced proliferation as well as fusion defects, correlating with *Smn* levels [71][~~68~~]. These results suggest that increased doubling time of myoblasts could be related to neuromuscular disease pathology. The decreased proliferation rate observed in the L-CMD myoblasts could be a direct consequence of *LMNA* mutations, as cell proliferation rate has previously been shown to be altered when lamin A/C abundance is increased or decreased. The abundance of lamin A/C has been found to be downregulated in certain cancers, and depletion of lamin A/C abundance in healthy primary human fibroblasts leads to downregulation of the Rb family of tumor suppressors and a defect in cell proliferation [72][~~69~~]. Additionally, in prostate tumor cell lines (LNCaP, DU145, and PC3), small hairpin RNA knockdown of lamin A/C decreased cell proliferation, whilst overexpression of lamin A/C stimulated cell growth [73][~~70~~]. Despite these findings, here, we did not go on to observe a reduction in lamin A/C abundance in myoblasts, as would be expected if downregulation of lamin A/C decreases cell proliferation rate. However, another study on lamin A knockdown in lung carcinoma-derived A549 cells was also not found to perturb proliferation [74][~~71~~].

The nuclear morphology defects that were observed in the L-CMD cells are likely the consequences of a compromised NL in the cells. Abnormalities in nuclear structure are a well-known characteristic of *LMNA* mutations and have been previously observed in

myoblasts from an Emery-Dreifuss muscular dystrophy (EDMD) patient with a confirmed *LMNA* mutation [75][~~72~~], myonuclei of muscle tissue from EDMD and Limb-Girdle (LGMD) muscular dystrophy patients carrying mutations in *LMNA* [76][~~73~~], as well as in skin fibroblasts from patients with a number of different laminopathies [77–80][~~74–77~~], and in myogenic cells derived from induced pluripotent stem cells (iPSCs) from patients with skeletal muscle laminopathies including L-CMD [81][~~78~~]. How this is linked to disease pathology has already been well-discussed in the form of the structural hypothesis, with the idea that *LMNA* mutations lead to a weakened NL that results in the nucleus being unable to resist high mechanical strain in tissues exposed to tension, such as skeletal muscle [82][~~79~~]. Of the different types of nuclear deformities observed, the L380S myoblasts exhibited many more donut shaped nuclei compared to the other L-CMD cell lines. It has previously been demonstrated that treatment of primary human skin fibroblasts with protein farnesyltransferase inhibitors (FTIs) resulted in a high frequency of cells with donut shaped nuclei [83][~~80~~], suggesting that the *LMNA* L380S mutation may affect farnesylation of lamin A/C.

Across all L-CMD cell lines differentiated into myotubes, it was noticed that the nuclei within the myotubes were extremely disordered, which has previously been observed in del.K32 myotubes [84][~~81~~]. Curiously, we also found that SUN2 was significantly reduced in abundance across L-CMD myotubes. It has been found that *SUN1* and *SUN2* variants disrupt myonuclear organization, as it has been found that myotubes from a patient carrying *SUN1* mutations displayed defects in myonuclear organization [85][~~82~~]. As well as this, events required for correct myonuclear arrangement, such as absence of recruitment of pericentrin, a centrosomal marker, to the nuclear envelope, and impaired microtubule nucleation [85][~~82~~]. Thus, perhaps reduction of SUN2 is contributing to nuclear disorganization in L-CMD myotubes. It would be of interest to upregulate SUN2 expression in L-CMD myotubes to determine whether this rescues myonuclear organization disruption, and whether this has any other effects on L-CMD myotube differentiation.

Across all of the L-CMD cell lines, it was found that on average around half of the myoblast and myotube nuclei were irregularly shaped. For the L-CMD R249W cell line, though, almost all myotube nuclei exhibited abnormalities, meaning that the number of abnormal nuclei was almost doubled in R249W myotubes compared to myoblasts. This could suggest that

nuclear abnormalities are exacerbated during differentiation in the R249W cells, which has not previously been described. Some emerin was also found to be mislocalized to the cytoplasm, perhaps specifically the ER, in R249W myoblasts, and not in any other L-CMD cells. This may suggest that the R249W mutation in particular may cause more severe nuclear defects. Emerin was found to be correctly localized in R249W myotubes, however, maybe not supporting the finding that nuclear defects are worsened in R249W myotubes. Previously, emerin has been found to mislocalize and aggregate in foci in iPSC-derived myoblasts and the cytoplasm of C2C12 myoblasts harbouring R249W mutations [81,86][~~78,83~~]. Emerin has been identified as a well-characterised binding partner of lamin A/C, [13][~~12~~], and it has been found that lamin A is involved in tethering emerin to the NE [87][~~84~~]. Consequently, mutations in *LMNA* may disrupt this interaction and cause emerin to become mislocalized. Here, even when some emerin was mislocalized in the R249W myoblasts, there remained proportion of emerin that was correctly localized to the NE. This result suggests that lamin A-emerin interactions are not entirely lost and are merely compromised by the *LMNA* mutation. Loss of emerin from the NE could have implications in L-CMD disease development, as correct localization is critical for a protein's function [88][~~85~~]. If a protein is in the wrong environment, it is unlikely to fold or assemble properly, and may also trigger secondary consequences such as ~~(e.g.~~ protein degradation pathways~~,)~~ that could lead to further detrimental effects inside of the cell [88][~~85~~]. Although emerin was only mislocalized in one L-CMD cell line, a reduction in emerin protein expression was observed across all L-CMD cell lines in myotubes compared to controls. It has previously been shown that mutant forms of emerin causing X-linked Emery-Dreifuss muscular dystrophy (EDMD) are mislocalised, and it has been proposed that an absence (caused by mutations that result in the deletion of *EMD*) or reduction of emerin at the NE may be responsible for the EDMD phenotype [89][~~86~~]. It has also been found that COS-7 cells expressing mutant emerin (Del236-241, an *EMD* variant found in EDMD patients) that mainly localizes to the cytoplasm exhibit aberrant cell cycle length [90][~~87~~]. Considering this has been linked to EDMD development, loss of emerin at the NE could also be contributing to L-CMD pathophysiology. This provides evidence that there may be some cross-over between the mechanisms behind EDMD and L-CMD disease pathways. This potentially can be expected as AD and AR-EDMD are also caused by *LMNA* mutations.

Whilst emerin was found to be mislocalized in the R249W myoblasts, the del.K32 myoblasts were the only cells to exhibit mislocalization of lamin A/C. In the del.K32 myoblasts, lamin A/C appeared to be aggregated in nuclear foci within the nucleoplasm. Increased nucleoplasmic aggregation of lamin A/C has been previously observed in L-CMD fibroblasts harbouring the same del.K32 mutation, as well as primary myoblasts derived from the *Lmna*^{dK32} mouse model of L-CMD [84]~~[81]~~. In this study, myotubes harbouring the del.K32 mutation were also found to have almost exclusively nucleoplasmic localization of lamin A/C, although this was not observed here [84]~~[81]~~. In the Bertrand *et al.* study, del.K32 myotubes were also found to have disrupted localization of other INM proteins such as emerin, lamin B1, SUN2 or nup153 (further information on where these proteins were mislocalized to is not provided), proving nuclear defects in cells harbouring the del.K32 *LMNA* mutation can also be severe [84]~~[81]~~. Absence of lamin A/C from the nuclear periphery and its accumulation in the nucleoplasm has been shown to be highly detrimental for myoblast differentiation in primary myoblasts derived from the *Lmna*^{dK32} mouse [91]~~[88]~~. This has been attributed to the inability of L-CMD post-mitotic myocytes to sequester muscle-specific NE transmembrane proteins in the nuclear envelope that are required for chromatin remodelling [91]~~[88]~~. Depending on their level of phosphorylation, A-type lamins are able to assemble under the INM (where they are primarily localized), but they may also reside in the nucleoplasm [92]~~[89]~~. A-type lamins at the nuclear periphery are necessary for the nuclear sequestration of NE transmembrane proteins [93–96]~~[90–93]~~, and for the interaction with the cytoskeleton via the LINC complex [97]~~[94]~~. Other A-type lamin functions such as the regulation of gene transcription, DNA repair, and regulation of cell cycle and mechanotransduction also require lamin A/C to be correctly localized at the NL [98–100]~~[95–97]~~.

Based on the evidence outlined above, it appeared that cells harbouring the R249W or del.K32 mutations had different nuclear defects than the L380S L-CMD patient cells. This could be a consequence of the region of the *LMNA* gene that is affected by the mutations. The R249W mutation is located at the ERK1/2 binding domain in *LMNA* and causes an arginine residue to be substituted with a tryptophan residue. Arginine and tryptophan have very different properties. Arginine is amphipathic, whilst tryptophan in comparison is extremely hydrophobic in nature [101].Arginine is known to be common in binding sites,

Formatted: Font: 12 pt, Font color: Black

therefore, if arginine is substituted with another amino acid with different properties, this may affect interactions at these domains. The del.K32 mutation causes an in-frame deletion affecting a lysine residue. Similarly, to arginine, lysine is also commonly found in protein binding sites [101] .The del.K32 variant is located in the head region of lamin A/C, which is known to be involved in lamin assembly. Consequently, mutations in this region may particularly lead to nuclear assembly defects. The L380S mutation affects the HCD2 (highly conserved domain) region of *LMNA*, located at the end of the central rod domain, next to coil 2.

Lamin A/C were found to be significantly reduced across L-CMD myotubes compared to controls. This reduction in lamin A/C expression could be linked to the nucleoplasmic aggregation of lamin A/C observed in the del.K32 myoblasts, as this may indicate lamin A/C is unstable and could lead to increased degradation of the protein. In myoblasts and myotubes derived from $Lmna^{\Delta K32/\Delta K32}$ mice, a mouse model of L-CMD, reduced levels of lamin A/C protein have also been observed, although *LMNA* mRNA levels were not reduced, suggesting a reduced translation efficiency or higher rate of degradation of mutant lamin A/C [91][~~88~~]. Reduced lamin A/C levels could likely contribute to the L-CMD phenotype, as $Lmna^{\Delta K32/\Delta K32}$ mice present with an even more severe phenotype than $Lmna^{-/-}$ mice (a lamin A/C deficient mouse model of AD-EDMD) [91][~~88~~]. Whilst $Lmna^{-/-}$ mice present with growth retardation, skeletal and cardiac muscle involvement, hypoglycemia and sudden cardiac death, this phenotype was exacerbated in $Lmna^{\Delta K32/\Delta K32}$ mice [91][~~88~~]. The result presented here that lamin A/C were reduced across all myotubes differentiated from each of the L-CMD cell lines harbouring different *LMNA* mutations corroborates Bertrand *et al.*'s findings and suggests reduced lamin A/C may be conserved across different L-CMD-causing mutations. This finding may help to guide future research in L-CMD, as a therapeutic approach could be to upregulate lamin A/C production. Based on the finding that lamin A/C is reduced in $Lmna^{\Delta K32/\Delta K32}$ mice, spliceosome-mediated RNA trans-splicing (SMaRT), an approach that targets RNA at the pre-mRNA level and converts endogenous mutated sequences into wild type ones has already been used to target the del.K32 L-CMD mutation [102][~~98~~]. To achieve this, 5'-RNA pre-*trans*-splicing molecules containing the first five exons of *Lmna* and targeting intron 5 of *Lmna* pre-mRNA were developed and their efficacy at

inducing *trans*-splicing events on *Lmna* were tested and confirmed at the protein level in C2C12 myoblasts [102]~~[98]~~. This approach was then tested *in-vivo* in newborn mice using adeno-associated virus (AAV) delivery, although the efficacy of *trans*-splicing events were low [102]~~[98]~~. Despite this, these results provide the first evidence for reprogramming *LMNA* mRNA in vitro.

Conclusion

By conducting a quantitative comparison of the proteome of L-CMD myoblasts and myotubes and healthy control cells, a number of differentially expression proteins have been identified as well as potential dysregulation of a number of different molecular and cellular processes and signalling pathways. Amongst these, molecular and cellular processes common to the dysregulated proteins included cellular development, cell cycle, and cellular growth and repair. Upon this discovery, further examination of L-CMD myoblasts and myotubes revealed defects in cell proliferation, as well as nuclear morphology abnormalities. In addition to this, reduction of lamin A/C protein expression levels, and lamin A/C binding partners, emerin and SUN2 were observed across all L-CMD myotubes. In del.K32 myoblasts, lamin A/C was found to aggregate in the nucleoplasm, and in R249W myoblasts emerin was mislocalized. Proteomic analysis also revealed a number of canonical pathways that may be dysregulated including the insulin signalling pathway and Huntington's disease pathway in L-CMD myotubes, and the synaptogenesis and necroptosis signalling pathway in L-CMD myoblasts, which require verification and further investigation in future studies. The ~~conserved~~ defects that were identified across the L-CMD cell lines may be associated with L-CMD pathophysiology, and might represent targets for the development of therapies. In future, it is important to study a greater number of cell lines harbouring the same mutations as the L-CMD cell lines used in this study, as well as different L-CMD causing mutations to determine whether the defects identified across the L-CMD cell lines are conserved features of L-CMD. Comparison of the proteomics data within this study with data from other published *LMNA* transcriptomic and proteomic datasets will also be useful to support the identification of potentially conserved changes to molecular pathways in L-CMD.

Supplementary Material

Supplementary File 1 (Word document containing Tables 1-3, and Figures 1 and 2)

Supplementary File 2 (Excel document containing supplementary Tables 1-4)

Data Availability Statement

The mass spectrometry proteomic data can be accessed for reviewing purposes at XXXXX

Following publication, the mass spectrometry proteomic data can be accessed at the following DOI: XXXX

Funding

This work was supported by funding from the EPSRC/MRC Doctoral Training Centre in Regenerative Medicine (Loughborough, Keele and Nottingham Universities);
Keele ACORN scheme, Keele University, UK; and the Orthopaedic Institute Ltd., RJAH Orthopaedic Hospital, Oswestry, UK (grant number RPG182). The Fusion Lumos mass spectrometer was purchased by BBSRC grant number BB/T017686/1

Conflicts of interest

The authors declare no conflict of interest.

Acknowledgements

We are grateful to The Platform for Immortalization of Human Cells, Institute of Myology, Paris, France, for providing the immortalized human myoblasts. The authors are particularly thankful to Professor Glenn Morris for his insight and advice during the preparation of this manuscript.

References

[1] Avila GM, González AP, Abad A, Fournier BG, León SR, Corral JAM, et al. Is the Next Generation Sequencing the Essential Tool for the Early Diagnostic Approach in Congenital Muscular Dystrophy? New Mutation in the Gene LMNA Associated with Serious Phenotype. Neurol India 2021;69:1835–7. https://doi.org/10.4103/0028-3886.333448.

[2] Hattori A, Komaki H, Kawatani M, Sakuma H, Saito Y, Nakagawa E, et al. A novel mutation in the LMNA gene causes congenital muscular dystrophy with dropped head and brain involvement. Neuromuscul Disord 2012;22:149–51.

[3] Quijano-Roy S, Mbieleu B, Bönnemann CG, Jeannet P-Y, Colomer J, Clarke NF, et al. De novo *LMNA* mutations cause a new form of congenital muscular dystrophy. Ann Neurol 2008;64:177–86. https://doi.org/10.1002/ana.21417.

[4] Ben Yaou R, Yun P, Dabaj I, Norato G, Donkervoort S, Xiong H, et al. International retrospective natural history study of LMNA-related congenital muscular dystrophy. Brain Commun 2021;3. https://doi.org/10.1093/braincomms/fcab075.

[5] Bonati U, Bechtel N, Heinimann K, Rutz E, Schneider J, Frank S, et al. Congenital muscular dystrophy with dropped head phenotype and cognitive impairment due to a novel mutation in the LMNA gene. Neuromuscular Disorders 2014;24:529–32. https://doi.org/10.1016/j.nmd.2014.02.004.

[6] Pasqualin LMA, Reed UC, Costa TVMM, Quedas E, Albuquerque MA V, Resende MBD, et al. Congenital muscular dystrophy with dropped head linked to the LMNA gene in a Brazilian cohort. Pediatr Neurol 2014;50:400–6.

[7] Karaoglu P, Quizon N, Pergande M, Wang H, Polat AI, Ersen A, et al. Dropped head congenital muscular dystrophy caused by de novo mutations in LMNA. Brain Dev 2017;39:361–4.

[8] Taddei A, Hediger F, Neumann FR, Gasser SM. The function of nuclear architecture: a genetic approach. Annu Rev Genet 2004;38:305–45. https://doi.org/10.1146/annurev.genet.37.110801.142705.

[9] Bridger JM, Foeger N, Kill IR, Herrmann H. The nuclear lamina. Both a structural framework and a platform for genome organization. FEBS J 2007;274:1354–61.

[10] Aebi U, Cohn J, Buhle L, Gerace L. The nuclear lamina is a meshwork of intermediate-type filaments. Nature 1986 323:6088 1986;323:560–4. https://doi.org/10.1038/323560a0.

[11] Crisp M, Liu Q, Roux K, Rattner JB, Shanahan C, Burke B, et al. Coupling of the nucleus and cytoplasm: Role of the LINC complex. J Cell Biol 2006;172:41–53. https://doi.org/10.1083/jcb.200509124.

[12] Haque F, Mazzeo D, Patel JT, Smallwood DT, Ellis JA, Shanahan CM, et al. Mammalian SUN protein interaction networks at the inner nuclear membrane and their role in laminopathy disease processes. Journal of Biological Chemistry 2010;285:3487–98. https://doi.org/10.1074/jbc.M109.071910.

[13] Clements L, Manilal S, Love DR, Morris GE. Direct interaction between emerin and lamin A. Biochem Biophys Res Commun 2000;267:709–14. https://doi.org/10.1006/bbrc.1999.2023.

[14] Gonzàlez JM, Navarro-Puche A, Casar B, Crespo P, Andrès V. Fast regulation of AP-1 activity through interaction of lamin A/C, ERK1/2, and c-Fos at the nuclear envelope. Journal of Cell Biology 2008;183:653–66. https://doi.org/10.1083/JCB.200805049.

[15] Moiseeva O, Bourdeau V, Vernier M, Dabauvalle MC, Ferbeyre G. Retinoblastoma-independent regulation of cell proliferation and senescence by the p53–p21 axis in lamin A/C-depleted cells. Aging Cell 2011;10:789–97. https://doi.org/10.1111/J.1474-9726.2011.00719.X.

[16] Swift J, Ivanovska IL, Buxboim A, Harada T, Dingal PCDP, Pinter J, et al. Nuclear lamin-A scales with tissue stiffness and enhances matrix-directed differentiation. Science (1979) 2013;341:1240104. https://doi.org/10.1126/science.1240104.

[17] Frock RL, Kudlow BA, Evans AM, Jameson SA, Hauschka SD, Kennedy BK. Lamin A/C and emerin are critical for skeletal muscle satellite cell differentiation. Genes Dev 2006;20:486–500. https://doi.org/10.1101/gad.1364906.

[18] Constantinescu D, Gray HL, Sammak PJ, Schatten GP, Csoka AB. Lamin A/C Expression Is a Marker of Mouse and Human Embryonic Stem Cell Differentiation. Stem Cells 2006;24:177–85. https://doi.org/10.1634/stemcells.2004-0159.

[19] Earle AJ, Kirby TJ, Fedorchak GR, Isermann P, Patel J, Iruvanti S, et al. Mutant lamins cause nuclear envelope rupture and DNA damage in skeletal muscle cells. Nat Mater 2020;19:464–73. https://doi.org/10.1038/s41563-019-0563-5.

[20] Maynard S, Keijzers G, Akbari M, Ezra M Ben, Hall A, Morevati M, et al. Lamin A/C promotes DNA base excision repair. Nucleic Acids Res 2019;47:11709–28.

[21] Barateau A, Vadrot N, Vicart P, Ferreiro A, Mayer M, Héron D, et al. A Novel Lamin A Mutant Responsible for Congenital Muscular Dystrophy Causes Distinct Abnormalities of the Cell Nucleus. PLoS One 2017;12:e0169189. https://doi.org/doi.org/10.1371/journal.pone.0169189.

[22] Barateau A, Vadrot N, Agbulut O, Vicart P, Batonnet-Pichon S, Buendia B. Distinct Fiber Type Signature in Mouse Muscles Expressing a Mutant Lamin A Responsible for Congenital Muscular Dystrophy in a Patient. Cells 2017;6.

[23] Gómez-Domínguez D, Epifano C, Miguel F de, Castaño AG, Vilaplana-Martí B, Martín A, et al. Consequences of Lmna Exon 4 Mutations in Myoblast Function. Cells 2020;9:1286. https://doi.org/10.3390/cells9051286.

[24] Bertrand AT, Brull A, Azibani F, Benarroch L, Chikhaoui K, Stewart CL, et al. Lamin A/C Assembly Defects in LMNA -Congenital Muscular Dystrophy Is Responsible for the Increased Severity of the Disease Compared with Emery-Dreifuss Muscular Dystrophy. Cells 2020;9:844. https://doi.org/doi.org/10.3390/cells9040844.

[25] Owens DJ, Messéant J, Moog S, Viggars M, Ferry A, Mamchaoui K, et al. Lamin-Related Congenital Muscular Dystrophy Alters Mechanical Signaling and Skeletal Muscle Growth. Int J Mol Sci 2020;22:306. https://doi.org/10.3390/ijms22010306.

[26] Owens DJ, Fischer M, Jabre S, Moog S, Mamchaoui K, Butler-Browne G, et al. Lamin Mutations Cause Increased YAP Nuclear Entry in Muscle Stem Cells. Cells 2020;9.

[27] Storey EC, Fuller HR. Genotype-Phenotype Correlations in Human Diseases Caused by Mutations of LINC Complex-Associated Genes: A Systematic Review and Meta-Summary. Cells 2022;11:4065. https://doi.org/10.3390/CELLS11244065/S1.

[28] Lefebvre S, Bürglen L, Reboullet S, Clermont O, Burlet P, Viollet L, et al. Identification and characterization of a spinal muscular atrophy-determining gene. Cell 1995;80:155–65. https://doi.org/10.1016/0092-8674(95)90460-3.

[29] Ramdas S, Servais L. New treatments in spinal muscular atrophy: an overview of currently available data. Expert Opin Pharmacother 2020;21:307–15. https://doi.org/10.1080/14656566.2019.1704732.

[30] Bertrand AT, Ziaei S, Ehret C, Duchemin H, Mamchaoui K, Bigot A, et al. Cellular microenvironments reveal defective mechanosensing responses and elevated YAP signaling in LMNA-mutated muscle precursors. J Cell Sci 2014;127:2873–84. https://doi.org/doi.org/10.1242/jcs.144907.

[31] Mamchaoui K, Trollet C, Bigot A, Negroni E, Chaouch S, Wolff A, et al. Immortalized pathological human myoblasts: Towards a universal tool for the study of neuromuscular disorders. Skelet Muscle 2011. https://doi.org/10.1186/2044-5040-1-34.

[32] Laemmli UK. Cleavage of structural proteins during the assembly of the head of bacteriophage T4. Nature 1970;227:680–5. https://doi.org/10.1038/227680a0.

[33] Welinder C, Ekblad L. Coomassie staining as loading control in Western blot analysis. J Proteome Res 2011;10:1416–9. https://doi.org/10.1021/pr1011476.

[34] Towbin H, Staehelin T, Gordon J. Electrophoretic transfer of proteins from polyacrylamide gels to nitrocellulose sheets: Procedure and some applications. Proc Natl Acad Sci U S A 1979;76:4350–4. https://doi.org/10.1073/pnas.76.9.4350.

[35] Manilal S, Randles KN, Aunac C, Thi Man N, Morris GE. A lamin A/C beta-strand containing the site of lipodystrophy mutations is a major surface epitope for a new panel of monoclonal antibodies. Biochim Biophys Acta Gen Subj 2004;1671. https://doi.org/10.1016/j.bbagen.2004.01.008.

[36] Manilal S, Sewry CA, Pereboev A, Thi Man N, Gobbi P, Hawkes S, et al. Distribution of emerin and lamins in the heart and implications for Emery-Dreifuss muscular dystrophy. Hum Mol Genet 1999;8:353–9. https://doi.org/10.1093/HMG/8.2.353.

[37] Manilal S, Nguyen TM, Sewry CA, Morris GE. The Emery-Dreifuss muscular dystrophy protein, emerin, is a nuclear membrane protein. Hum Mol Genet 1996;5:801–8. https://doi.org/10.1093/hmg/5.6.801.

[38] Sheffield J. ImageJ, A Useful Tool for Biological Image Processing and Analysis. Microscopy and Microanalysis 2007;13:200–1. https://doi.org/10.1017/S1431927607076611.

[39] Reiter L, Rinner O, Picotti P, Hüttenhain R, Beck M, Brusniak M-Y, et al. mProphet : A general and flexible data model and algorithm for automated SRM data processing and statistical error estimation. Nat Methods 2011;8.

[40] Jen Y, Weintraub H, Benezra R. Overexpression of Id protein inhibits the muscle differentiation program: In vivo association of Id with E2A proteins. Genes Dev 1992;6:1466–79. https://doi.org/10.1101/gad.6.8.1466.

[41] Quinn LBS, Anderson BG, Drivdahl RH, Alvarez B, Argilés JM. Overexpression of interleukin-15 induces skeletal muscle hypertrophy in vitro: Implications for treatment of muscle wasting disorders. Exp Cell Res 2002;280:55–63. https://doi.org/10.1006/excr.2002.5624.

[42] Pieczenik SR, Neustadt J. Mitochondrial dysfunction and molecular pathways of disease. Exp Mol Pathol 2007;83:84–92. https://doi.org/10.1016/j.yexmp.2006.09.008.

[43] van Tienen FHJ, Lindsey PJ, Kamps MAF, Krapels IP, Ramaekers FCS, Brunner HG, et al. Assessment of fibroblast nuclear morphology aids interpretation of LMNA variants. European Journal of Human Genetics 2018;27:389–99. https://doi.org/10.1038/s41431-018-0294-0.

[44] Sinensky M, Fantle K, Trujillo M, McLain T, Kupfer A, Dalton M. The processing pathway of prelamin A. J Cell Sci 1994;107:61–7. https://doi.org/10.1242/JCS.107.1.61.

[45] Hill AV. Muscular activity and carbohydrate metabolism. Science (1979) 1924;60:505–14. https://doi.org/10.1126/SCIENCE.60.1562.505.

[46] Schneider SM, Sridhar V, Bettis AK, Heath-Barnett H, Balog-Alvarez CJ, Guo LJ, et al. Glucose Metabolism as a Pre-clinical Biomarker for the Golden Retriever Model of Duchenne Muscular Dystrophy. Mol Imaging Biol 2018;20:780–8. https://doi.org/10.1007/S11307-018-1174-2/FIGURES/5.

[47] Nghiem PP, Bello L, Stoughton WB, López SM, Vidal AH, Hernandez B V., et al. Changes in Muscle Metabolism are Associated with Phenotypic Variability in Golden Retriever Muscular Dystrophy. Yale J Biol Med 2017;90:351.

[48] Timpani CA, Hayes A, Rybalka E. Revisiting the dystrophin-ATP connection: How half a century of research still implicates mitochondrial dysfunction in Duchenne Muscular Dystrophy aetiology. Med Hypotheses 2015;85:1021–33. https://doi.org/10.1016/J.MEHY.2015.08.015.

[49] Onopiuk M, Brutkowski W, Wierzbicka K, Wojciechowska S, Szczepanowska J, Fronk J, et al. Mutation in dystrophin-encoding gene affects energy metabolism in mouse myoblasts. Biochem Biophys Res Commun 2009;386:463–6. https://doi.org/10.1016/J.BBRC.2009.06.053.

[50] Sharma U, Atri S, Sharma MC, Sarkar C, Jagannathan NR. Skeletal muscle metabolism in Duchenne muscular dystrophy (DMD): an in-vitro proton NMR spectroscopy study. Magn Reson Imaging 2003;21:145–53. https://doi.org/10.1016/S0730-725X(02)00646-X.

[51] Chi MMY, Hintz CS, McKee D, Felder S, Grant N, Kaiser KK, et al. Effect of Duchenne muscular dystrophy on enzymes of energy metabolism in individual muscle fibers. Metabolism 1987;36:761–7. https://doi.org/10.1016/0026-0495(87)90113-2.

[52] Martin PT, Freeze HH. Glycobiology of neuromuscular disorders. Glycobiology 2003;13:67R-75R. https://doi.org/10.1093/GLYCOB/CWG077.

[53] Méjat A, Decostre V, Li J, Renou L, Kesari A, Hantaï D, et al. Lamin A/C-mediated neuromuscular junction defects in Emery-Dreifuss muscular dystrophy. J Cell Biol 2009;184:31–44. https://doi.org/10.1083/jcb.200811035.

[54] Sang TK, Li C, Liu W, Rodriguez A, Abrams JM, Zipursky SL, et al. Inactivation of Drosophila Apaf-1 related killer suppresses formation of polyglutamine aggregates and blocks polyglutamine pathogenesis. Hum Mol Genet 2005;14:357–72. https://doi.org/10.1093/hmg/ddi032.

[55] Hickey MA, Chesselet MF. Apoptosis in Huntington's disease. Prog Neuropsychopharmacol Biol Psychiatry 2003;27:255-. https://doi.org/10.1016/S0278-5846(03)00021-6.

[56] Yang D, Wang CE, Zhao B, Li W, Ouyang Z, Liu Z, et al. Expression of Huntington's disease protein results in apoptotic neurons in the brains of cloned transgenic pigs. Hum Mol Genet 2010;19:3983–94. https://doi.org/10.1093/hmg/ddq313.

[57] Vis JC, Schipper E, de Boer-van H, Verbeek MM, de Waal RMW, Wesseling P, et al. Expression pattern of apoptosis-related markers in Huntington's disease. Acta Neuropathol 2005;109:321–8. https://doi.org/10.1007/s00401-004-0957-5.

[58] Degterev A, Hitomi J, Germscheid M, Ch'en IL, Korkina O, Teng X, et al. Identification of RIP1 kinase as a specific cellular target of necrostatins. Nat Chem Biol 2008;4:313–21. https://doi.org/10.1038/nchembio.83.

[59] Smith CCT, Davidson SM, Lim SY, Simpkin JC, Hothersall JS, Yellon DM. Necrostatin: A potentially novel cardioprotective agent? Cardiovasc Drugs Ther 2007;21:227–33. https://doi.org/10.1007/s10557-007-6035-1.

[60] Lin J, Li H, Yang M, Ren J, Huang Z, Han F, et al. A Role of RIP3-Mediated Macrophage Necrosis in Atherosclerosis Development. Cell Rep 2013;3:200–10. https://doi.org/10.1016/j.celrep.2012.12.012.

[61] Linkermann A, Bräsen JH, Himmerkus N, Liu S, Huber TB, Kunzendorf U, et al. Rip1 (Receptor-interacting protein kinase 1) mediates necroptosis and contributes to renal ischemia/reperfusion injury. Kidney Int 2012;81:751–61. https://doi.org/10.1038/ki.2011.450.

[62] Oerlemans MIFJ, Liu J, Arslan F, Den Ouden K, Van Middelaar BJ, Doevendans PA, et al. Inhibition of RIP1-dependent necrosis prevents adverse cardiac remodeling after myocardial ischemia-reperfusion in vivo. Basic Res Cardiol 2012;107:207. https://doi.org/10.1007/s00395-012-0270-8.

[63] Zhang DW, Shao J, Lin J, Zhang N, Lu BJ, Lin SC, et al. RIP3, an energy metabolism regulator that switches TNF-induced cell death from apoptosis to necrosis. Science (1979) 2009;325:332–6. https://doi.org/10.1126/science.1172308.

[64] Wu J, Huang Z, Ren J, Zhang Z, He P, Li Y, et al. Mlkl knockout mice demonstrate the indispensable role of Mlkl in necroptosis. Cell Res 2013;23:994–1006. https://doi.org/10.1038/cr.2013.91.

[65] Welz PS, Wullaert A, Vlantis K, Kondylis V, Fernández-Majada V, Ermolaeva M, et al. FADD prevents RIP3-mediated epithelial cell necrosis and chronic intestinal inflammation. Nature 2011;477:330–4. https://doi.org/10.1038/nature10273.

[66] Ito Y, Ofengeim D, Najafov A, Das S, Saberi S, Li Y, et al. RIPK1 mediates axonal degeneration by promoting inflammation and necroptosis in ALS. Science (1979) 2016;353:603–8. https://doi.org/10.1126/science.aaf6803.

[67] Zhang S, Su Y, Ying Z, Guo D, Pan C, Guo J, et al. RIP1 kinase inhibitor halts the progression of an immune-induced demyelination disease at the stage of monocyte elevation. Proc Natl Acad Sci U S A 2019;116:5675–80. https://doi.org/10.1073/pnas.1819917116.

[68] Chehade L, Deguise MO, De Repentigny Y, Yaworski R, Beauvais A, Gagnon S, et al. Suppression of the necroptotic cell death pathways improves survival in Smn2B/− mice. Front Cell Neurosci 2022;16:408. https://doi.org/doi.org/10.3389/fncel.2022.972029.

[69] Bencze M, Meng J, Pini V, Conti F, Muntoni F, Morgan J. Necroptosis, a programmed form of necrosis, participates in muscle degeneration in Duchenne muscular dystrophy. Neuromuscular Disorders 2017;27:S98. https://doi.org/10.1016/j.nmd.2017.06.029.

[70] Blau HM, Webster C, Pavlath GK. Defective myoblasts identified in Duchenne muscular dystrophy. Proceedings of the National Academy of Sciences 1983;80:4856–60. https://doi.org/10.1073/PNAS.80.15.4856.

[71] Shafey D, Côté PD, Kothary R. Hypomorphic Smn knockdown C2C12 myoblasts reveal intrinsic defects in myoblast fusion and myotube morphology. Exp Cell Res 2005;311:49–61. https://doi.org/10.1016/J.YEXCR.2005.08.019.

[72] Moiseeva O, Bourdeau V, Vernier M, Dabauvalle MC, Ferbeyre G. Retinoblastoma-independent regulation of cell proliferation and senescence by the p53–p21 axis in lamin A/C-depleted cells. Aging Cell 2011;10:789–97. https://doi.org/10.1111/J.1474-9726.2011.00719.X.

[73] Kong L, Schäfer G, Bu H, Zhang Y, Zhang Y, Klocker H. Lamin A/C protein is overexpressed in tissue-invading prostate cancer and promotes prostate cancer cell growth, migration and invasion through the PI3K/AKT/PTEN pathway. Carcinogenesis 2012;33:751–9. https://doi.org/10.1093/CARCIN/BGS022.

[74] Harada T, Swift J, Irianto J, Shin JW, Spinler KR, Athirasala A, et al. Nuclear lamin stiffness is a barrier to 3D migration, but softness can limit survival. Journal of Cell Biology 2014;204:669–82. https://doi.org/10.1083/JCB.201308029.

[75] Kandert S, Wehnert M, Müller CR, Buendia B, Dabauvalle M-C. Impaired nuclear functions lead to increased senescence and inefficient differentiation in human myoblasts with a dominant p.R545C mutation in the LMNA gene. Eur J Cell Biol 2009;88:593–608.

[76] Park Y-E, Hayashi YK, Goto K, Komaki H, Hayashi Y, Inuzuka T, et al. Nuclear changes in skeletal muscle extend to satellite cells in autosomal dominant Emery-Dreifuss muscular dystrophy/limb-girdle muscular dystrophy 1B. Neuromuscul Disord 2009;19:29–36. https://doi.org/10.1016/j.nmd.2008.09.018.

[77] Muchir A, Medioni J, Laluc M, Massart C, Arimura T, van der Kooi AJ, et al. Nuclear envelope alterations in fibroblasts from patients with muscular dystrophy, cardiomyopathy, and partial lipodystrophy carrying lamin A/C gene mutations. Muscle Nerve 2004;30:444–50. https://doi.org/10.1002/mus.20122.

[78] Favreau C, Dubosclard E, Östlund C, Vigouroux C, Capeau J, Wehnert M, et al. Expression of lamin A mutated in the carboxyl-terminal tail generates an aberrant nuclear phenotype similar to that observed in cells from patients with Dunnigan-type partial lipodystrophy and Emery-Dreifuss muscular dystrophy. Exp Cell Res 2003;282:14–23. https://doi.org/10.1006/EXCR.2002.5669.

[79] Muchir A, van Engelen BG, Lammens M, Mislow JM, McNally E, Schwartz K, et al. Nuclear envelope alterations in fibroblasts from LGMD1B patients carrying nonsense Y259X

heterozygous or homozygous mutation in lamin A/C gene. Exp Cell Res 2003;291:352–62. https://doi.org/10.1016/j.yexcr.2003.07.002.

[80] Vigouroux C, Auclair M, Dubosclard E, Pouchelet M, Capeau J, Courvalin JC, et al. Nuclear envelope disorganization in fibroblasts from lipodystrophic patients with heterozygous R482Q/W mutations in the lamin A/C gene. J Cell Sci 2001;114:4459–68. https://doi.org/10.1242/jcs.114.24.4459.

[81] Steele-Stallard HB, Pinton L, Sarcar S, Ozdemir T, Maffioletti SM, Zammit PS, et al. Modeling Skeletal Muscle Laminopathies Using Human Induced Pluripotent Stem Cells Carrying Pathogenic LMNA Mutations. Front Physiol 2018;9:1332.

[82] Davidson PM, Lammerding J. Broken nuclei – lamins, nuclear mechanics, and disease. Trends Cell Biol 2014;24:247–56. https://doi.org/10.1016/j.tcb.2013.11.004.

[83] Verstraeten VLRM, Peckham LA, Olive M, Capell BC, Collins FS, Nabel EG, et al. Protein farnesylation inhibitors cause donut-shaped cell nuclei attributable to a centrosome separation defect. Proc Natl Acad Sci U S A 2011;108. https://doi.org/10.1073/pnas.1019532108.

[84] Bertrand AT, Brull A, Azibani F, Benarroch L, Chikhaoui K, Stewart CL, et al. Lamin A/C Assembly Defects in LMNA -Congenital Muscular Dystrophy Is Responsible for the Increased Severity of the Disease Compared with Emery-Dreifuss Muscular Dystrophy. Cells 2020;9.

[85] Meinke P, Mattioli E, Haque F, Antoku S, Columbaro M, Straatman KR, et al. Muscular Dystrophy-Associated SUN1 and SUN2 Variants Disrupt Nuclear-Cytoskeletal Connections and Myonuclear Organization. PLoS Genet 2014;10:e1004605. https://doi.org/10.1371/journal.pgen.1004605.

[86] Gómez-Domínguez D, Epifano C, Miguel F de, Castaño AG, Vilaplana-Martí B, Martín A, et al. Consequences of Lmna Exon 4 Mutations in Myoblast Function. Cells 2020;9.

[87] Vaughan OA, Alvarez-Reyes M, Bridger JM, Broers JLV, Ramaekers FCS, Wehnert M, et al. Both emerin and lamin C depend on lamin A for localization at the nuclear envelope. J Cell Sci 2001;114:2577–90. https://doi.org/10.1242/jcs.114.14.2577.

[88] Hegde RS, Zavodszky E. Recognition and Degradation of Mislocalized Proteins in Health and Disease. Cold Spring Harb Perspect Biol 2019;11:a033902. https://doi.org/10.1101/CSHPERSPECT.A033902.

[89] Fairley EA, Kendrick-Jones J, Ellis JA. The Emery-Dreifuss muscular dystrophy phenotype arises from aberrant targeting and binding of emerin at the inner nuclear membrane. J Cell Sci 1999;112 (Pt 1:2571–82.

[90] Fairley EAL, Riddell A, Ellis JA, Kendrick-Jones J. The cell cycle dependent mislocalisation of emerin may contribute to the Emery-Dreifuss muscular dystrophy phenotype. J Cell Sci 2002;115:341–54.

[91] Bertrand AT, Renou L, Papadopoulos A, Beuvin M, Lacène E, Massart C, et al. DelK32-lamin A/C has abnormal location and induces incomplete tissue maturation and severe metabolic defects leading to premature death. Hum Mol Genet 2012;21:1037–48. https://doi.org/10.1093/HMG/DDR534.

[92] Torvaldson E, Kochin V, Eriksson JE. Phosphorylation of lamins determine their structural properties and signaling functions. Nucleus 2015;6:166–71.

[93] Sullivan T, Escalante-Alcalde D, Bhatt H, Anver M, Bhat N, Nagashima K, et al. Loss of A-type lamin expression compromises nuclear envelope integrity leading to muscular dystrophy. Journal of Cell Biology 1999;147:913–9. https://doi.org/10.1083/jcb.147.5.913.

[94] Thanisch K, Song C, Engelkamp D, Koch J, Wang A, Hallberg E, et al. Nuclear envelope localization of LEMD2 is developmentally dynamic and lamin A/C dependent yet insufficient for heterochromatin tethering. Differentiation 2017;94. https://doi.org/10.1016/j.diff.2016.12.002.

[95] Malik P, Korfali N, Srsen V, Lazou V, Batrakou DG, Zuleger N, et al. Cell-specific and lamin-dependent targeting of novel transmembrane proteins in the nuclear envelope. Cellular and Molecular Life Sciences 2010;67. https://doi.org/10.1007/s00018-010-0257-2.

[96] Libotte T, Zaim H, Abraham S, Padmakumar VC, Schneider M, Lu W, et al. Lamin A/C–dependent Localization of Nesprin-2, a Giant Scaffolder at the Nuclear Envelope. Https://DoiOrg/101091/MbcE04-11-1009 2005;16:3411–24. https://doi.org/10.1091/MBC.E04-11-1009.

[97] Crisp M, Liu Q, Roux K, Rattner JB, Shanahan C, Burke B, et al. Coupling of the nucleus and cytoplasm. J Cell Biol 2006;172:41–53. https://doi.org/10.1083/jcb.200509124.

[98] Ungricht R, Kutay U. Establishment of NE asymmetry-targeting of membrane proteins to the inner nuclear membrane. Curr Opin Cell Biol 2015;34. https://doi.org/10.1016/j.ceb.2015.04.005.

[99] Andrés V, González JM. Role of A-type lamins in signaling, transcription, and chromatin organization. J Cell Biol 2009;187:945–57. https://doi.org/10.1083/jcb.200904124.

[100] Parnaik VK. Role of Nuclear Lamins in Nuclear Organization, Cellular Signaling, and Inherited Diseases. Int Rev Cell Mol Biol 2008;266. https://doi.org/10.1016/S1937-6448(07)66004-3.

[101] Betts MJ, Russell RB. Amino Acid Properties and Consequences of Substitutions. In: Barnes MR, Gray IC, editors. Bioinformatics for Geneticists, John Wiley & Sons, Ltd; 2003, p. 289–316. https://doi.org/10.1002/0470867302.CH14.

[102] Azibani F, Brull A, Arandel L, Beuvin M, Nelson I, Jollet A, et al. Gene Therapy via Trans-Splicing for LMNA-Related Congenital Muscular Dystrophy. Mol Ther Nucleic Acids 2018;10:376–86. https://doi.org/10.1016/J.OMTN.2017.12.012.

~~[1] Avila GM, González AP, Abad A, Fournier BG, León SR, Corral JAM, et al. Is the Next Generation Sequencing the Essential Tool for the Early Diagnostic Approach in Congenital Muscular Dystrophy? New Mutation in the Gene LMNA Associated with Serious Phenotype. Neurol India 2021;69:1835–7. https://doi.org/10.4103/0028-3886.333448.~~

~~[2] Hattori A, Komaki H, Kawatani M, Sakuma H, Saito Y, Nakagawa E, et al. A novel mutation in the LMNA gene causes congenital muscular dystrophy with dropped head and brain involvement. Neuromuscul Disord 2012;22:149–51.~~

~~[3] Quijano-Roy S, Mbieleu B, Bönnemann CG, Jeannet P-Y, Colomer J, Clarke NF, et al. De novo *LMNA* mutations cause a new form of congenital muscular dystrophy. Ann Neurol 2008;64:177–86. https://doi.org/10.1002/ana.21417.~~

[4] Bonati U, Bechtel N, Heinimann K, Rutz E, Schneider J, Frank S, et al. Congenital muscular dystrophy with dropped head phenotype and cognitive impairment due to a novel mutation in the LMNA gene. Neuromuscular Disorders 2014;24:529–32. https://doi.org/10.1016/j.nmd.2014.02.004.

[5] Pasqualin LMA, Reed UC, Costa TVMM, Quedas E, Albuquerque MA V, Resende MBD, et al. Congenital muscular dystrophy with dropped head linked to the LMNA gene in a Brazilian cohort. Pediatr Neurol 2014;50:400–6.

[6] Karaoglu P, Quizon N, Pergande M, Wang H, Polat AI, Ersen A, et al. Dropped head congenital muscular dystrophy caused by de novo mutations in LMNA. Brain Dev 2017;39:361–4.

[7] Taddei A, Hediger F, Neumann FR, Gasser SM. The function of nuclear architecture: a genetic approach. Annu Rev Genet 2004;38:305–45. https://doi.org/10.1146/annurev.genet.37.110801.142705.

[8] Bridger JM, Foeger N, Kill IR, Herrmann H. The nuclear lamina. Both a structural framework and a platform for genome organization. FEBS J 2007;274:1354–61.

[9] Aebi U, Cohn J, Buhle L, Gerace L. The nuclear lamina is a meshwork of intermediate-type filaments. Nature 1986 323:6088 1986;323:560–4. https://doi.org/10.1038/323560a0.

[10] Crisp M, Liu Q, Roux K, Rattner JB, Shanahan C, Burke B, et al. Coupling of the nucleus and cytoplasm: Role of the LINC complex. J Cell Biol 2006;172:41–53. https://doi.org/10.1083/jcb.200509124.

[11] Haque F, Mazzeo D, Patel JT, Smallwood DT, Ellis JA, Shanahan CM, et al. Mammalian SUN protein interaction networks at the inner nuclear membrane and their role in laminopathy disease processes. Journal of Biological Chemistry 2010;285:3487–98. https://doi.org/10.1074/jbc.M109.071910.

[12] Clements L, Manilal S, Love DR, Morris GE. Direct interaction between emerin and lamin A. Biochem Biophys Res Commun 2000;267:709–14. https://doi.org/10.1006/bbrc.1999.2023.

[13] Gonzàlez JM, Navarro-Puche A, Casar B, Crespo P, Andrès V. Fast regulation of AP-1 activity through interaction of lamin A/C, ERK1/2, and c-Fos at the nuclear envelope. Journal of Cell Biology 2008;183:653–66. https://doi.org/10.1083/JCB.200805049.

[14] Moiseeva O, Bourdeau V, Vernier M, Dabauvalle MC, Ferbeyre G. Retinoblastoma-independent regulation of cell proliferation and senescence by the p53–p21 axis in lamin A/C-depleted cells. Aging Cell 2011;10:789–97. https://doi.org/10.1111/J.1474-9726.2011.00719.X.

[15] Swift J, Ivanovska IL, Buxboim A, Harada T, Dingal PCDP, Pinter J, et al. Nuclear lamin-A scales with tissue stiffness and enhances matrix-directed differentiation. Science (1979) 2013;341:1240104. https://doi.org/10.1126/science.1240104.

[16] Frock RL, Kudlow BA, Evans AM, Jameson SA, Hauschka SD, Kennedy BK. Lamin A/C and emerin are critical for skeletal muscle satellite cell differentiation. Genes Dev 2006;20:486–500. https://doi.org/10.1101/gad.1364906.

[17] Constantinescu D, Gray HL, Sammak PJ, Schatten GP, Csoka AB. Lamin A/C Expression Is a Marker of Mouse and Human Embryonic Stem Cell Differentiation. Stem Cells 2006;24:177–85. https://doi.org/10.1634/stemcells.2004-0159.

[18] Earle AJ, Kirby TJ, Fedorchak GR, Isermann P, Patel J, Iruvanti S, et al. Mutant lamins cause nuclear envelope rupture and DNA damage in skeletal muscle cells. Nat Mater 2020;19:464–73. https://doi.org/10.1038/s41563-019-0563-5.

[19] Maynard S, Keijzers G, Akbari M, Ezra M Ben, Hall A, Morevati M, et al. Lamin A/C promotes DNA base excision repair. Nucleic Acids Res 2019;47:11709–28.

[20] Barateau A, Vadrot N, Vicart P, Ferreiro A, Mayer M, Héron D, et al. A Novel Lamin A Mutant Responsible for Congenital Muscular Dystrophy Causes Distinct Abnormalities of the Cell Nucleus. PLoS One 2017;12:e0169189. https://doi.org/doi.org/10.1371/journal.pone.0169189.

[21] Barateau A, Vadrot N, Agbulut O, Vicart P, Batonnet-Pichon S, Buendia B. Distinct Fiber Type Signature in Mouse Muscles Expressing a Mutant Lamin A Responsible for Congenital Muscular Dystrophy in a Patient. Cells 2017;6.

[22] Gómez-Domínguez D, Epifano C, Miguel F de, Castaño AG, Vilaplana-Martí B, Martín A, et al. Consequences of Lmna Exon 4 Mutations in Myoblast Function. Cells 2020;9:1286. https://doi.org/10.3390/cells9051286.

[23] Bertrand AT, Brull A, Azibani F, Benarroch L, Chikhaoui K, Stewart CL, et al. Lamin A/C Assembly Defects in LMNA -Congenital Muscular Dystrophy Is Responsible for the Increased Severity of the Disease Compared with Emery-Dreifuss Muscular Dystrophy. Cells 2020;9:844. https://doi.org/doi.org/10.3390/cells9040844.

[24] Owens DJ, Messéant J, Moog S, Viggars M, Ferry A, Mamchaoui K, et al. Lamin-Related Congenital Muscular Dystrophy Alters Mechanical Signaling and Skeletal Muscle Growth. Int J Mol Sci 2020;22:306. https://doi.org/10.3390/ijms22010306.

[25] Owens DJ, Fischer M, Jabre S, Moog S, Mamchaoui K, Butler-Browne G, et al. Lamin Mutations Cause Increased YAP Nuclear Entry in Muscle Stem Cells. Cells 2020;9.

[26] Storey EC, Fuller HR. Genotype-Phenotype Correlations in Human Diseases Caused by Mutations of LINC Complex-Associated Genes: A Systematic Review and Meta-Summary. Cells 2022;11:4065. https://doi.org/10.3390/CELLS11244065/S1.

[27] Lefebvre S, Bürglen L, Reboullet S, Clermont O, Burlet P, Viollet L, et al. Identification and characterization of a spinal muscular atrophy-determining gene. Cell 1995;80:155–65. https://doi.org/10.1016/0092-8674(95)90460-3.

[28] Ramdas S, Servais L. New treatments in spinal muscular atrophy: an overview of currently available data. Expert Opin Pharmacother 2020;21:307–15. https://doi.org/10.1080/14656566.2019.1704732.

[29] Bertrand AT, Ziaei S, Ehret C, Duchemin H, Mamchaoui K, Bigot A, et al. Cellular microenvironments reveal defective mechanosensing responses and elevated YAP signaling in LMNA-mutated muscle precursors. J Cell Sci 2014;127:2873–84. https://doi.org/doi.org/10.1242/jcs.144907.

[30] Mamchaoui K, Trollet C, Bigot A, Negroni E, Chaouch S, Wolff A, et al. Immortalized pathological human myoblasts: Towards a universal tool for the study of neuromuscular disorders. Skelet Muscle 2011. https://doi.org/10.1186/2044-5040-1-34.

[31] Laemmli UK. Cleavage of structural proteins during the assembly of the head of bacteriophage T4. Nature 1970;227:680–5. https://doi.org/10.1038/227680a0.

[32] Welinder C, Ekblad L. Coomassie staining as loading control in Western blot analysis. J Proteome Res 2011;10:1416–9. https://doi.org/10.1021/pr1011476.

[33] Towbin H, Staehelin T, Gordon J. Electrophoretic transfer of proteins from polyacrylamide gels to nitrocellulose sheets: Procedure and some applications. Proc Natl Acad Sci U S A 1979;76:4350–4. https://doi.org/10.1073/pnas.76.9.4350.

[34] Manilal S, Randles KN, Aunac C, Thi Man N, Morris GE. A lamin A/C beta-strand containing the site of lipodystrophy mutations is a major surface epitope for a new panel of monoclonal antibodies. Biochim Biophys Acta Gen Subj 2004;1671. https://doi.org/10.1016/j.bbagen.2004.01.008.

[35] Manilal S, Sewry CA, Pereboev A, Thi Man N, Gobbi P, Hawkes S, et al. Distribution of emerin and lamins in the heart and implications for Emery-Dreifuss muscular dystrophy. Hum Mol Genet 1999;8:353–9. https://doi.org/10.1093/HMG/8.2.353.

[36] Manilal S, Nguyen TM, Sewry CA, Morris GE. The Emery-Dreifuss muscular dystrophy protein, emerin, is a nuclear membrane protein. Hum Mol Genet 1996;5:801–8. https://doi.org/10.1093/hmg/5.6.801.

[37] Sheffield J. ImageJ, A Useful Tool for Biological Image Processing and Analysis. Microscopy and Microanalysis 2007;13:200–1. https://doi.org/10.1017/S1431927607076611.

[38] Reiter L, Rinner O, Picotti P, Hüttenhain R, Beck M, Brusniak M-Y, et al. mProphet : A general and flexible data model and algorithm for automated SRM data processing and statistical error estimation. Nat Methods 2011;8.

[39] Jen Y, Weintraub H, Benezra R. Overexpression of Id protein inhibits the muscle differentiation program: In vivo association of Id with E2A proteins. Genes Dev 1992;6:1466–79. https://doi.org/10.1101/gad.6.8.1466.

[40] Quinn LBS, Anderson BG, Drivdahl RH, Alvarez B, Argilés JM. Overexpression of interleukin-15 induces skeletal muscle hypertrophy in vitro: Implications for treatment of muscle wasting disorders. Exp Cell Res 2002;280:55–63. https://doi.org/10.1006/excr.2002.5624.

[41] Pieczenik SR, Neustadt J. Mitochondrial dysfunction and molecular pathways of disease. Exp Mol Pathol 2007;83:84–92. https://doi.org/10.1016/j.yexmp.2006.09.008.

[42] Hill AV. Muscular activity and carbohydrate metabolism. Science (1979) 1924;60:505–14. https://doi.org/10.1126/SCIENCE.60.1562.505.

[43] Schneider SM, Sridhar V, Bettis AK, Heath-Barnett H, Balog-Alvarez CJ, Guo LJ, et al. Glucose Metabolism as a Pre-clinical Biomarker for the Golden Retriever Model of Duchenne Muscular Dystrophy. Mol Imaging Biol 2018;20:780–8. https://doi.org/10.1007/S11307-018-1174-2/FIGURES/5.

[44] Nghiem PP, Bello L, Stoughton WB, López SM, Vidal AH, Hernandez B V., et al. Changes in Muscle Metabolism are Associated with Phenotypic Variability in Golden Retriever Muscular Dystrophy. Yale J Biol Med 2017;90:351.

[45] Timpani CA, Hayes A, Rybalka E. Revisiting the dystrophin-ATP connection: How half a century of research still implicates mitochondrial dysfunction in Duchenne Muscular Dystrophy aetiology. Med Hypotheses 2015;85:1021–33. https://doi.org/10.1016/J.MEHY.2015.08.015.

[46] Onopiuk M, Brutkowski W, Wierzbicka K, Wojciechowska S, Szczepanowska J, Fronk J, et al. Mutation in dystrophin-encoding gene affects energy metabolism in mouse myoblasts. Biochem Biophys Res Commun 2009;386:463–6. https://doi.org/10.1016/J.BBRC.2009.06.053.

[47] Sharma U, Atri S, Sharma MC, Sarkar C, Jagannathan NR. Skeletal muscle metabolism in Duchenne muscular dystrophy (DMD): an in-vitro proton NMR spectroscopy study. Magn Reson Imaging 2003;21:145–53. https://doi.org/10.1016/S0730-725X(02)00646-X.

[48] Chi MMY, Hintz CS, McKee D, Felder S, Grant N, Kaiser KK, et al. Effect of Duchenne muscular dystrophy on enzymes of energy metabolism in individual muscle fibers. Metabolism 1987;36:761–7. https://doi.org/10.1016/0026-0495(87)90113-2.

[49] Martin PT, Freeze HH. Glycobiology of neuromuscular disorders. Glycobiology 2003;13:67R-75R. https://doi.org/10.1093/GLYCOB/CWG077.

[50] Méjat A, Decostre V, Li J, Renou L, Kesari A, Hantaï D, et al. Lamin A/C-mediated neuromuscular junction defects in Emery-Dreifuss muscular dystrophy. J Cell Biol 2009;184:31–44. https://doi.org/10.1083/jcb.200811035.

[51] Sang TK, Li C, Liu W, Rodriguez A, Abrams JM, Zipursky SL, et al. Inactivation of Drosophila Apaf-1 related killer suppresses formation of polyglutamine aggregates and blocks polyglutamine pathogenesis. Hum Mol Genet 2005;14:357–72. https://doi.org/10.1093/hmg/ddi032.

[52] Hickey MA, Chesselet MF. Apoptosis in Huntington's disease. Prog Neuropsychopharmacol Biol Psychiatry 2003;27:255-. https://doi.org/10.1016/S0278-5846(03)00021-6.

[53] Yang D, Wang CE, Zhao B, Li W, Ouyang Z, Liu Z, et al. Expression of Huntington's disease protein results in apoptotic neurons in the brains of cloned transgenic pigs. Hum Mol Genet 2010;19:3983–94. https://doi.org/10.1093/hmg/ddq313.

[54] Vis JC, Schipper E, de Boer-van H, Verbeek MM, de Waal RMW, Wesseling P, et al. Expression pattern of apoptosis-related markers in Huntington's disease. Acta Neuropathol 2005;109:321–8. https://doi.org/10.1007/s00401-004-0957-5.

[55] Degterev A, Hitomi J, Germscheid M, Ch'en IL, Korkina O, Teng X, et al. Identification of RIP1 kinase as a specific cellular target of necrostatins. Nat Chem Biol 2008;4:313–21. https://doi.org/10.1038/nchembio.83.

[56] Smith CCT, Davidson SM, Lim SY, Simpkin JC, Hothersall JS, Yellon DM. Necrostatin: A potentially novel cardioprotective agent? Cardiovasc Drugs Ther 2007;21:227–33. https://doi.org/10.1007/s10557-007-6035-1.

[57] Lin J, Li H, Yang M, Ren J, Huang Z, Han F, et al. A Role of RIP3-Mediated Macrophage Necrosis in Atherosclerosis Development. Cell Rep 2013;3:200–10. https://doi.org/10.1016/j.celrep.2012.12.012.

[58] Linkermann A, Bräsen JH, Himmerkus N, Liu S, Huber TB, Kunzendorf U, et al. Rip1 (Receptor-interacting protein kinase 1) mediates necroptosis and contributes to renal

ischemia/reperfusion injury. Kidney Int 2012;81:751–61. https://doi.org/10.1038/ki.2011.450.

[59] Oerlemans MIFJ, Liu J, Arslan F, Den Ouden K, Van Middelaar BJ, Doevendans PA, et al. Inhibition of RIP1-dependent necrosis prevents adverse cardiac remodeling after myocardial ischemia-reperfusion in vivo. Basic Res Cardiol 2012;107:207. https://doi.org/10.1007/s00395-012-0270-8.

[60] Zhang DW, Shao J, Lin J, Zhang N, Lu BJ, Lin SC, et al. RIP3, an energy metabolism regulator that switches TNF-induced cell death from apoptosis to necrosis. Science (1979) 2009;325:332–6. https://doi.org/10.1126/science.1172308.

[61] Wu J, Huang Z, Ren J, Zhang Z, He P, Li Y, et al. Mlkl knockout mice demonstrate the indispensable role of Mlkl in necroptosis. Cell Res 2013;23:994–1006. https://doi.org/10.1038/cr.2013.91.

[62] Welz PS, Wullaert A, Vlantis K, Kondylis V, Fernández-Majada V, Ermolaeva M, et al. FADD prevents RIP3-mediated epithelial cell necrosis and chronic intestinal inflammation. Nature 2011;477:330–4. https://doi.org/10.1038/nature10273.

[63] Ito Y, Ofengeim D, Najafov A, Das S, Saberi S, Li Y, et al. RIPK1 mediates axonal degeneration by promoting inflammation and necroptosis in ALS. Science (1979) 2016;353:603–8. https://doi.org/10.1126/science.aaf6803.

[64] Zhang S, Su Y, Ying Z, Guo D, Pan C, Guo J, et al. RIP1 kinase inhibitor halts the progression of an immune-induced demyelination disease at the stage of monocyte elevation. Proc Natl Acad Sci U S A 2019;116:5675–80. https://doi.org/10.1073/pnas.1819917116.

[65] Chehade L, Deguise MO, De Repentigny Y, Yaworski R, Beauvais A, Gagnon S, et al. Suppression of the necroptotic cell death pathways improves survival in Smn2B/− mice. Front Cell Neurosci 2022;16:408. https://doi.org/doi.org/10.3389/fncel.2022.972029.

[66] Bencze M, Meng J, Pini V, Conti F, Muntoni F, Morgan J. Necroptosis, a programmed form of necrosis, participates in muscle degeneration in Duchenne muscular dystrophy. Neuromuscular Disorders 2017;27:S98. https://doi.org/10.1016/j.nmd.2017.06.029.

[67] Blau HM, Webster C, Pavlath GK. Defective myoblasts identified in Duchenne muscular dystrophy. Proceedings of the National Academy of Sciences 1983;80:4856–60. https://doi.org/10.1073/PNAS.80.15.4856.

[68] Shafey D, Côté PD, Kothary R. Hypomorphic Smn knockdown C2C12 myoblasts reveal intrinsic defects in myoblast fusion and myotube morphology. Exp Cell Res 2005;311:49–61. https://doi.org/10.1016/J.YEXCR.2005.08.019.

[69] Moiseeva O, Bourdeau V, Vernier M, Dabauvalle MC, Ferbeyre G. Retinoblastoma-independent regulation of cell proliferation and senescence by the p53–p21 axis in lamin A/C-depleted cells. Aging Cell 2011;10:789–97. https://doi.org/10.1111/J.1474-9726.2011.00719.X.

[70] Kong L, Schäfer G, Bu H, Zhang Y, Zhang Y, Klocker H. Lamin A/C protein is overexpressed in tissue-invading prostate cancer and promotes prostate cancer cell growth, migration and invasion through the PI3K/AKT/PTEN pathway. Carcinogenesis 2012;33:751–9. https://doi.org/10.1093/CARCIN/BGS022.

[71] Harada T, Swift J, Irianto J, Shin JW, Spinler KR, Athirasala A, et al. Nuclear lamin stiffness is a barrier to 3D migration, but softness can limit survival. Journal of Cell Biology 2014;204:669–82. https://doi.org/10.1083/JCB.201308029.

[72] Kandert S, Wehnert M, Müller CR, Buendia B, Dabauvalle M-C. Impaired nuclear functions lead to increased senescence and inefficient differentiation in human myoblasts with a dominant p.R545C mutation in the LMNA gene. Eur J Cell Biol 2009;88:593–608.

[73] Park Y-E, Hayashi YK, Goto K, Komaki H, Hayashi Y, Inuzuka T, et al. Nuclear changes in skeletal muscle extend to satellite cells in autosomal dominant Emery-Dreifuss muscular dystrophy/limb-girdle muscular dystrophy 1B. Neuromuscul Disord 2009;19:29–36. https://doi.org/10.1016/j.nmd.2008.09.018.

[74] Muchir A, Medioni J, Laluc M, Massart C, Arimura T, van der Kooi AJ, et al. Nuclear envelope alterations in fibroblasts from patients with muscular dystrophy, cardiomyopathy, and partial lipodystrophy carrying lamin A/C gene mutations. Muscle Nerve 2004;30:444–50. https://doi.org/10.1002/mus.20122.

[75] Favreau C, Dubosclard E, Östlund C, Vigouroux C, Capeau J, Wehnert M, et al. Expression of lamin A mutated in the carboxyl-terminal tail generates an aberrant nuclear phenotype similar to that observed in cells from patients with Dunnigan-type partial lipodystrophy and Emery-Dreifuss muscular dystrophy. Exp Cell Res 2003;282:14–23. https://doi.org/10.1006/EXCR.2002.5669.

[76] Muchir A, van Engelen BG, Lammens M, Mislow JM, McNally E, Schwartz K, et al. Nuclear envelope alterations in fibroblasts from LGMD1B patients carrying nonsense Y259X heterozygous or homozygous mutation in lamin A/C gene. Exp Cell Res 2003;291:352–62. https://doi.org/10.1016/j.yexcr.2003.07.002.

[77] Vigouroux C, Auclair M, Dubosclard E, Pouchelet M, Capeau J, Courvalin JC, et al. Nuclear envelope disorganization in fibroblasts from lipodystrophic patients with heterozygous R482Q/W mutations in the lamin A/C gene. J Cell Sci 2001;114:4459–68. https://doi.org/10.1242/jcs.114.24.4459.

[78] Steele-Stallard HB, Pinton L, Sarcar S, Ozdemir T, Maffioletti SM, Zammit PS, et al. Modeling Skeletal Muscle Laminopathies Using Human Induced Pluripotent Stem Cells Carrying Pathogenic LMNA Mutations. Front Physiol 2018;9:1332.

[79] Davidson PM, Lammerding J. Broken nuclei — lamins, nuclear mechanics, and disease. Trends Cell Biol 2014;24:247–56. https://doi.org/10.1016/j.tcb.2013.11.004.

[80] Verstraeten VLRM, Peckham LA, Olive M, Capell BC, Collins FS, Nabel EG, et al. Protein farnesylation inhibitors cause donut-shaped cell nuclei attributable to a centrosome separation defect. Proc Natl Acad Sci U S A 2011;108. https://doi.org/10.1073/pnas.1019532108.

[81] Bertrand AT, Brull A, Azibani F, Benarroch L, Chikhaoui K, Stewart CL, et al. Lamin A/C Assembly Defects in LMNA -Congenital Muscular Dystrophy Is Responsible for the Increased Severity of the Disease Compared with Emery-Dreifuss Muscular Dystrophy. Cells 2020;9.

[82] Meinke P, Mattioli E, Haque F, Antoku S, Columbaro M, Straatman KR, et al. Muscular Dystrophy-Associated SUN1 and SUN2 Variants Disrupt Nuclear-Cytoskeletal Connections and

Myonuclear Organization. PLoS Genet 2014;10:e1004605. https://doi.org/10.1371/journal.pgen.1004605.

[83] Gómez-Domínguez D, Epifano C, Miguel F de, Castaño AG, Vilaplana-Martí B, Martín A, et al. Consequences of Lmna Exon 4 Mutations in Myoblast Function. Cells 2020;9.

[84] Vaughan OA, Alvarez-Reyes M, Bridger JM, Broers JLV, Ramaekers FCS, Wehnert M, et al. Both emerin and lamin C depend on lamin A for localization at the nuclear envelope. J Cell Sci 2001;114:2577–90. https://doi.org/10.1242/jcs.114.14.2577.

[85] Hegde RS, Zavodszky E. Recognition and Degradation of Mislocalized Proteins in Health and Disease. Cold Spring Harb Perspect Biol 2019;11:a033902. https://doi.org/10.1101/CSHPERSPECT.A033902.

[86] Fairley EA, Kendrick-Jones J, Ellis JA. The Emery-Dreifuss muscular dystrophy phenotype arises from aberrant targeting and binding of emerin at the inner nuclear membrane. J Cell Sci 1999;112 (Pt 1:2571–82.

[87] Fairley EAL, Riddell A, Ellis JA, Kendrick-Jones J. The cell cycle dependent mislocalisation of emerin may contribute to the Emery-Dreifuss muscular dystrophy phenotype. J Cell Sci 2002;115:341–54.

[88] Bertrand AT, Renou L, Papadopoulos A, Beuvin M, Lacène E, Massart C, et al. DelK32-lamin A/C has abnormal location and induces incomplete tissue maturation and severe metabolic defects leading to premature death. Hum Mol Genet 2012;21:1037–48. https://doi.org/10.1093/HMG/DDR534.

[89] Torvaldson E, Kochin V, Eriksson JE. Phosphorylation of lamins determine their structural properties and signaling functions. Nucleus 2015;6:166–71.

[90] Sullivan T, Escalante-Alcalde D, Bhatt H, Anver M, Bhat N, Nagashima K, et al. Loss of A-type lamin expression compromises nuclear envelope integrity leading to muscular dystrophy. Journal of Cell Biology 1999;147:913–9. https://doi.org/10.1083/jcb.147.5.913.

[91] Thanisch K, Song C, Engelkamp D, Koch J, Wang A, Hallberg E, et al. Nuclear envelope localization of LEMD2 is developmentally dynamic and lamin A/C dependent yet insufficient for heterochromatin tethering. Differentiation 2017;94. https://doi.org/10.1016/j.diff.2016.12.002.

[92] Malik P, Korfali N, Srsen V, Lazou V, Batrakou DG, Zuleger N, et al. Cell-specific and lamin-dependent targeting of novel transmembrane proteins in the nuclear envelope. Cellular and Molecular Life Sciences 2010;67. https://doi.org/10.1007/s00018-010-0257-2.

[93] Libotte T, Zaim H, Abraham S, Padmakumar VC, Schneider M, Lu W, et al. Lamin A/C–dependent Localization of Nesprin-2, a Giant Scaffolder at the Nuclear Envelope. Https://DoiOrg/101091/MbcE04-11-1009 2005;16:3411–24. https://doi.org/10.1091/MBC.E04-11-1009.

[94] Crisp M, Liu Q, Roux K, Rattner JB, Shanahan C, Burke B, et al. Coupling of the nucleus and cytoplasm. J Cell Biol 2006;172:41–53. https://doi.org/10.1083/jcb.200509124.

[95] Ungricht R, Kutay U. Establishment of NE asymmetry-targeting of membrane proteins to the inner nuclear membrane. Curr Opin Cell Biol 2015;34. https://doi.org/10.1016/j.ceb.2015.04.005.

[96] Andrés V, González JM. Role of A-type lamins in signaling, transcription, and chromatin organization. J Cell Biol 2009;187:945–57. https://doi.org/10.1083/jcb.200904124.

[97] Parnaik VK. Role of Nuclear Lamins in Nuclear Organization, Cellular Signaling, and Inherited Diseases. Int Rev Cell Mol Biol 2008;266. https://doi.org/10.1016/S1937-6448(07)66004-3.

[98] Azibani F, Brull A, Arandel L, Beuvin M, Nelson I, Jollet A, et al. Gene Therapy via Trans-Splicing for LMNA-Related Congenital Muscular Dystrophy. Mol Ther Nucleic Acids 2018;10:376–86. https://doi.org/10.1016/J.OMTN.2017.12.012.

Figure legends

Figure 1- Quantitative proteomics analysis revealed 348 dysregulated proteins in L-CMD myoblasts and myotubes compared to healthy controls. Using SWATH-MS analysis, dysregulated proteins were identified in L-CMD (R249W, L380S, del.K32) myoblasts and myotubes compared to controls (C5d, C25, C41). (A) Venn diagram illustrating the limited overlap of downregulated proteins that were identified in L-CMD myoblasts and L-CMD myotubes and showing no overlap between the upregulated proteins identified in L-CMD myoblasts and L-CMD myotubes. (B) Heatmap illustrating a total of 348 differentially expressed proteins were identified across the L-CMD myoblasts and L-CMD myotubes and the size of their fold-change, there were four commonalities across the L-CMD samples, with two proteins downregulated in L-CMD myoblasts and L-CMD myotubes, and two proteins upregulated in L-CMD myoblasts but downregulated in L-CMD myotubes. (C) Enriched molecular and cellular functions that were most common to the dysregulated proteins with the number of proteins associated with each term. (D) Enriched canonical pathways that were associated with the dysregulated proteins and the number of proteins associated with each term. A negative Z-score suggests inhibition, whilst a positive Z-score indicates potential activation. For terms where no activity pattern is available, this indicates that IPA® was not able to predict activity for a pathway.

Figure 2- Differentially expressed proteins identified in L-CMD myoblasts compared to myotubes, and control myoblasts compared to myotubes. There was limited overlap between the differentially expressed proteins that were identified in L-CMD myoblasts versus L-CMD myotubes, compared to control myoblasts versus control myotubes. (A) Venn diagram illustrating only 3 proteins were commonly upregulated in L-CMD and control myoblasts compared to L-CMD and control myotubes. (B) Venn diagram showing 28 proteins were commonly downregulated in L-CMD and control myoblasts compared to L-CMD and control myotubes. (C) Enriched canonical pathways that were associated with the dysregulated proteins and the number of proteins associated with each term. A negative Z-score suggests inhibition, whilst a positive Z-score indicates potential activation. For terms where no activity pattern is available, this indicates that IPA® was not able to predict activity for a pathway.

Figure 3- L-CMD myoblasts exhibited increased proliferation rate and nuclear deformities. (A) Cell proliferation rate is increased in L-CMD myoblasts and is expressed as doubling time in myoblasts from L-CMD patients (L380S, R249W, del.K32) compared to controls (C5d, C25, C41). Individual values for each cell line are presented, as well as the average for each group, with error bars indicating standard deviation from the mean. Asterisk (*) indicates significance (p=0.023). (B)

Representative images of control (C5d, C25, C41) and L-CMD (del.K32, R249W, L380S) myotubes stained with DAPI. On average, control myotubes had 16 nuclei per myotube, whilst L-CMD myotubes had a similar amount of nuclei, an average of 14 nuclei per myotube (ten myotubes were counted per cell line). Compared to the other L- CMD and control myotubes, however, the del.K32 L-CMD myotubes had a reduced number of nuclei per myotube. On average, the L-CMD myotubes contained 9 nuclei. (C) Abnormal L-CMD (L380S, del.K32, R249W) myoblast and myotube nuclei were characterised based on the defect type using lamin A/C immunostaining (yellow) and DAPI (blue). (a) Nuclear blebbing is defined as protrusions from the nucleus, sometimes these are seen to become detached from the nucleus itself, (b) honeycomb nuclei have multiple distinct holes that sometimes resemble a honeycomb, (c) nuclear shape abnormalities are nuclei that are shaped differently to control nuclei, elongated nuclei are an example of this, (d) donut shaped nuclei have a single hole through the centre, (e) correctly shaped control nuclei for comparison. (D) Graph depicting the percentage (%) of abnormal nuclei identified in L-CMD and control myoblasts. (E) Graph depicting the percentage (%) of abnormal nuclei identified in L-CMD and control myotubes.

Figure 4- Lamin A/C is significantly reduced in L-CMD myotubes compared to controls and nucleoplasmic aggregation was found in del.K32 myoblasts only. Lamin A/C expression was compared in control (C5d, C25, C41) and L-CMD (R249W, del.K32, L380S) myoblasts (A,B,C) and myotubes (D,E). (A, C) In L-CMD myoblasts, lamin A appeared reduced compared to controls, although this finding was not statistically significant (p=0.244), whilst lamin C did not appear obviously reduced (p=0.805). (B) However, it was noticed that lamin A was of a lower molecular weight in L-CMD myoblasts compared to controls. (D, E) In L-CMD myotubes, lamin A and C were both reduced with statistical significance compared to controls (p=0.044, p=0.043). ns indicates not significant, Asterisk (*) denotes statistical significance. (F) Representative immunocytochemistry images showing lamin A/C (yellow) and DAPI (blue) staining in control myoblasts and myotubes (C5d, C25, C41). Lamin A/C was found to be correctly localized at the nuclear envelope across all control myoblasts and myotubes. (G) Representative immunocytochemistry images showing lamin A/C (yellow) and DAPI (blue) staining in L-CMD myoblasts and myotubes (L380S, del.K32, R249W). Lamin A/C was found in nucleoplasmic aggregates in del.K32 myoblasts, as indicated by white arrows.

Figure 5- Emerin is significantly reduced in expression in L-CMD myotubes compared to controls and mislocalized in R249W myoblasts only. (A) Representative immunocytochemistry images showing emerin (magenta) and DAPI (blue) staining in control (C5d, C25, C41) and L-CMD (R249W, del.K32, L380S) myoblasts and myotubes. Emerin was found to be correctly localized at the nuclear envelope across all control myoblasts and myotubes, and all L-CMD myoblasts and myotubes except R249W L-CMD myoblasts where emerin was observed at the nuclear envelope and in the cytoplasm. (A) Emerin was not found to be significantly reduced in L-CMD myoblasts (L380S, R249W, del.K32) compared to age matched controls (C5d, C25, C41) (p=0.097). (C) Emerin was however significantly decreased L-CMD myotubes compared to controls (p=0.040). ns indicates not significant, Asterisk (*) denotes statistical significance.

Figure 6- SUN2 is significantly reduced in expression in L-CMD myotubes compared to controls, and is correctly localized to the nuclear envelope in all L-CMD cell lines. (A) Representative immunocytochemistry images showing SUN2 (magenta) and DAPI (blue) staining in control (C5d,

C25, C41) and L-CMD (R249W, del.K32, L380S) myoblasts and myotubes. SUN2 was correctly localized at the nuclear envelope across all control myoblasts and myotubes, and all L-CMD myoblasts and myotubes. There did, however, appear to be reduced staining of SUN2 across L-CMD cells. (B) Expression SUN2 was not found to be reduced in L-CMD myoblasts compared to controls (p=0.401). (C) In myotubes, expression of SUN2 was significantly increased (p=0.049). ns indicates not significant, Asterisk (*) denotes statistical significance.

Proteomic characterisation of human *LMNA*-related congenital muscular dystrophy muscle cells

Emily C Storey[1,2], Ian Holt[1,2], Sharon Brown[1,2], Silvia Synowsky[3], Sally Shirran[3], Heidi R Fuller[1,2]*

[1]Wolfson Centre for Inherited Neuromuscular Disease, RJAH Orthopaedic Hospital, Oswestry, SY10 7AG, UK. [2]The School of Pharmacy and Bioengineering, Keele University, ST5 5BG, UK. [3]BSRC Mass Spectrometry and Proteomics Facility, University of St Andrews, KY16 9ST, UK

* Correspondence to h.r.fuller@keele.ac.uk

Abstract

LMNA-related congenital muscular dystrophy (L-CMD) is caused by mutations in the *LMNA* gene, encoding lamin A/C. To further understand the molecular mechanisms of L-CMD*,* proteomic profiling using DIA mass spectrometry was conducted on immortalized myoblasts and myotubes from controls and L-CMD donors each harbouring a different *LMNA* mutation (R249W, del.32K and L380S). Compared to controls, 124 and 228 differentially abundant proteins were detected in L-CMD myoblasts and myotubes, respectively, and were associated with enriched canonical pathways including synaptogenesis and necroptosis in myoblasts, and Huntington's disease and insulin secretion in myotubes. Abnormal nuclear morphology and reduced lamin A/C and emerin abundance was evident in all L-CMD cell lines compared to controls, while nucleoplasmic aggregation of lamin A/C was restricted to del.32K cells, and mislocalisation of emerin was restricted to R249W cells. Abnormal nuclear morphology indicates loss of nuclear lamina integrity as a common feature of L-CMD, likely rendering muscle cells vulnerable to mechanically induced stress, while differences between L-CMD cell lines in emerin and lamin A localisation suggests that some molecular alterations in L-CMD are mutation specific. Nonetheless, identifying common proteomic alterations and

molecular pathways across all three L-CMD lines has highlighted potential targets for the development of non-mutation specific therapies.

Key words
L-CMD; lamin A; LMNA; congenital muscular dystrophy; emerin; SUN2; proteome; proteomics

1. Introduction

LMNA-related congenital muscular dystrophy (L-CMD, ORPHA:157973) is an extremely rare genetic condition, with an estimated incidence of <1/1,000,000 [1] caused by mutations in the *LMNA* gene that encodes the type V intermediate filament proteins, lamins A and C [2,3]. L-CMD has been described as the most severe of the striated muscle laminopathies and is characterized by onset before the age of 2 years old [3,4]. Distinct features include major muscle atrophy and weakness, mainly affecting the axial muscles, leading to a complete absence of or limited motor achievements [3,4]. A hallmark of L-CMD is a "dropped head" due to weakness of muscles in the neck [2,5–7], and other characteristics include the presence of multiple joint contractures, and life-threatening severe respiratory insufficiency, requiring mechanical ventilation [3,4]. Cardiac arrhythmias have been identified in L-CMD patients, suggesting there is some cardiac involvement in this disease [3,4]. Current treatment options are limited to physiotherapy, surgery to treat contractures, as well as managing the risk of respiratory and cardiac manifestations which are common causes of premature death.

Lamins A and C, along with B-type lamins, are the major components of the nuclear lamina (NL) [8–10]. Lamin A/C are connected to other nuclear envelope (NE) proteins through their mutual association with the Linker of Nucleoskeleton and Cytoskeleton (LINC) complex, which functions to connect the NL to the cytoskeleton in mammalian cells [11]. Lamin A/C is known to interact directly with LINC complex proteins Sad1 and UNC84 domain containing SUN proteins 1 and 2 [12], and associated protein, emerin [13], and is involved with a wide variety of cellular processes including the regulation of cell stability, cell motility,

mechanosensing, gene regulation, chromosome organization, DNA damage repair, telomere protection, and cell differentiation, including myogenesis [14–20]. Lamin A/C has been widely studied in many of these contexts, and in recent years, some progress has been made to elucidate the pathophysiological mechanisms of L-CMD, downstream of *LMNA* mutations. It was noted, for example, that fibroblasts from an individual with a severe L-CMD and lipodystrophy phenotype harbouring a heterozygous *LMNA* R388P mutation senesced prematurely, had abnormal cellular morphology and a small percentage of abnormally shaped nuclei [21]. In C2C12 cells transfected with lamin A carrying the same mutation, mutant lamin A mostly accumulated within the nucleoplasm, with less lamin A being correctly localized at the nuclear periphery [22]. Additionally, altered anchorage of the inner nuclear membrane protein and interaction partner of lamin A/C, emerin, and LAP2α, another nuclear envelope protein, was evident [22]. In C2C12 cells in which the R249W *LMNA* mutation, a common cause of L-CMD, was introduced by CRISPR/Cas9 editing, mislocalised emerin was detected at the endoplasmic reticulum, nuclei showed a significant reduction in their circularity index, and there was evidence of DNA damage and impaired myogenic differentiation [23]. Similarly, skin fibroblasts from L-CMD individuals carrying R249W and del.K32 *LMNA* mutations also exhibited mislocalised lamin A/C, which was almost exclusively found in the nucleoplasm [24]. In the del.K32 myoblasts from a mouse model of L-CMD, a strong reduction of lamin A/C was noted, in addition to partially mislocalized emerin. The cells were found to have impaired differentiation, with highly misshapen myonuclei, that were elongated, enlarged, and situated in the middle of myotubes [24]. In addition to emerin, lamin B1 and SUN2 were also mislocalized in del.K32 mouse myotubes, in contrast to the apparent correct localization of lamin B1 and SUN1 in the respective myoblasts, suggesting that the nuclear defects are exacerbated by differentiation [24]. There is evidence too that L-CMD causing mutations interfere with mechanosignalling pathways in skeletal muscle, subsequently affecting muscle growth [25]. Human muscle stem cells carrying either the del.K32, R249W or L380S *LMNA* mutations were each found to have impaired myogenic fusion, due to disorganized cadherin/β catenin adhesion complexes, stretched myotubes and overloaded muscle fibres with aberrant regulation of the yes-associated protein (YAP) [25,26]. Skeletal muscle from *Lmna*-CMD mice was also unable to hypertrophy in response to functional overload, due to defective accretion of activated satellite cells [25,26].

The wide range of *LMNA* mutations known to cause L-CMD complicates gene therapy development for the condition [27], and it may be too late for gene therapy to be fully effective by the time a diagnosis is made. Variable severity and symptom onset time with little obvious relationship to the mutation further complicates matters [3,4]. Alternatively, therapies tailored towards conserved features of L-CMD might, in combination with gene therapy, offer maximum benefit to patients. This approach is gaining momentum for another inherited neuromuscular disease, spinal muscular atrophy, where gene replacement strategies have shown incomplete efficiency [28,29]. While the studies described above have generated valuable insights into the cellular consequences of L-CMD, identification of targets for therapy development is hindered by limited insights into the molecular pathways downstream from *LMNA* to modulate pathogenesis.

Here, we have conducted targeted and unbiased proteomic analyses on immortalized myoblasts and myotubes from healthy controls compared to three individuals with L-CMD, each harbouring a different *LMNA* mutation (i.e., R249W, del.32K and L380S), with the aim of determining whether the L-CMD cells may share a core molecular signature.

2. Materials and Methods

2.1. Cell culture

Immortalized myoblast cell lines were from three human control donors without neuromuscular disease, and from three individuals with L-CMD (**Supplementary File 1, Table 1**) [3,30]. They were immortalized by transduction with human telomerase reverse transcriptase (hTERT) and cyclin-dependent kinase-4 (Cdk4-R24C mutant) containing retroviral vectors, at the Institut de Myologie, Paris, as described previously [31]. Myoblasts were cultured in skeletal muscle cell growth medium (Cat No: C-23060; PromoCell GmbH, Heidelberg, Germany) containing supplement mix (Cat No: C-39365; PromoCell) with 10% Fetal Bovine Serum (Cat No: 10270; Gibco; Thermo Fisher Scientific, Paisley, UK) and Penicillin-Streptomycin (Cat No: 15140122; Gibco; Thermo Fisher Scientific). Differentiation was induced once myoblasts had reached approximately 80-90% confluency by washing

adherent myoblasts in serum free medium and then culturing in DMEM (Cat No: 31966-021; Gibco; Thermo Fisher Scientific) supplemented with Insulin-Transferrin-Selenium-Ethanolamine (ITS-X) (Cat No: 51500-056; Gibco; Thermo Fisher Scientific) and Penicillin-Streptomycin (Cat No: 15140122; Gibco; Thermo Fisher Scientific) without the addition of serum. After a further four days of cell culture, approximately 80% of the cells had fused into myotubes.

2.2. Cell proliferation assay

Control (C5d, C25, C41) and L-CMD (L380S, del.K32, R249W) myoblasts were grown in complete medium, as described above, seeded in T25 cell culture flasks at a density of 30,000 cells per flask (approximately 1% of the maximum confluency of a T25 flask). The cells were maintained in a humidified incubator (LEEC, Nottingham, UK) at 37°C and 5% CO_2 for three days during their exponential growth phase. After this point, the media was removed from the flask and cells were trypsinized and counted. Each cell line was grown in three T25 flasks (to provide technical replicates), and each flask was counted four times. Before the final cell count, each of the cell lines were less than 50% confluent, indicating that the myoblasts were still growing exponentially. A total of 12 measurements were performed for each cell line. Doubling time (DT) for each cell was calculated using the following equation: $DT = \ln(2) \times t/(\ln(C2) - (\ln(C1))$. Here, t represents the culture duration in hours, C2 is the number of cells at the end of the culture, and C1 is the number of seeded cells at the beginning of the experiment.

2.3. Western blotting

Myoblast and myotube pellets were resuspended in RIPA buffer (p.25% deoxycholic acid, 1mM ethylenediaminetetracetic acid, 150mM sodium chloride and 50mM TRIS-HCl buffer, pH 7.4), left on ice for 5 min, then sonicated briefly for 10s. Samples were centrifuged for 5 min at 13,000 RPM (MSE, Heathfield, UK; Harrier 18/80R) at 4°C to pellet any insoluble material. Protein extracts were then subject to SDS-PAGE and western blotting. Samples were then briefly heated in 2x Laemmli buffer [32] (4% sodium dodecyl sulfate, 10% 2-mercaptoethanol, 20% glycerol, 0.125 M TRIS-HCl) at 95°C for 3 min and subjected to SDS-PAGE (Biorad, Hercules, CA, USA) using 4-12% Bis-Tris 15-well precast gels (Cat No: NW04125BOX; Life Technologies; Invitrogen). A small section from the top of the gel was

excised and stained with Coomassie blue (Cat No: 20278; Thermo Scientific; ThermoFisher Scientific) as an internal loading control for total protein, as previously described [33]. The proteins in the remaining gel were transferred to nitrocellulose membrane by western blotting overnight [34]. Membranes were blocked with 4% powdered milk, and then incubated with primary antibodies; mouse anti-lamin A/C (MANLAC1 4A7; 1:100 [35]), mouse anti-emerin (MANNEM1 5D10; 1:100 [36,37]), rabbit anti-SUN2 (HPA001209; 1:500, Merck Life Science, Gillingham, UK) in western blot buffer (1% BSA, 10% horse serum, 10% fetal calf serum in PBS with 0.05% triton) for 1-2 h, followed by incubation with secondary antibodies; HRP-labelled rabbit anti-mouse immunoglobulins (Cat No: P026002-2; Dako; Agilent; 1:1000) or HRP-labelled goat anti-rabbit immunoglobulins (Cat No: P0448; Dako; Agilent; 1:1000). Membranes were then incubated with West Pico chemiluminescent substrate (Cat No: 34580; Thermo Fisher Scientific; Thermo Fisher Scientific), or SuperSignal™ West Femto chemiluminescent substrate (Cat No: 10391544; Thermo Fisher Scientific; Thermo Fisher Scientific) for low signal detection and visualized using a Gel Image Documentation system (Biorad, Hercules, CA, USA). Densitometry measurements of antibody reactive bands were obtained using ImageJ software (version 1.8.0_112) and were normalized to densitometry measurements of the Coomassie stained gel [38].

2.4. Immunofluorescent microscopy

Immortalized myoblasts were fixed in acetone:methanol (50:50) for 5-10 min and incubated with primary antibody, mouse anti-emerin (MANEM1 5D10; 1:4 [36,37]), rabbit anti-lamin A/C (MANLAC1 4A7; 1:4 [35]), and rabbit anti-SUN2 (HPA001209, 1:100, Merck Life Science, Gillingham, UK) in blocking buffer (1% FBS and 1% HS in PBS) for 1 h. After incubation with secondary antibody, goat anti-mouse immunoglobulins Alexa Fluor® 488 or 546 (Cat No: A11029, Cat no: A11030; Life Technologies; 1:400) or goat anti-rabbit immunoglobulins Alexa Fluor® 546 (Cat No: A11010; Life Technologies; 1:400), coverslips were mounted with ProLong™ Gold Antifade Mountant with DAPI (Cat No: P36941, Thermo Fisher Scientific), and cells were imaged using Leica SP5 confocal microscope with 63x oil immersion objective.

2.5. Quantitative DIA-MS proteomics analysis

2.5.1. Sample preparation

Protein was extracted from myoblast and myotube samples from healthy control donors (n=3) and L-CMD patients harbouring mutations in *LMNA* (n=3) using 250µL of extraction buffer (8M urea (Cat no: U0631; Sigma Aldrich), 100mM ammonium bicarbonate, 2% sodium deoxycholate in sterile dH_2O). Samples were sonicated at 5 microns for 10s and centrifuged at 13000 RPM for 5 min at 4°C to pellet insoluble material. A small aliquot of cell extract from each sample was used to determine protein concentration, whilst the remaining samples were stored at -80°C for downstream analysis. The protein concentration of each sample was determined using the Pierce™ BCA Protein Assay Kit. A minimum of 30µg of protein is needed to perform quantitative DIA MS analysis with a bespoke identification library therefore we ensured each sample contained more than the minimum protein concentration.

Each sample (50µg) was diluted with extraction buffer to obtain equal concentrations and then reduced with 5mM tris(2-carboxyethyl) phosphine (TCEP) at 30°C for 1 h followed by alkylation with 10mM iodoacetamide (IAA) in darkness at room temperature for 30 min. The reaction was quenched with 20mM DTT to deactivate any unreacted reagents. The samples were diluted to 1.5M urea and subsequently digested overnight with sequencing grade trypsin in a ratio of 1µg of protease to 50µg protein.

The peptides were subjected to cleanup using C18 columns, and the cleaned, digested sample was then dried and resuspended to 1µg/µl in loading buffer (100% water, 0.1% formic acid). Data independent acquisition was performed on individual samples (DIA-MS). In addition, a pool of all the samples was prepared, and a portion subjected to nanoLC MS/MS analysis using data dependent acquisition (DDA-MS). The remnant of the pooled sample was then fractionated on high pH C18 Reverse Phase into 12 fractions before analysing the fractions individually in DDA mode.

2.5.2. Data dependent acquisition (DDA)

Peptides (5 µg) were subjected to LCMS/MS using an Ultimate 3000 RSLC (Thermo Fisher Scientific) coupled to an Orbitrap Fusion Lumos mass spectrometer (Thermo Fisher Scientific). The peptides were injected onto a Pepmap100 C18 5µm 0.3 × 5 mm reverse-

phase trap for pre-concentration and desalted with loading buffer, at 5 µL/min for 10 min. The trap was then switched in-line with the analytical column (Easy-spray Pepmap RSLC C18 2µm, 50cm x75um ID). Peptides were eluted from the column using a linear solvent gradient using the following gradient: linear 4–40% of buffer B over 120 min, linear 40–60% of buffer B for 30 min, sharp increase to 95% buffer B within 0.1 min, isocratic 95% of buffer B for 15 min, sharp decrease to 2% buffer B within 0.1 min and isocratic 2% buffer B for 15 min. The mass spectrometer was operated in DDA positive ion mode with a cycle time of 1.5 s. The Orbitrap was selected as the MS1 detector at a resolution of 120000 with a scan range of from m/z 375 to 1500. Peptides with charge states 2 to 5 were selected for fragmentation in the ion trap using HCD as collision energy.

The raw data files were converted into mgf using MSconvert (ProteoWizard) and searched using Mascot with trypsin as the cleavage enzyme and carbamidomethylation as a fixed modification of cysteines, against the Swissprot database, restricted only to proteins from humans. Note that the iRT peptides were added to this database. The mass accuracy for the MS scan was set to 20 ppm and for the fragment ion mass to 0.6 Da.

2.5.3. Data independent acquisition (DIA) mode

For quantitative MS, sample (5 µg) was injected onto the same LCMS set up as above with the same gradient, however data acquisition was performed in data independent acquisition (DIA) mode. The DIA MS method alternates between a MS scan and a tMS2 scan containing 24 scan windows. The MS scan has the following parameters: the Orbitrap at 120000 resolution is selected as detector with a m/z range from 400 to 1000. The tMS2 scan uses HCD as activation energy with fragments detected in the Orbitrap at 30000 resolution. The first 20 m/z windows are 20 mass units wide from 410 to 790 followed by a 30m/z window from 790-820, a 40m/z window from 820-860, a 50m/z window from 860-910 and a 60m/z window from 910-970.

All Mascot searches using the DIA data were exported as .dat file and assembled to a spectral library in Skyline by associating each peptide to its respective protein. After the quantitative spectra were imported, peaks were reintegrated using the mProphet peak scoring model [39] To identify differentially expressed proteins, the sum total area value for

each protein identified by ≥2 peptides in the L-CMD (n=3) and control samples (n=3) was averaged, and only proteins with an average fold change of <0.8 and >1.25 with a $p < 0.05$ (as determined by a t-test) across the three L-CMD samples compared to controls were considered in further analysis.

2.5.4. QIAGEN Ingenuity Pathway Analysis (IPA®)

Dysregulated pathways were identified downstream of *LMNA* mutations in L-CMD patient myoblasts and myotubes (compared to controls) using QIAGEN Ingenuity Pathway Analysis (IPA®) software (QIAGEN; https://digitalinsights.qiagen.com/products-overview/discovery-insights-portfolio/analysis-and-visualization/qiagen-ipa/). The fold change value for each protein along with the assigned p-value was inputted into IPA® in the form of an Excel spreadsheet. IPA® uses right-tailed Fisher's Exact Test to calculate the p-value determining the probability that each cellular and molecular function or canonical pathway assigned to that dataset is due to chance alone, and the final lists of functions and pathways were ranked accordingly to the resulting p-value. IPA® also produces a Z-score for enriched canonical pathways. The Z-score is a prediction of whether a pathway is activated or inhibited based on the direction of expression change in the input dataset. This is done by comparing the IPA® database, which predicts what to expect when an upstream regulator interacts with its downstream target, to the direction of differential gene/protein expression that was observed in the input dataset. Z-score of ≥2 represents the prediction of activation, while Z-score ≤ -2 represents the prediction of inhibition.

2.6. Statistical analysis

All statistical analysis were carried out using GraphPad Prism Version 9.0.0. for Windows (GraphPad Software, San Diego, CA, USA, www.graphpad.com). Western blot densitometry measurements were assessed using unpaired, two-tailed t-tests, with unequal variance to determine significant differences between L-CMD myoblast and myotube samples and healthy controls. To determine if changes in protein expression in L-CMD myoblasts and myotubes were significantly different to controls after MS analysis, multiple unpaired two-tailed t-tests were performed assuming unequal variance applying no correction for multiple comparisons. Also following MS analysis, significant protein expression changes were

determined between L-CMD myoblasts and L-CMD myotubes, as well as control myoblasts and control myotubes. For this, paired two-tailed t-tests with unequal variance were used.

3. Results

3.1. Quantitative proteomic identification of differentially expressed protein profiles in L-CMD cells compared to healthy controls

To determine whether there is a molecular signature of L-CMD in myoblasts and myotubes that is conserved across each of the three different mutations (R249W, L380S, del.K32) a quantitative proteomic comparison was made with control cells (C5d, C25, C41) using Data Independent Acquisition MS This approach identified a total of 10,977 proteins in total with a Mascot significance threshold for of $p<0.05$ (**Supplementary File 2**). Following the subsequent filtering steps described in the methods section, 124 and 228 proteins met the criteria for differential abundance in the L-CMD myoblasts and myotubes, respectively, compared to control cells (**Figure 1A & B**). Of these, 85 and 171 proteins were downregulated in the L-CMD myoblasts and myotubes, respectively, compared to controls. Two proteins, BCL7B (B-cell CLL/lymphoma 7 protein family member B) and transketolase, were commonly downregulated in both L-CMD myoblasts and myotubes compared to control cells. No commonly upregulated proteins were identified between the 39 and 57 proteins that were significantly increased in L-CMD myoblasts and myotubes, respectively, compared to controls (**Figure 1A & B**), though two proteins, DNA primase large subunit and F-box/LRR-repeat protein 3, were upregulated in L-CMD myoblasts but downregulated in L-CMD myotubes. Lamin A/C itself met the criteria for reduced abundance in the L-CMD myotubes compared to controls (ratio=0.450, p=0.038). Other LINC complex-associated proteins including lamin B1 and B2, emerin, FHL1, SUN1 and SUN2, and nesprin-1 and nesprin 2, were detected but did not meet the criteria for differential abundance. In the case of SUN2 and emerin, this was most likely due to the technical variability in the detection and measurement of individual peptides within each sample, as confirmed by inspection of the raw proteomics data.

Ingenuity pathway analysis (IPA®) identified enriched molecular and cellular functions with which the dysregulated proteins in the L-CMD cells were associated. The top five terms were cell death and survival (n=11, p=1.18 x 10^{-02}-7.27 x 10^{-04}), cellular growth and proliferation (n=10, p=1.36 x 10^{-02}–3.19 x 10^{-04}), cell cycle (n=6, p=1.03 x 10^{-02}–3.92x 10^{-04}), DNA replication, recombination, and repair (n=4, p=1.03x 10^{-02}-3.92 x 10^{-04}), and cellular development (n=11, p=1.03 x 10^{-02}-3.19 x 10^{-04}) (**Figure 1C**). Differentially expressed proteins in the L-CMD myotubes were also associated with cellular development (n=39, p=9.46 x 10^{-03}-7.13 x 10^{-05}), while other enriched molecular and cellular functions included cell morphology (n=32, p=9.46 x 10^{-03}-7.13 x 10^{-05}), small molecule biochemistry (n=30, p=9.46 x 10^{-03}-1.56 x 10^{-06}), drug metabolism (n=6, p=9.46 x 10^{-03}-1.56 x 10^{-06}) and carbohydrate metabolism (n=31, p=1.18 x 10^{-02}-7.27 x 10^{-04}) (**Figure 1C**).

IPA® also identified significantly enriched canonical pathways among the list of differentially expressed proteins in L-CMD cells compared to controls. In the dataset comparing L-CMD and control myoblasts, top enriched canonical pathways included the white adipose tissue browning pathway (n=3, p=0.035), SNARE signalling pathway (n=3, p=0.034), ferroptosis signalling pathway (n=3, p=0.031), p38MAPK signalling (n=3, p=0.025), ATM signalling (n=3, p=0.015), apelin adipocyte signalling pathway (n=3, p=0.023), PDGF signalling (n=3, p=0.010), and LPS/IL-1 mediated inhibition of RXR function (n=5, p=0.043). For these pathways, it was not possible to predict an activity pattern. The necroptosis pathway, however, had a z-score of -2, indicating a predicted downregulation (n=4, p=0.009), whilst the synaptogenesis signalling pathway was assigned a z-score of 1.342, suggesting the pathway is upregulated (n=5, p=0.025) (**Figure 1D**). In the L-CMD versus control myotube dataset, top enriched canonical pathways included the protein ubiquitination pathway (n=6, p=0.047), sperm motility (n=6, p=0.035), role of macrophages, fibroblasts and endothelial cells in rheumatoid arthritis (n=7, p=0.037), xenobiotic metabolism signalling (n=8, p=0.007), and RAR activation (n=10, p=<0.001), none of which had predicted directionality of activation. HIF1α signaling (n=6, p=0.014454) and protein kinase A signalling (n=8, p=0.042) had z-scores of 0, whilst the insulin secretion signalling pathway (n=6, p=0.046) and Huntington's disease signalling (n=11, p=<0.001) had positive z-scores of 0.816, suggesting activation, and the xenobiotic metabolism general signalling pathway (n=6, p=0.002) had a negative z-score of -0.816, predicting inhibition (**Figure 1C**). There were no enriched

canonical pathways in common between the differentially expressed proteins that were identified in the L-CMD myoblasts and myotubes.

To gain insights into whether the molecular response associated with myoblast differentiation was similar in the L-CMD cells compared to controls, the differentially expressed proteins identified in L-CMD myoblasts vs their respective myotubes were compared with those that were differentially expressed in the control myotubes vs their respective myoblasts. A total of 136 proteins were differentially expressed in control myoblasts compared to their myotubes, whilst 570 proteins were differentially expressed in L-CMD myoblasts compared to their myotubes. Of these, only 3 proteins were commonly upregulated and 28 commonly downregulated in L-CMD and control myoblasts compared to their respective myotubes (**Figure 2A & B**). The lack of overlap of differentially expressed proteins in the L-CMD and control myoblast vs myotube datasets, therefore implies that proteins that are involved at different points during muscle cell differentiation are dysregulated in L-CMD myoblasts and/or myotubes.

Top canonical pathways identified by IPA® for the differentially expressed proteins in the control myoblasts vs myotubes comparison included cell cycle control of chromosomal replication (n=15, *p*=1.31E-15), ID1 signalling pathway (n-15, *p*=1.87E-07), IL-15 production (n=12, *p*=1.89E-07), and reelin signalling in neurons (n=12, p=7.16E-07), which had negative z-scores of -3.4, -3.4, -3.5, and -2.1, respectively, indicating predicted inhibition, whilst role of tissue factor in cancer (n=12, *p*=9.88E-08) was also an enriched pathway, but had no predicted activity (**Figure 2C**). For the proteins identified in the L-CMD myoblasts vs their myotubes, top enriched canonical pathways were very different and included dilated cardiomyopathy signalling pathway (n=41, *p*=5.18E-24) and calcium signalling (n=44, p=9.92E-20), which had z-scores of -5 and -0.6, suggesting inhibition, actin cytoskeleton signalling (n=50, *p*=1.79E-22) and oxidative phosphorylation (n=32, *p*=1.32E-19) which had z-scores of 2.2 and 5.7, suggesting activation, and mitochondrial dysfunction (n=41, *p*=2.05E-21), for which activity could not be predicted (**Figure 2C**). Whilst top canonical pathways for the dysregulated proteins in the control myotubes included ID1 signalling and IL-15 production, which are pathways known to be involved in muscle cell differentiation or skeletal muscle hypertrophy [40,41], the top canonical pathways for the dysregulated

proteins in the L-CMD myotubes included pathways associated with disease states including dilated cardiomyopathy signalling and mitochondrial dysfunction [42].

3.2. L-CMD myoblasts have a decreased proliferation rate and both myoblasts and myotubes exhibit nuclear morphology abnormalities

Next, we investigated the doubling time of each myoblast cell line, to determine the relevance of the finding described above that ten differentially abundant proteins in the L-CMD myoblast cell lines were associated with cell growth and proliferation canonical pathways. On average, the L-CMD myoblasts had a longer doubling time compared to the control cells during their exponential growth phase (36.24hrs vs 26.72 hrs, $p = 0.023$), indicating that the L-CMD cells had a decreased proliferation rate (**Figure 3A**). The quantitative proteomics analysis also identified that 32 proteins differentially abundant in the L-CMD myotubes compared to controls were associated with cell morphology. In culture, there were no obvious differences in the gross cellular morphology of L-CMD myoblasts compared to controls (**Supplementary File 1, Figures 1-2**). All L-CMD and control myoblasts appeared small and uniform in shape, except for the C5d control cell line which appeared to have slightly larger cells that were less uniform in shape, with some myoblasts appearing elongated. Across all cell lines, the myotubes also appeared similar in morphology when growing in culture (**Supplementary File 1, Figures 1-2**). Immunofluorescence microscopy analysis using DAPI nuclear staining, however, demonstrated that each of the L-CMD cell line myotubes exhibited disordered nuclei that did not all appear to fuse together properly and their placement within the myotube was more random and irregular compared to control myotube nuclei (**Figure 3B**). In contrast, control myotubes contained consistently fused nuclei that formed elongated, thick structures. In addition, some L-CMD myotubes were shorter, contained less nuclei or formed myotubes with “clumps” of nuclei which were not elongated.

To determine whether the L-CMD myoblasts used in this study also have nuclear morphology abnormalities, a classification method described previously by van Tienen *et al.* (2018) was used to analyse immunofluorescence microscopy images from L-CMD myoblast and myotube cultures [43]. Lamin A/C immunostaining in combination with DAPI allowed

the nuclear envelope and nuclear defects to be visualized more clearly than with DAPI alone. A representative example of each type of abnormality that was identified is given in **Figure 3C**. Approximately 49% and 50% of myoblast nuclei were classified as abnormal in the L380S and del.K32 L-CMD myoblasts, while 47% and 54% of the nuclei in the myotubes for the respective cell lines were abnormally shaped (**Figure 3D and E**). The R249W L-CMD cells exhibited an increased amount of abnormally shaped nuclei in myotubes (95%) compared to myoblasts (54%), suggesting that nuclear defects in this L-CMD cell line are exacerbated during differentiation (**Figure 3D and E**). In comparison, only 4% of control myoblasts had nuclear abnormalities, which is comparable to the previous study by van Tienen et al., where 4.8% of healthy cell nuclei were abnormal, and only 2% of control myotube nuclei appeared to have abnormalities (**Figure 3D and E**). Nuclear shape abnormalities (NSA) were the most frequent abnormalities seen across all three L-CMD myoblasts and myotubes, followed by blebs. L-CMD L380S myoblasts also exhibited many nuclei with donut shapes, which was not observed in the other L-CMD cell lines. In comparison to the L-CMD nuclei, the control cell nuclei were spherical or slightly oval, as expected.

3.3. Lamin A/C is reduced in expression in L-CMD myotubes compared to controls and is partially mislocalized in L-CMD del.K32 myoblasts

With lamin A/C having been identified by quantitative proteomics analysis as reduced in abundance in the L-CMD myotubes compared to controls (ratio=0.450, p=0.038), we next determined the relative levels of lamin A/C in myoblast and myotubes extracts using quantitative western blotting analysis. Quantitative western blotting analysis of myoblast cell extracts indicated slight, non-statistically significant reduction in lamin A, but not lamin C levels in the L-CMD cells compared to healthy controls (by 54.55%, p=0.244) (**Figure 4A &E**). The lamin A band exhibited a slightly faster electrophoretic mobility in the L-CMD myoblasts compared to control myoblasts (**Figure 4A & C**) that was not apparent in the myotube extracts (**Figure 4B**), where lamin A appeared to be of comparable molecular weight in the L-CMD and control samples. The lower molecular weight lamin A band in L-CMD myoblasts may indicate the presence of truncated lamin A in each of the L-CMD cell lines or a degraded form of mature lamin A, potentially due to lamin A being more unstable

in the L-CMD myoblasts. It was also observed that there were higher molecular weight lamin A bands that were present in addition to the lamin A bands at the expected molecular weight (70kDa) in C25 and C41 control myoblast samples, as well as in all of the control myotube samples. This could indicate the presence of pre-lamin A, which would have a slightly higher molecular weight than mature lamin A [44], however further experiments are needed to confirm this. In myotube extracts, both lamin A and C were reduced in the L-CMD cells vs controls (by 98.68%, p=0.044, and by 63.29%, p=0.043, respectively) (**Figure 4B & D)**.

With the observations of reduced levels of lamin A/C and differences in its molecular weight in L-CMD cells compared to controls, we next wished to determine whether lamin A/C is correctly localized in the L-CMD cells, which may help to gain insights into the cause and / or consequence of its reduced expression. In the L-CMD myoblasts harbouring the R249W and L380S mutations, lamin A/C was observed at the nuclear envelope, possibly with some diffuse lamin A/C immunoreactivity also in the nucleoplasm, to a greater extent than was evident in the control myoblasts (**Figure 4F & G**). Technically, this was unreliable to quantify, particularly in the R249W cell line, due to the abnormal nuclear morphologies causing wrinkling and invaginations around the nuclei. In the L-CMD del.K32 myoblasts, some lamin A/C was evident at the nuclear envelope, but most appeared to be present in nuclear aggregates within the nucleoplasm in all cells examined (out of 100 cells) (**Figure 4G**). This nuclear aggregation was not apparent in myotubes derived from the del.K32 cell line, and localization of lamin A/C in myotubes from the R249W and L380S cell lines also appeared to be relatively consistent with the distribution seen in healthy controls. To note, *LMNA* protein expression was not quantifiable using immunofluorescence microscopy and could not be compared to western blot analysis of total *LMNA* protein as samples were not imaged using consistent laser intensity.

3.4. Emerin is mislocalized to the cytoplasm in L-CMD R249W myoblasts and is reduced in expression in L-CMD myotubes compared to controls

The lamin A/C binding protein, emerin, was clearly localized at the nuclear envelope in all control myoblast and myotube cell lines examined, though some emerin was found to be mislocalized to the cytoplasm in approximately one third of the L-CMD myoblasts examined

that harboured the R249W mutation (**Figure 5A**). On average across the three L-CMD myoblast cell lines, emerin was not significantly different to controls (p=0.097) (**Figure 5B**). In L-CMD myotubes, emerin was, however, significantly reduced compared to controls (by 74.25%, p=0.040) (**Figure 5C**). An incidental finding, prompted by this observation, is that emerin expression generally appeared to be decreased on average by 81.37% in fully formed control myotubes, compared to their respective proliferating and differentiating myoblasts across six different cell lines. The most prominent reduction in emerin expression levels occurred between the second and third day (corresponding to timepoints 4 and 5) following differentiation initiation (timepoint 3) (**Supplementary File 1, Figure 3**). A similar pattern was noted in the L-CMD cell lines, albeit with emerin being less easily detectable at each timepoint examined (**Supplementary File 1, Figure 3**).

3.5. SUN2 was correctly localized at the nuclear envelope in L-CMD cells and reduced in expression in myotubes

SUN2 is a known interaction partner of lamin A at the INM (Crisp, et al., 2006), and is dependent on lamin A for its correct localization at the NE (Haque et al., 2010). SUN2 appeared to be correctly localised at the NE in the control and L-CMD myoblasts and myotubes, suggesting that the *LMNA* mutations harboured in the L-CMD cells do not affect SUN2 localization (**Figure 6A**). The intensity of SUN2 staining appeared reduced in L-CMD myoblasts and myotubes compared to control cells, when imaged using a consistent laser intensity (**Figure 6A**). When measured, it was found that in L-CMD myoblasts, SUN2 staining intensity was reduced by 32.23% compared to controls, but this reduction was not statistically significant (p= 0.439). In L-CMD myotubes, however, SUN2 staining was reduced by 85.35%, which was statistically significant (p= 0.010). Quantitative western blotting analysis confirmed this result, showing that SUN2 was not significantly different in expression in the L-CMD myoblasts compared to controls (p=0.401) (**Figure 6B)**. In the myotube samples, SUN2 was significantly reduced in L-CMD myotubes compared to controls (by 52.21%, p=0.049) (**Figure 6C)**.

4. Discussion

In the past couple of decades, quantitative proteomics has gained popularity as a useful method for identifying and quantifying all the proteins within a biological sample on a large-scale in an unbiased manner. Proteomic studies have advanced our understanding of cellular signalling networks and have improved diagnosis and molecular understanding of disease mechanisms. Comparison of the proteome of L-CMD cells to controls, a total of 124 differentially expressed proteins were identified in the L-CMD myoblasts, and 228 proteins were identified in the L-CMD myotubes, which could be potentially linked to the development of the disease. It was noted that there were more dysregulated proteins in the L-CMD myotubes than the L-CMD myoblasts, compared to controls, indicating that processes are potentially more impaired in L-CMD myotubes. There was also found to be very little cross over between the dysregulated proteins that were identified in the L-CMD myoblasts and myotubes. This implies the processes and signalling pathways that are dysregulated in L-CMD myoblasts and myotubes differ. This was substantiated by the finding that the molecular and cellular pathways and the canonical pathways associated with the dysregulated proteins were different for the L-CMD myoblasts and myotubes.

Several particularly interesting canonical pathways were found to be associated with the dysregulated proteins that were identified in the L-CMD myoblasts and myotubes. A substantial number of the dysregulated proteins in myotubes were linked to carbohydrate metabolism. The two major energy sources for muscle contraction are glycogen and fatty acids, whose metabolic pathways converge into actyl-CoA for final oxidation via the Krebs cycle and the respiratory chain, therefore carbohydrate metabolism is important for muscle function [45]. Metabolic dysfunction has been observed in Duchenne muscular dystrophy, and is characterised by reduced glycolytic and oxidative enzymes, decreased and abnormal mitochondria, decreased ATP, and increased oxidative stress [46–51]. However, alterations in carbohydrate metabolism are often associated with neuromuscular disorders [52], therefore it may not be a direct consequence of *LMNA* mutations in L-CMD, and instead may be a result of muscle damage or abnormal function. Interestingly the insulin secretion signalling pathway, which is also a component of carbohydrate metabolism, was additionally found to be upregulated in L-CMD myotubes compared to controls.

The synaptogenesis signalling pathway was found to be elevated in L-CMD myoblasts compared to controls. Synaptogenesis is the formation of synapses between neurons in the nervous system. NMJ defects have been previously observed in models of autosomal dominant Emery-Dreifuss muscular dystrophy (AD-EDMD), which, similarly to L-CMD, is caused by *LMNA* mutations [53]. Two AD-EDMD mouse models *($Lmna^{H222P/H222P}$, $Lmna^{-/-}$)* were found to show innervation defects including misexpression of electrical activity-dependent genes and altered epigenetic chromatin modifications, as well as aberrant NMJ architecture [53]. Considering these results, it is plausible to infer that NMJ defects contribute to L-CMD pathophysiology, though confirmation would further investigation.

Huntington's disease signalling was upregulated in L-CMD myotubes compared to controls, and upon further examination of the dysregulated proteins involved in this pathway, two proteins that are involved in apoptosis were of particular interest; apoptotic protease-activating factor 1 (Apaf-1) and caspase-7. Apoptosis dysregulation has been identified as a feature of a number of neurodegenerative diseases, including Huntington's disease [54–57] In L-CMD myoblasts, it was found that the necroptosis pathway, another method of cell death, was significantly downregulated. Necroptosis has been found to be of central pathophysiological relevance in a variety of disease states including myocardial infarction and stroke [58,59], atherosclerosis [60], ischemia-reperfusion injury [61,62], pancreatitis [63,64], inflammatory bowel diseases [65], as well as neurological disorders [66,67]. More recently, necroptosis has been implicated in neuromuscular diseases including Duchenne muscular dystrophy (DMD) and spinal muscular atrophy (SMA) [68,69]. Considering the necroptosis pathway's emerging role in neuromuscular conditions as well as identification of its dysregulation in L-CMD myoblasts, it merits further verification.

We found that L-CMD myoblasts had a significantly decreased proliferation rate compared to controls. Furthermore, cellular growth and proliferation as well as cell development were enriched canonical terms associated with the differentially expressed proteins that were identified in L-CMD myoblasts using quantitative proteomics. This may suggest that *in-vivo* myoblasts fail to proliferate adequately, which could consequently hinder muscle regeneration and repair, as myoblast proliferation is a key step in this process. This would

therefore impact L-CMD patients muscle integrity if it is subject to any damage or injury. For example, in models of other neuromuscular diseases, cell proliferation rate has previously been found to be altered compared to that of healthy controls. Satellite cells cultured from Duchenne muscular dystrophy patients (DMD) have been found to have an increased generation time, ceasing to proliferate beyond 100-1,000 cells, but still were capable of forming myotubes when differentiation was induced [70]. In a study on spinal muscular atrophy (SMA), C2C12 myoblasts with differing levels of survival motor neuron protein (*Smn*) knockdown have reduced proliferation as well as fusion defects, correlating with *Smn* levels [71]. These results suggest that increased doubling time of myoblasts could be related to neuromuscular disease pathology. The decreased proliferation rate observed in the L-CMD myoblasts could be a direct consequence of *LMNA* mutations, as cell proliferation rate has previously been shown to be altered when lamin A/C abundance is increased or decreased. The abundance of lamin A/C has been found to be downregulated in certain cancers, and depletion of lamin A/C abundance in healthy primary human fibroblasts leads to downregulation of the Rb family of tumor suppressors and a defect in cell proliferation [72]. Additionally, in prostate tumor cell lines (LNCaP, DU145, and PC3), small hairpin RNA knockdown of lamin A/C decreased cell proliferation, whilst overexpression of lamin A/C stimulated cell growth [73]. Despite these findings, here, we did not go on to observe a reduction in lamin A/C abundance in myoblasts, as would be expected if downregulation of lamin A/C decreases cell proliferation rate. However, another study on lamin A knockdown in lung carcinoma-derived A549 cells was also not found to perturb proliferation [74].

The nuclear morphology defects that were observed in the L-CMD cells are likely the consequences of a compromised NL in the cells. Abnormalities in nuclear structure are a well-known characteristic of *LMNA* mutations and have been previously observed in myoblasts from an Emery-Dreifuss muscular dystrophy (EDMD) patient with a confirmed *LMNA* mutation [75], myonuclei of muscle tissue from EDMD and Limb-Girdle (LGMD) muscular dystrophy patients carrying mutations in *LMNA* [76], as well as in skin fibroblasts from patients with a number of different laminopathies [77–80], and in myogenic cells derived from induced pluripotent stem cells (iPSCs) from patients with skeletal muscle laminopathies including L-CMD [81]. How this is linked to disease pathology has already been well-discussed in the form of the structural hypothesis, with the idea that *LMNA*

mutations lead to a weakened NL that results in the nucleus being unable to resist high mechanical strain in tissues exposed to tension, such as skeletal muscle [82]. Of the different types of nuclear deformities observed, the L380S myoblasts exhibited many more donut shaped nuclei compared to the other L-CMD cell lines. It has previously been demonstrated that treatment of primary human skin fibroblasts with protein farnesyltransferase inhibitors (FTIs) resulted in a high frequency of cells with donut shaped nuclei [83], suggesting that the *LMNA* L380S mutation may affect farnesylation of lamin A/C.

Across all L-CMD cell lines differentiated into myotubes, it was noticed that the nuclei within the myotubes were extremely disordered, which has previously been observed in del.K32 myotubes [84]. Curiously, we also found that SUN2 was significantly reduced in abundance across L-CMD myotubes. It has been found that *SUN1* and *SUN2* variants disrupt myonuclear organization, as it has been found that myotubes from a patient carrying *SUN1* mutations displayed defects in myonuclear organization [85]. As well as this, events required for correct myonuclear arrangement, such as absence of recruitment of pericentrin, a centrosomal marker, to the nuclear envelope, and impaired microtubule nucleation [85]. Thus, perhaps reduction of SUN2 is contributing to nuclear disorganization in L-CMD myotubes. It would be of interest to upregulate SUN2 expression in L-CMD myotubes to determine whether this rescues myonuclear organization disruption, and whether this has any other effects on L-CMD myotube differentiation.

Across all of the L-CMD cell lines, it was found that on average around half of the myoblast and myotube nuclei were irregularly shaped. For the L-CMD R249W cell line, though, almost all myotube nuclei exhibited abnormalities, meaning that the number of abnormal nuclei was almost doubled in R249W myotubes compared to myoblasts. This could suggest that nuclear abnormalities are exacerbated during differentiation in the R249W cells, which has not previously been described. Some emerin was also found to be mislocalized to the cytoplasm, perhaps specifically the ER, in R249W myoblasts, and not in any other L-CMD cells. This may suggest that the R249W mutation in particular may cause more severe nuclear defects. Emerin was found to be correctly localized in R249W myotubes, however, maybe not supporting the finding that nuclear defects are worsened in R249W myotubes. Previously, emerin has been found to mislocalize and aggregate in foci in iPSC-derived myoblasts and the cytoplasm of C2C12 myoblasts harbouring R249W mutations [81,86].

Emerin has been identified as a well-characterised binding partner of lamin A/C, [13], and it has been found that lamin A is involved in tethering emerin to the NE [87]. Consequently, mutations in *LMNA* may disrupt this interaction and cause emerin to become mislocalized. Here, even when some emerin was mislocalized in the R249W myoblasts, there remained proportion of emerin that was correctly localized to the NE. This result suggests that lamin A-emerin interactions are not entirely lost and are merely compromised by the *LMNA* mutation. Loss of emerin from the NE could have implications in L-CMD disease development, as correct localization is critical for a protein's function [88]. If a protein is in the wrong environment, it is unlikely to fold or assemble properly, and may also trigger secondary consequences such as protein degradation pathways, that could lead to further detrimental effects inside of the cell [88]. Although emerin was only mislocalized in one L-CMD cell line, a reduction in emerin protein expression was observed across all L-CMD cell lines in myotubes compared to controls. It has previously been shown that mutant forms of emerin causing X-linked Emery-Dreifuss muscular dystrophy (EDMD) are mislocalised, and it has been proposed that an absence (caused by mutations that result in the deletion of *EMD*) or reduction of emerin at the NE may be responsible for the EDMD phenotype [89]. It has also been found that COS-7 cells expressing mutant emerin (Del236-241, an *EMD* variant found in EDMD patients) that mainly localizes to the cytoplasm exhibit aberrant cell cycle length [90]. Considering this has been linked to EDMD development, loss of emerin at the NE could also be contributing to L-CMD pathophysiology. This provides evidence that there may be some cross-over between the mechanisms behind EDMD and L-CMD disease pathways. This potentially can be expected as AD and AR-EDMD are also caused by *LMNA* mutations.

Whilst emerin was found to be mislocalized in the R249W myoblasts, the del.K32 myoblasts were the only cells to exhibit mislocalization of lamin A/C. In the del.K32 myoblasts, lamin A/C appeared to be aggregated in nuclear foci within the nucleoplasm. Increased nucleoplasmic aggregation of lamin A/C has been previously observed in L-CMD fibroblasts harbouring the same del.K32 mutation, as well as primary myoblasts derived from the *Lmna*^{dK32} mouse model of L-CMD [84]. In this study, myotubes harbouring the del.K32 mutation were also found to have almost exclusively nucleoplasmic localization of lamin A/C, although this was not observed here [84]. In the Bertrand *et al.* study, del.K32 myotubes were also found to have disrupted localization of other INM proteins such as

emerin, lamin B1, SUN2 or nup153 (further information on where these proteins were mislocalized to is not provided), proving nuclear defects in cells harbouring the del.K32 *LMNA* mutation can also be severe [84]. Absence of lamin A/C from the nuclear periphery and its accumulation in the nucleoplasm has been shown to be highly detrimental for myoblast differentiation in primary myoblasts derived from the *Lmna*^{dK32} mouse [91]. This has been attributed to the inability of L-CMD post-mitotic myocytes to sequester muscle-specific NE transmembrane proteins in the nuclear envelope that are required for chromatin remodelling [91]. Depending on their level of phosphorylation, A-type lamins are able to assemble under the INM (where they are primarily localized), but they may also reside in the nucleoplasm [92]. A-type lamins at the nuclear periphery are necessary for the nuclear sequestration of NE transmembrane proteins [93–96], and for the interaction with the cytoskeleton via the LINC complex [97]. Other A-type lamin functions such as the regulation of gene transcription, DNA repair, and regulation of cell cycle and mechanotransduction also require lamin A/C to be correctly localized at the NL [98–100].

Based on the evidence outlined above, it appeared that cells harbouring the R249W or del.K32 mutations had different nuclear defects than the L380S L-CMD patient cells. This could be a consequence of the region of the *LMNA* gene that is affected by the mutations. The R249W mutation is located at the ERK1/2 binding domain in *LMNA* and causes an arginine residue to be substituted with a tryptophan residue. Arginine and tryptophan have very different properties. Arginine is amphipathic, whilst tryptophan in comparison is extremely hydrophobic in nature [101].Arginine is known to be common in binding sites, therefore, if arginine is substituted with another amino acid with different properties, this may affect interactions at these domains. The del.K32 mutation causes an in-frame deletion affecting a lysine residue. Similarly, to arginine, lysine is also commonly found in protein binding sites [101] .The del.K32 variant is located in the head region of lamin A/C, which is known to be involved in lamin assembly. Consequently, mutations in this region may particularly lead to nuclear assembly defects. The L380S mutation affects the HCD2 (highly conserved domain) region of *LMNA*, located at the end of the central rod domain, next to coil 2.

Lamin A/C were found to be significantly reduced across L-CMD myotubes compared to controls. This reduction in lamin A/C expression could be linked to the nucleoplasmic aggregation of lamin A/C observed in the del.K32 myoblasts, as this may indicate lamin A/C is unstable and could lead to increased degradation of the protein. In myoblasts and myotubes derived from *Lmna*$^{\Delta K32/\Delta K32}$ mice, a mouse model of L-CMD, reduced levels of lamin A/C protein have also been observed, although *LMNA* mRNA levels were not reduced, suggesting a reduced translation efficiency or higher rate of degradation of mutant lamin A/C [91]. Reduced lamin A/C levels could likely contribute to the L-CMD phenotype, as *Lmna*$^{\Delta K32/\Delta K32}$ mice present with an even more severe phenotype than *Lmna*$^{-/-}$ mice (a lamin A/C deficient mouse model of AD-EDMD) [91]. Whilst *Lmna*$^{-/-}$ mice present with growth retardation, skeletal and cardiac muscle involvement, hypoglycemia and sudden cardiac death, this phenotype was exacerbated in *Lmna*$^{\Delta K32/\Delta K32}$ mice [91]. The result presented here that lamin A/C were reduced across all myotubes differentiated from each of the L-CMD cell lines harbouring different *LMNA* mutations corroborates Bertrand *et al.*'s findings and suggests reduced lamin A/C may be conserved across different L-CMD-causing mutations. This finding may help to guide future research in L-CMD, as a therapeutic approach could be to upregulate lamin A/C production. Based on the finding that lamin A/C is reduced in *Lmna*$^{\Delta K32/\Delta K32}$ mice, spliceosome-mediated RNA trans-splicing (SMaRT), an approach that targets RNA at the pre-mRNA level and converts endogenous mutated sequences into wild type ones has already been used to target the del.K32 L-CMD mutation [102]. To achieve this, 5'-RNA pre-*trans*-splicing molecules containing the first five exons of *Lmna* and targeting intron 5 of *Lmna* pre-mRNA were developed and their efficacy at inducing *trans*-splicing events on *Lmna* were tested and confirmed at the protein level in C2C12 myoblasts [102]. This approach was then tested *in-vivo* in newborn mice using adeno-associated virus (AAV) delivery, although the efficacy of *trans*-splicing events were low [102]. Despite this, these results provide the first evidence for reprogramming *LMNA* mRNA in vitro.

Conclusion

By conducting a quantitative comparison of the proteome of L-CMD myoblasts and myotubes and healthy control cells, a number of differentially expression proteins have

been identified as well as potential dysregulation of a number of different molecular and cellular processes and signalling pathways. Amongst these, molecular and cellular processes common to the dysregulated proteins included cellular development, cell cycle, and cellular growth and repair. Upon this discovery, further examination of L-CMD myoblasts and myotubes revealed defects in cell proliferation, as well as nuclear morphology abnormalities. In addition to this, reduction of lamin A/C protein expression levels, and lamin A/C binding partners, emerin and SUN2 were observed across all L-CMD myotubes. In del.K32 myoblasts, lamin A/C was found to aggregate in the nucleoplasm, and in R249W myoblasts emerin was mislocalized. Proteomic analysis also revealed a number of canonical pathways that may be dysregulated including the insulin signalling pathway and Huntington's disease pathway in L-CMD myotubes, and the synaptogenesis and necroptosis signalling pathway in L-CMD myoblasts, which require verification and further investigation in future studies. The defects that were identified across the L-CMD cell lines may be associated with L-CMD pathophysiology, and might represent targets for the development of therapies. In future, it is important to study a greater number of cell lines harbouring the same mutations as the L-CMD cell lines used in this study, as well as different L-CMD causing mutations to determine whether the defects identified across the L-CMD cell lines are conserved features of L-CMD. Comparison of the proteomics data within this study with data from other published *LMNA* transcriptomic and proteomic datasets will also be useful to support the identification of potentially conserved changes to molecular pathways in L-CMD.

Supplementary Material

Supplementary File 1 (Word document containing Tables 1-3, and Figures 1 and 2)

Supplementary File 2 (Excel document containing supplementary Tables 1-4)

Data Availability Statement

The mass spectrometry proteomic data can be accessed for reviewing purposes at XXXXX

Following publication, the mass spectrometry proteomic data can be accessed at the following DOI: XXXX

Funding

This work was supported by funding from the EPSRC/MRC Doctoral Training Centre in Regenerative Medicine (Loughborough, Keele and Nottingham Universities);
Keele ACORN scheme, Keele University, UK; and the Orthopaedic Institute Ltd., RJAH Orthopaedic Hospital, Oswestry, UK (grant number RPG182). The Fusion Lumos mass spectrometer was purchased by BBSRC grant number BB/T017686/1

Conflicts of interest

The authors declare no conflict of interest.

Acknowledgements

We are grateful to The Platform for Immortalization of Human Cells, Institute of Myology, Paris, France, for providing the immortalized human myoblasts. The authors are particularly thankful to Professor Glenn Morris for his insight and advice during the preparation of this manuscript.

References

[1] Avila GM, González AP, Abad A, Fournier BG, León SR, Corral JAM, et al. Is the Next Generation Sequencing the Essential Tool for the Early Diagnostic Approach in Congenital Muscular Dystrophy? New Mutation in the Gene LMNA Associated with Serious Phenotype. Neurol India 2021;69:1835–7. https://doi.org/10.4103/0028-3886.333448.

[2] Hattori A, Komaki H, Kawatani M, Sakuma H, Saito Y, Nakagawa E, et al. A novel mutation in the LMNA gene causes congenital muscular dystrophy with dropped head and brain involvement. Neuromuscul Disord 2012;22:149–51.

[3] Quijano-Roy S, Mbieleu B, Bönnemann CG, Jeannet P-Y, Colomer J, Clarke NF, et al. De novo *LMNA* mutations cause a new form of congenital muscular dystrophy. Ann Neurol 2008;64:177–86. https://doi.org/10.1002/ana.21417.

[4] Ben Yaou R, Yun P, Dabaj I, Norato G, Donkervoort S, Xiong H, et al. International retrospective natural history study of LMNA-related congenital muscular dystrophy. Brain Commun 2021;3. https://doi.org/10.1093/braincomms/fcab075.

[5] Bonati U, Bechtel N, Heinimann K, Rutz E, Schneider J, Frank S, et al. Congenital muscular dystrophy with dropped head phenotype and cognitive impairment due to a novel mutation in the LMNA gene. Neuromuscular Disorders 2014;24:529–32. https://doi.org/10.1016/j.nmd.2014.02.004.

[6] Pasqualin LMA, Reed UC, Costa TVMM, Quedas E, Albuquerque MA V, Resende MBD, et al. Congenital muscular dystrophy with dropped head linked to the LMNA gene in a Brazilian cohort. Pediatr Neurol 2014;50:400–6.

[7] Karaoglu P, Quizon N, Pergande M, Wang H, Polat AI, Ersen A, et al. Dropped head congenital muscular dystrophy caused by de novo mutations in LMNA. Brain Dev 2017;39:361–4.

[8] Taddei A, Hediger F, Neumann FR, Gasser SM. The function of nuclear architecture: a genetic approach. Annu Rev Genet 2004;38:305–45. https://doi.org/10.1146/annurev.genet.37.110801.142705.

[9] Bridger JM, Foeger N, Kill IR, Herrmann H. The nuclear lamina. Both a structural framework and a platform for genome organization. FEBS J 2007;274:1354–61.

[10] Aebi U, Cohn J, Buhle L, Gerace L. The nuclear lamina is a meshwork of intermediate-type filaments. Nature 1986 323:6088 1986;323:560–4. https://doi.org/10.1038/323560a0.

[11] Crisp M, Liu Q, Roux K, Rattner JB, Shanahan C, Burke B, et al. Coupling of the nucleus and cytoplasm: Role of the LINC complex. J Cell Biol 2006;172:41–53. https://doi.org/10.1083/jcb.200509124.

[12] Haque F, Mazzeo D, Patel JT, Smallwood DT, Ellis JA, Shanahan CM, et al. Mammalian SUN protein interaction networks at the inner nuclear membrane and their role in laminopathy disease processes. Journal of Biological Chemistry 2010;285:3487–98. https://doi.org/10.1074/jbc.M109.071910.

[13] Clements L, Manilal S, Love DR, Morris GE. Direct interaction between emerin and lamin A. Biochem Biophys Res Commun 2000;267:709–14. https://doi.org/10.1006/bbrc.1999.2023.

[14] Gonzàlez JM, Navarro-Puche A, Casar B, Crespo P, Andrès V. Fast regulation of AP-1 activity through interaction of lamin A/C, ERK1/2, and c-Fos at the nuclear envelope. Journal of Cell Biology 2008;183:653–66. https://doi.org/10.1083/JCB.200805049.

[15] Moiseeva O, Bourdeau V, Vernier M, Dabauvalle MC, Ferbeyre G. Retinoblastoma-independent regulation of cell proliferation and senescence by the p53–p21 axis in lamin A/C-depleted cells. Aging Cell 2011;10:789–97. https://doi.org/10.1111/J.1474-9726.2011.00719.X.

[16] Swift J, Ivanovska IL, Buxboim A, Harada T, Dingal PCDP, Pinter J, et al. Nuclear lamin-A scales with tissue stiffness and enhances matrix-directed differentiation. Science (1979) 2013;341:1240104. https://doi.org/10.1126/science.1240104.

[17] Frock RL, Kudlow BA, Evans AM, Jameson SA, Hauschka SD, Kennedy BK. Lamin A/C and emerin are critical for skeletal muscle satellite cell differentiation. Genes Dev 2006;20:486–500. https://doi.org/10.1101/gad.1364906.

[18] Constantinescu D, Gray HL, Sammak PJ, Schatten GP, Csoka AB. Lamin A/C Expression Is a Marker of Mouse and Human Embryonic Stem Cell Differentiation. Stem Cells 2006;24:177–85. https://doi.org/10.1634/stemcells.2004-0159.

[19] Earle AJ, Kirby TJ, Fedorchak GR, Isermann P, Patel J, Iruvanti S, et al. Mutant lamins cause nuclear envelope rupture and DNA damage in skeletal muscle cells. Nat Mater 2020;19:464–73. https://doi.org/10.1038/s41563-019-0563-5.

[20] Maynard S, Keijzers G, Akbari M, Ezra M Ben, Hall A, Morevati M, et al. Lamin A/C promotes DNA base excision repair. Nucleic Acids Res 2019;47:11709–28.

[21] Barateau A, Vadrot N, Vicart P, Ferreiro A, Mayer M, Héron D, et al. A Novel Lamin A Mutant Responsible for Congenital Muscular Dystrophy Causes Distinct Abnormalities of the Cell Nucleus. PLoS One 2017;12:e0169189. https://doi.org/doi.org/10.1371/journal.pone.0169189.

[22] Barateau A, Vadrot N, Agbulut O, Vicart P, Batonnet-Pichon S, Buendia B. Distinct Fiber Type Signature in Mouse Muscles Expressing a Mutant Lamin A Responsible for Congenital Muscular Dystrophy in a Patient. Cells 2017;6.

[23] Gómez-Domínguez D, Epifano C, Miguel F de, Castaño AG, Vilaplana-Martí B, Martín A, et al. Consequences of Lmna Exon 4 Mutations in Myoblast Function. Cells 2020;9:1286. https://doi.org/10.3390/cells9051286.

[24] Bertrand AT, Brull A, Azibani F, Benarroch L, Chikhaoui K, Stewart CL, et al. Lamin A/C Assembly Defects in LMNA -Congenital Muscular Dystrophy Is Responsible for the Increased Severity of the Disease Compared with Emery-Dreifuss Muscular Dystrophy. Cells 2020;9:844. https://doi.org/doi.org/10.3390/cells9040844.

[25] Owens DJ, Messéant J, Moog S, Viggars M, Ferry A, Mamchaoui K, et al. Lamin-Related Congenital Muscular Dystrophy Alters Mechanical Signaling and Skeletal Muscle Growth. Int J Mol Sci 2020;22:306. https://doi.org/10.3390/ijms22010306.

[26] Owens DJ, Fischer M, Jabre S, Moog S, Mamchaoui K, Butler-Browne G, et al. Lamin Mutations Cause Increased YAP Nuclear Entry in Muscle Stem Cells. Cells 2020;9.

[27] Storey EC, Fuller HR. Genotype-Phenotype Correlations in Human Diseases Caused by Mutations of LINC Complex-Associated Genes: A Systematic Review and Meta-Summary. Cells 2022;11:4065. https://doi.org/10.3390/CELLS11244065/S1.

[28] Lefebvre S, Bürglen L, Reboullet S, Clermont O, Burlet P, Viollet L, et al. Identification and characterization of a spinal muscular atrophy-determining gene. Cell 1995;80:155–65. https://doi.org/10.1016/0092-8674(95)90460-3.

[29] Ramdas S, Servais L. New treatments in spinal muscular atrophy: an overview of currently available data. Expert Opin Pharmacother 2020;21:307–15. https://doi.org/10.1080/14656566.2019.1704732.

[30] Bertrand AT, Ziaei S, Ehret C, Duchemin H, Mamchaoui K, Bigot A, et al. Cellular microenvironments reveal defective mechanosensing responses and elevated YAP signaling in LMNA-mutated muscle precursors. J Cell Sci 2014;127:2873–84. https://doi.org/doi.org/10.1242/jcs.144907.

[31] Mamchaoui K, Trollet C, Bigot A, Negroni E, Chaouch S, Wolff A, et al. Immortalized pathological human myoblasts: Towards a universal tool for the study of neuromuscular disorders. Skelet Muscle 2011. https://doi.org/10.1186/2044-5040-1-34.

[32] Laemmli UK. Cleavage of structural proteins during the assembly of the head of bacteriophage T4. Nature 1970;227:680–5. https://doi.org/10.1038/227680a0.

[33] Welinder C, Ekblad L. Coomassie staining as loading control in Western blot analysis. J Proteome Res 2011;10:1416–9. https://doi.org/10.1021/pr1011476.

[34] Towbin H, Staehelin T, Gordon J. Electrophoretic transfer of proteins from polyacrylamide gels to nitrocellulose sheets: Procedure and some applications. Proc Natl Acad Sci U S A 1979;76:4350–4. https://doi.org/10.1073/pnas.76.9.4350.

[35] Manilal S, Randles KN, Aunac C, Thi Man N, Morris GE. A lamin A/C beta-strand containing the site of lipodystrophy mutations is a major surface epitope for a new panel of monoclonal antibodies. Biochim Biophys Acta Gen Subj 2004;1671. https://doi.org/10.1016/j.bbagen.2004.01.008.

[36] Manilal S, Sewry CA, Pereboev A, Thi Man N, Gobbi P, Hawkes S, et al. Distribution of emerin and lamins in the heart and implications for Emery-Dreifuss muscular dystrophy. Hum Mol Genet 1999;8:353–9. https://doi.org/10.1093/HMG/8.2.353.

[37] Manilal S, Nguyen TM, Sewry CA, Morris GE. The Emery-Dreifuss muscular dystrophy protein, emerin, is a nuclear membrane protein. Hum Mol Genet 1996;5:801–8. https://doi.org/10.1093/hmg/5.6.801.

[38] Sheffield J. ImageJ, A Useful Tool for Biological Image Processing and Analysis. Microscopy and Microanalysis 2007;13:200–1. https://doi.org/10.1017/S1431927607076611.

[39] Reiter L, Rinner O, Picotti P, Hüttenhain R, Beck M, Brusniak M-Y, et al. mProphet : A general and flexible data model and algorithm for automated SRM data processing and statistical error estimation. Nat Methods 2011;8.

[40] Jen Y, Weintraub H, Benezra R. Overexpression of Id protein inhibits the muscle differentiation program: In vivo association of Id with E2A proteins. Genes Dev 1992;6:1466–79. https://doi.org/10.1101/gad.6.8.1466.

[41] Quinn LBS, Anderson BG, Drivdahl RH, Alvarez B, Argilés JM. Overexpression of interleukin-15 induces skeletal muscle hypertrophy in vitro: Implications for treatment of muscle wasting disorders. Exp Cell Res 2002;280:55–63. https://doi.org/10.1006/excr.2002.5624.

[42] Pieczenik SR, Neustadt J. Mitochondrial dysfunction and molecular pathways of disease. Exp Mol Pathol 2007;83:84–92. https://doi.org/10.1016/j.yexmp.2006.09.008.

[43] van Tienen FHJ, Lindsey PJ, Kamps MAF, Krapels IP, Ramaekers FCS, Brunner HG, et al. Assessment of fibroblast nuclear morphology aids interpretation of LMNA variants. European Journal of Human Genetics 2018;27:389–99. https://doi.org/10.1038/s41431-018-0294-0.

[44] Sinensky M, Fantle K, Trujillo M, McLain T, Kupfer A, Dalton M. The processing pathway of prelamin A. J Cell Sci 1994;107:61–7. https://doi.org/10.1242/JCS.107.1.61.

[45] Hill AV. Muscular activity and carbohydrate metabolism. Science (1979) 1924;60:505–14. https://doi.org/10.1126/SCIENCE.60.1562.505.

[46] Schneider SM, Sridhar V, Bettis AK, Heath-Barnett H, Balog-Alvarez CJ, Guo LJ, et al. Glucose Metabolism as a Pre-clinical Biomarker for the Golden Retriever Model of Duchenne Muscular Dystrophy. Mol Imaging Biol 2018;20:780–8. https://doi.org/10.1007/S11307-018-1174-2/FIGURES/5.

[47] Nghiem PP, Bello L, Stoughton WB, López SM, Vidal AH, Hernandez B V., et al. Changes in Muscle Metabolism are Associated with Phenotypic Variability in Golden Retriever Muscular Dystrophy. Yale J Biol Med 2017;90:351.

[48] Timpani CA, Hayes A, Rybalka E. Revisiting the dystrophin-ATP connection: How half a century of research still implicates mitochondrial dysfunction in Duchenne Muscular Dystrophy aetiology. Med Hypotheses 2015;85:1021–33. https://doi.org/10.1016/J.MEHY.2015.08.015.

[49] Onopiuk M, Brutkowski W, Wierzbicka K, Wojciechowska S, Szczepanowska J, Fronk J, et al. Mutation in dystrophin-encoding gene affects energy metabolism in mouse myoblasts. Biochem Biophys Res Commun 2009;386:463–6. https://doi.org/10.1016/J.BBRC.2009.06.053.

[50] Sharma U, Atri S, Sharma MC, Sarkar C, Jagannathan NR. Skeletal muscle metabolism in Duchenne muscular dystrophy (DMD): an in-vitro proton NMR spectroscopy study. Magn Reson Imaging 2003;21:145–53. https://doi.org/10.1016/S0730-725X(02)00646-X.

[51] Chi MMY, Hintz CS, McKee D, Felder S, Grant N, Kaiser KK, et al. Effect of Duchenne muscular dystrophy on enzymes of energy metabolism in individual muscle fibers. Metabolism 1987;36:761–7. https://doi.org/10.1016/0026-0495(87)90113-2.

[52] Martin PT, Freeze HH. Glycobiology of neuromuscular disorders. Glycobiology 2003;13:67R-75R. https://doi.org/10.1093/GLYCOB/CWG077.

[53] Méjat A, Decostre V, Li J, Renou L, Kesari A, Hantaï D, et al. Lamin A/C-mediated neuromuscular junction defects in Emery-Dreifuss muscular dystrophy. J Cell Biol 2009;184:31–44. https://doi.org/10.1083/jcb.200811035.

[54] Sang TK, Li C, Liu W, Rodriguez A, Abrams JM, Zipursky SL, et al. Inactivation of Drosophila Apaf-1 related killer suppresses formation of polyglutamine aggregates and blocks polyglutamine pathogenesis. Hum Mol Genet 2005;14:357–72. https://doi.org/10.1093/hmg/ddi032.

[55] Hickey MA, Chesselet MF. Apoptosis in Huntington's disease. Prog Neuropsychopharmacol Biol Psychiatry 2003;27:255-. https://doi.org/10.1016/S0278-5846(03)00021-6.

[56] Yang D, Wang CE, Zhao B, Li W, Ouyang Z, Liu Z, et al. Expression of Huntington's disease protein results in apoptotic neurons in the brains of cloned transgenic pigs. Hum Mol Genet 2010;19:3983–94. https://doi.org/10.1093/hmg/ddq313.

[57] Vis JC, Schipper E, de Boer-van H, Verbeek MM, de Waal RMW, Wesseling P, et al. Expression pattern of apoptosis-related markers in Huntington's disease. Acta Neuropathol 2005;109:321–8. https://doi.org/10.1007/s00401-004-0957-5.

[58] Degterev A, Hitomi J, Germscheid M, Ch'en IL, Korkina O, Teng X, et al. Identification of RIP1 kinase as a specific cellular target of necrostatins. Nat Chem Biol 2008;4:313–21. https://doi.org/10.1038/nchembio.83.

[59] Smith CCT, Davidson SM, Lim SY, Simpkin JC, Hothersall JS, Yellon DM. Necrostatin: A potentially novel cardioprotective agent? Cardiovasc Drugs Ther 2007;21:227–33. https://doi.org/10.1007/s10557-007-6035-1.

[60] Lin J, Li H, Yang M, Ren J, Huang Z, Han F, et al. A Role of RIP3-Mediated Macrophage Necrosis in Atherosclerosis Development. Cell Rep 2013;3:200–10. https://doi.org/10.1016/j.celrep.2012.12.012.

[61] Linkermann A, Bräsen JH, Himmerkus N, Liu S, Huber TB, Kunzendorf U, et al. Rip1 (Receptor-interacting protein kinase 1) mediates necroptosis and contributes to renal ischemia/reperfusion injury. Kidney Int 2012;81:751–61. https://doi.org/10.1038/ki.2011.450.

[62] Oerlemans MIFJ, Liu J, Arslan F, Den Ouden K, Van Middelaar BJ, Doevendans PA, et al. Inhibition of RIP1-dependent necrosis prevents adverse cardiac remodeling after myocardial ischemia-reperfusion in vivo. Basic Res Cardiol 2012;107:207. https://doi.org/10.1007/s00395-012-0270-8.

[63] Zhang DW, Shao J, Lin J, Zhang N, Lu BJ, Lin SC, et al. RIP3, an energy metabolism regulator that switches TNF-induced cell death from apoptosis to necrosis. Science (1979) 2009;325:332–6. https://doi.org/10.1126/science.1172308.

[64] Wu J, Huang Z, Ren J, Zhang Z, He P, Li Y, et al. Mlkl knockout mice demonstrate the indispensable role of Mlkl in necroptosis. Cell Res 2013;23:994–1006. https://doi.org/10.1038/cr.2013.91.

[65] Welz PS, Wullaert A, Vlantis K, Kondylis V, Fernández-Majada V, Ermolaeva M, et al. FADD prevents RIP3-mediated epithelial cell necrosis and chronic intestinal inflammation. Nature 2011;477:330–4. https://doi.org/10.1038/nature10273.

[66] Ito Y, Ofengeim D, Najafov A, Das S, Saberi S, Li Y, et al. RIPK1 mediates axonal degeneration by promoting inflammation and necroptosis in ALS. Science (1979) 2016;353:603–8. https://doi.org/10.1126/science.aaf6803.

[67] Zhang S, Su Y, Ying Z, Guo D, Pan C, Guo J, et al. RIP1 kinase inhibitor halts the progression of an immune-induced demyelination disease at the stage of monocyte elevation. Proc Natl Acad Sci U S A 2019;116:5675–80. https://doi.org/10.1073/pnas.1819917116.

[68] Chehade L, Deguise MO, De Repentigny Y, Yaworski R, Beauvais A, Gagnon S, et al. Suppression of the necroptotic cell death pathways improves survival in Smn2B/− mice. Front Cell Neurosci 2022;16:408. https://doi.org/doi.org/10.3389/fncel.2022.972029.

[69] Bencze M, Meng J, Pini V, Conti F, Muntoni F, Morgan J. Necroptosis, a programmed form of necrosis, participates in muscle degeneration in Duchenne muscular dystrophy. Neuromuscular Disorders 2017;27:S98. https://doi.org/10.1016/j.nmd.2017.06.029.

[70] Blau HM, Webster C, Pavlath GK. Defective myoblasts identified in Duchenne muscular dystrophy. Proceedings of the National Academy of Sciences 1983;80:4856–60. https://doi.org/10.1073/PNAS.80.15.4856.

[71] Shafey D, Côté PD, Kothary R. Hypomorphic Smn knockdown C2C12 myoblasts reveal intrinsic defects in myoblast fusion and myotube morphology. Exp Cell Res 2005;311:49–61. https://doi.org/10.1016/J.YEXCR.2005.08.019.

[72] Moiseeva O, Bourdeau V, Vernier M, Dabauvalle MC, Ferbeyre G. Retinoblastoma-independent regulation of cell proliferation and senescence by the p53–p21 axis in lamin A/C-depleted cells. Aging Cell 2011;10:789–97. https://doi.org/10.1111/J.1474-9726.2011.00719.X.

[73] Kong L, Schäfer G, Bu H, Zhang Y, Zhang Y, Klocker H. Lamin A/C protein is overexpressed in tissue-invading prostate cancer and promotes prostate cancer cell growth, migration and invasion through the PI3K/AKT/PTEN pathway. Carcinogenesis 2012;33:751–9. https://doi.org/10.1093/CARCIN/BGS022.

[74] Harada T, Swift J, Irianto J, Shin JW, Spinler KR, Athirasala A, et al. Nuclear lamin stiffness is a barrier to 3D migration, but softness can limit survival. Journal of Cell Biology 2014;204:669–82. https://doi.org/10.1083/JCB.201308029.

[75] Kandert S, Wehnert M, Müller CR, Buendia B, Dabauvalle M-C. Impaired nuclear functions lead to increased senescence and inefficient differentiation in human myoblasts with a dominant p.R545C mutation in the LMNA gene. Eur J Cell Biol 2009;88:593–608.

[76] Park Y-E, Hayashi YK, Goto K, Komaki H, Hayashi Y, Inuzuka T, et al. Nuclear changes in skeletal muscle extend to satellite cells in autosomal dominant Emery-Dreifuss muscular dystrophy/limb-girdle muscular dystrophy 1B. Neuromuscul Disord 2009;19:29–36. https://doi.org/10.1016/j.nmd.2008.09.018.

[77] Muchir A, Medioni J, Laluc M, Massart C, Arimura T, van der Kooi AJ, et al. Nuclear envelope alterations in fibroblasts from patients with muscular dystrophy, cardiomyopathy, and partial lipodystrophy carrying lamin A/C gene mutations. Muscle Nerve 2004;30:444–50. https://doi.org/10.1002/mus.20122.

[78] Favreau C, Dubosclard E, Östlund C, Vigouroux C, Capeau J, Wehnert M, et al. Expression of lamin A mutated in the carboxyl-terminal tail generates an aberrant nuclear phenotype similar to that observed in cells from patients with Dunnigan-type partial lipodystrophy and Emery-Dreifuss muscular dystrophy. Exp Cell Res 2003;282:14–23. https://doi.org/10.1006/EXCR.2002.5669.

[79] Muchir A, van Engelen BG, Lammens M, Mislow JM, McNally E, Schwartz K, et al. Nuclear envelope alterations in fibroblasts from LGMD1B patients carrying nonsense Y259X

heterozygous or homozygous mutation in lamin A/C gene. Exp Cell Res 2003;291:352–62. https://doi.org/10.1016/j.yexcr.2003.07.002.

[80] Vigouroux C, Auclair M, Dubosclard E, Pouchelet M, Capeau J, Courvalin JC, et al. Nuclear envelope disorganization in fibroblasts from lipodystrophic patients with heterozygous R482Q/W mutations in the lamin A/C gene. J Cell Sci 2001;114:4459–68. https://doi.org/10.1242/jcs.114.24.4459.

[81] Steele-Stallard HB, Pinton L, Sarcar S, Ozdemir T, Maffioletti SM, Zammit PS, et al. Modeling Skeletal Muscle Laminopathies Using Human Induced Pluripotent Stem Cells Carrying Pathogenic LMNA Mutations. Front Physiol 2018;9:1332.

[82] Davidson PM, Lammerding J. Broken nuclei – lamins, nuclear mechanics, and disease. Trends Cell Biol 2014;24:247–56. https://doi.org/10.1016/j.tcb.2013.11.004.

[83] Verstraeten VLRM, Peckham LA, Olive M, Capell BC, Collins FS, Nabel EG, et al. Protein farnesylation inhibitors cause donut-shaped cell nuclei attributable to a centrosome separation defect. Proc Natl Acad Sci U S A 2011;108. https://doi.org/10.1073/pnas.1019532108.

[84] Bertrand AT, Brull A, Azibani F, Benarroch L, Chikhaoui K, Stewart CL, et al. Lamin A/C Assembly Defects in LMNA -Congenital Muscular Dystrophy Is Responsible for the Increased Severity of the Disease Compared with Emery-Dreifuss Muscular Dystrophy. Cells 2020;9.

[85] Meinke P, Mattioli E, Haque F, Antoku S, Columbaro M, Straatman KR, et al. Muscular Dystrophy-Associated SUN1 and SUN2 Variants Disrupt Nuclear-Cytoskeletal Connections and Myonuclear Organization. PLoS Genet 2014;10:e1004605. https://doi.org/10.1371/journal.pgen.1004605.

[86] Gómez-Domínguez D, Epifano C, Miguel F de, Castaño AG, Vilaplana-Martí B, Martín A, et al. Consequences of Lmna Exon 4 Mutations in Myoblast Function. Cells 2020;9.

[87] Vaughan OA, Alvarez-Reyes M, Bridger JM, Broers JLV, Ramaekers FCS, Wehnert M, et al. Both emerin and lamin C depend on lamin A for localization at the nuclear envelope. J Cell Sci 2001;114:2577–90. https://doi.org/10.1242/jcs.114.14.2577.

[88] Hegde RS, Zavodszky E. Recognition and Degradation of Mislocalized Proteins in Health and Disease. Cold Spring Harb Perspect Biol 2019;11:a033902. https://doi.org/10.1101/CSHPERSPECT.A033902.

[89] Fairley EA, Kendrick-Jones J, Ellis JA. The Emery-Dreifuss muscular dystrophy phenotype arises from aberrant targeting and binding of emerin at the inner nuclear membrane. J Cell Sci 1999;112 (Pt 1:2571–82.

[90] Fairley EAL, Riddell A, Ellis JA, Kendrick-Jones J. The cell cycle dependent mislocalisation of emerin may contribute to the Emery-Dreifuss muscular dystrophy phenotype. J Cell Sci 2002;115:341–54.

[91] Bertrand AT, Renou L, Papadopoulos A, Beuvin M, Lacène E, Massart C, et al. DelK32-lamin A/C has abnormal location and induces incomplete tissue maturation and severe metabolic defects leading to premature death. Hum Mol Genet 2012;21:1037–48. https://doi.org/10.1093/HMG/DDR534.

[92] Torvaldson E, Kochin V, Eriksson JE. Phosphorylation of lamins determine their structural properties and signaling functions. Nucleus 2015;6:166–71.

[93] Sullivan T, Escalante-Alcalde D, Bhatt H, Anver M, Bhat N, Nagashima K, et al. Loss of A-type lamin expression compromises nuclear envelope integrity leading to muscular dystrophy. Journal of Cell Biology 1999;147:913–9. https://doi.org/10.1083/jcb.147.5.913.

[94] Thanisch K, Song C, Engelkamp D, Koch J, Wang A, Hallberg E, et al. Nuclear envelope localization of LEMD2 is developmentally dynamic and lamin A/C dependent yet insufficient for heterochromatin tethering. Differentiation 2017;94. https://doi.org/10.1016/j.diff.2016.12.002.

[95] Malik P, Korfali N, Srsen V, Lazou V, Batrakou DG, Zuleger N, et al. Cell-specific and lamin-dependent targeting of novel transmembrane proteins in the nuclear envelope. Cellular and Molecular Life Sciences 2010;67. https://doi.org/10.1007/s00018-010-0257-2.

[96] Libotte T, Zaim H, Abraham S, Padmakumar VC, Schneider M, Lu W, et al. Lamin A/C–dependent Localization of Nesprin-2, a Giant Scaffolder at the Nuclear Envelope. Https://DoiOrg/101091/MbcE04-11-1009 2005;16:3411–24. https://doi.org/10.1091/MBC.E04-11-1009.

[97] Crisp M, Liu Q, Roux K, Rattner JB, Shanahan C, Burke B, et al. Coupling of the nucleus and cytoplasm. J Cell Biol 2006;172:41–53. https://doi.org/10.1083/jcb.200509124.

[98] Ungricht R, Kutay U. Establishment of NE asymmetry-targeting of membrane proteins to the inner nuclear membrane. Curr Opin Cell Biol 2015;34. https://doi.org/10.1016/j.ceb.2015.04.005.

[99] Andrés V, González JM. Role of A-type lamins in signaling, transcription, and chromatin organization. J Cell Biol 2009;187:945–57. https://doi.org/10.1083/jcb.200904124.

[100] Parnaik VK. Role of Nuclear Lamins in Nuclear Organization, Cellular Signaling, and Inherited Diseases. Int Rev Cell Mol Biol 2008;266. https://doi.org/10.1016/S1937-6448(07)66004-3.

[101] Betts MJ, Russell RB. Amino Acid Properties and Consequences of Substitutions. In: Barnes MR, Gray IC, editors. Bioinformatics for Geneticists, John Wiley & Sons, Ltd; 2003, p. 289–316. https://doi.org/10.1002/0470867302.CH14.

[102] Azibani F, Brull A, Arandel L, Beuvin M, Nelson I, Jollet A, et al. Gene Therapy via Trans-Splicing for LMNA-Related Congenital Muscular Dystrophy. Mol Ther Nucleic Acids 2018;10:376–86. https://doi.org/10.1016/J.OMTN.2017.12.012.

Figure legends

Figure 1- Quantitative proteomics analysis revealed 348 dysregulated proteins in L-CMD myoblasts and myotubes compared to healthy controls. Using SWATH-MS analysis, dysregulated proteins were identified in L-CMD (R249W, L380S, del.K32) myoblasts and myotubes compared to controls (C5d, C25, C41). (A) Venn diagram illustrating the limited overlap of downregulated proteins that were identified in L-CMD myoblasts and L-CMD myotubes and showing no overlap between the upregulated proteins identified in L-CMD myoblasts and L-CMD myotubes. (B) Heatmap illustrating a total of 348 differentially expressed proteins were identified across the L-CMD myoblasts and L-CMD myotubes and the size of their fold-change, there were four commonalities across the L-CMD samples, with two proteins downregulated in L-CMD myoblasts and L-CMD myotubes, and two proteins upregulated in L-CMD myoblasts but downregulated in L-CMD myotubes. (C) Enriched molecular and cellular functions that were most common to the dysregulated proteins with the number of proteins associated with each term. (D) Enriched canonical pathways that were associated with the dysregulated proteins and the number of proteins associated with each term. A negative Z-score suggests inhibition, whilst a positive Z-score indicates potential activation. For terms where no activity pattern is available, this indicates that IPA® was not able to predict activity for a pathway.

Figure 2- Differentially expressed proteins identified in L-CMD myoblasts compared to myotubes, and control myoblasts compared to myotubes. There was limited overlap between the differentially expressed proteins that were identified in L-CMD myoblasts versus L-CMD myotubes, compared to control myoblasts versus control myotubes. (A) Venn diagram illustrating only 3 proteins were commonly upregulated in L-CMD and control myoblasts compared to L-CMD and control myotubes. (B) Venn diagram showing 28 proteins were commonly downregulated in L-CMD and control myoblasts compared to L-CMD and control myotubes. (C) Enriched canonical pathways that were associated with the dysregulated proteins and the number of proteins associated with each term. A negative Z-score suggests inhibition, whilst a positive Z-score indicates potential activation. For terms where no activity pattern is available, this indicates that IPA® was not able to predict activity for a pathway.

Figure 3- L-CMD myoblasts exhibited increased proliferation rate and nuclear deformities. (A) Cell proliferation rate is increased in L-CMD myoblasts and is expressed as doubling time in myoblasts from L-CMD patients (L380S, R249W, del.K32) compared to controls (C5d, C25, C41). Individual values for each cell line are presented, as well as the average for each group, with error bars indicating standard deviation from the mean. Asterisk (*) indicates significance (p=0.023). (B) Representative images of control (C5d, C25, C41) and L-CMD (del.K32, R249W, L380S) myotubes stained with DAPI. On average, control myotubes had 16 nuclei per myotube, whilst L-CMD myotubes had a similar amount of nuclei, an average of 14 nuclei per myotube (ten myotubes were counted per cell line). Compared to the other L- CMD and control myotubes, however, the del.K32 L-CMD myotubes had a reduced number of nuclei per myotube. On average, the L-CMD myotubes contained 9 nuclei. (C) Abnormal L-CMD (L380S, del.K32, R249W) myoblast and myotube nuclei were characterised based on the defect type using lamin A/C immunostaining (yellow) and DAPI (blue). (a) Nuclear blebbing is defined as protrusions from the nucleus, sometimes these are seen to become detached from the nucleus itself, (b) honeycomb nuclei have multiple distinct holes that sometimes resemble a honeycomb, (c) nuclear shape abnormalities are nuclei that are shaped differently to

control nuclei, elongated nuclei are an example of this, (d) donut shaped nuclei have a single hole through the centre, (e) correctly shaped control nuclei for comparison. (D) Graph depicting the percentage (%) of abnormal nuclei identified in L-CMD and control myoblasts. (E) Graph depicting the percentage (%) of abnormal nuclei identified in L-CMD and control myotubes.

Figure 4- Lamin A/C is significantly reduced in L-CMD myotubes compared to controls and nucleoplasmic aggregation was found in del.K32 myoblasts only. Lamin A/C expression was compared in control (C5d, C25, C41) and L-CMD (R249W, del.K32, L380S) myoblasts (A,B,C) and myotubes (D,E). (A, C) In L-CMD myoblasts, lamin A appeared reduced compared to controls, although this finding was not statistically significant (p=0.244), whilst lamin C did not appear obviously reduced (p=0.805). (B) However, it was noticed that lamin A was of a lower molecular weight in L-CMD myoblasts compared to controls. (D, E) In L-CMD myotubes, lamin A and C were both reduced with statistical significance compared to controls (p=0.044, p=0.043). ns indicates not significant, Asterisk (*) denotes statistical significance. (F) Representative immunocytochemistry images showing lamin A/C (yellow) and DAPI (blue) staining in control myoblasts and myotubes (C5d, C25, C41). Lamin A/C was found to be correctly localized at the nuclear envelope across all control myoblasts and myotubes. (G) Representative immunocytochemistry images showing lamin A/C (yellow) and DAPI (blue) staining in L-CMD myoblasts and myotubes (L380S, del.K32, R249W). Lamin A/C was found in nucleoplasmic aggregates in del.K32 myoblasts, as indicated by white arrows.

Figure 5- Emerin is significantly reduced in expression in L-CMD myotubes compared to controls and mislocalized in R249W myoblasts only. (A) Representative immunocytochemistry images showing emerin (magenta) and DAPI (blue) staining in control (C5d, C25, C41) and L-CMD (R249W, del.K32, L380S) myoblasts and myotubes. Emerin was found to be correctly localized at the nuclear envelope across all control myoblasts and myotubes, and all L-CMD myoblasts and myotubes except R249W L-CMD myoblasts where emerin was observed at the nuclear envelope and in the cytoplasm. (A) Emerin was not found to be significantly reduced in L-CMD myoblasts (L380S, R249W, del.K32) compared to age matched controls (C5d, C25, C41) (p=0.097). (C) Emerin was however significantly decreased L-CMD myotubes compared to controls (p=0.040). ns indicates not significant, Asterisk (*) denotes statistical significance.

Figure 6- SUN2 is significantly reduced in expression in L-CMD myotubes compared to controls, and is correctly localized to the nuclear envelope in all L-CMD cell lines. (A) Representative immunocytochemistry images showing SUN2 (magenta) and DAPI (blue) staining in control (C5d, C25, C41) and L-CMD (R249W, del.K32, L380S) myoblasts and myotubes. SUN2 was correctly localized at the nuclear envelope across all control myoblasts and myotubes, and all L-CMD myoblasts and myotubes. There did, however, appear to be reduced staining of SUN2 across L-CMD cells. (B) Expression SUN2 was not found to be reduced in L-CMD myoblasts compared to controls (p=0.401). (C) In myotubes, expression of SUN2 was significantly increased (p=0.049). ns indicates not significant, Asterisk (*) denotes statistical significance.

Figure 3 R

Click here to access/download;Figure;Figure 3 NEW 2024.tiff

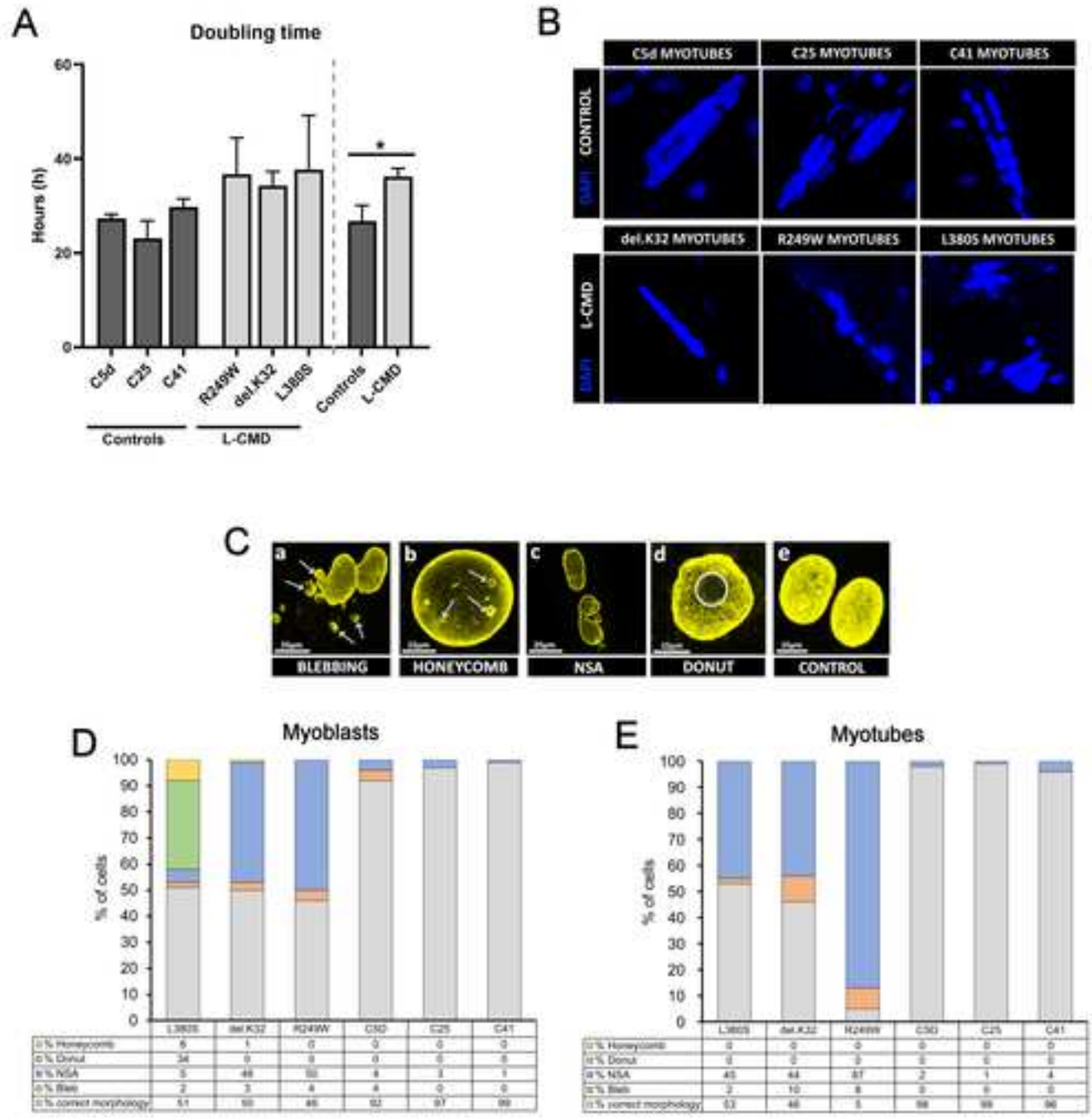

Figure 4 R

Click here to access/download;Figure;Figure 4 NEW 2024.tiff

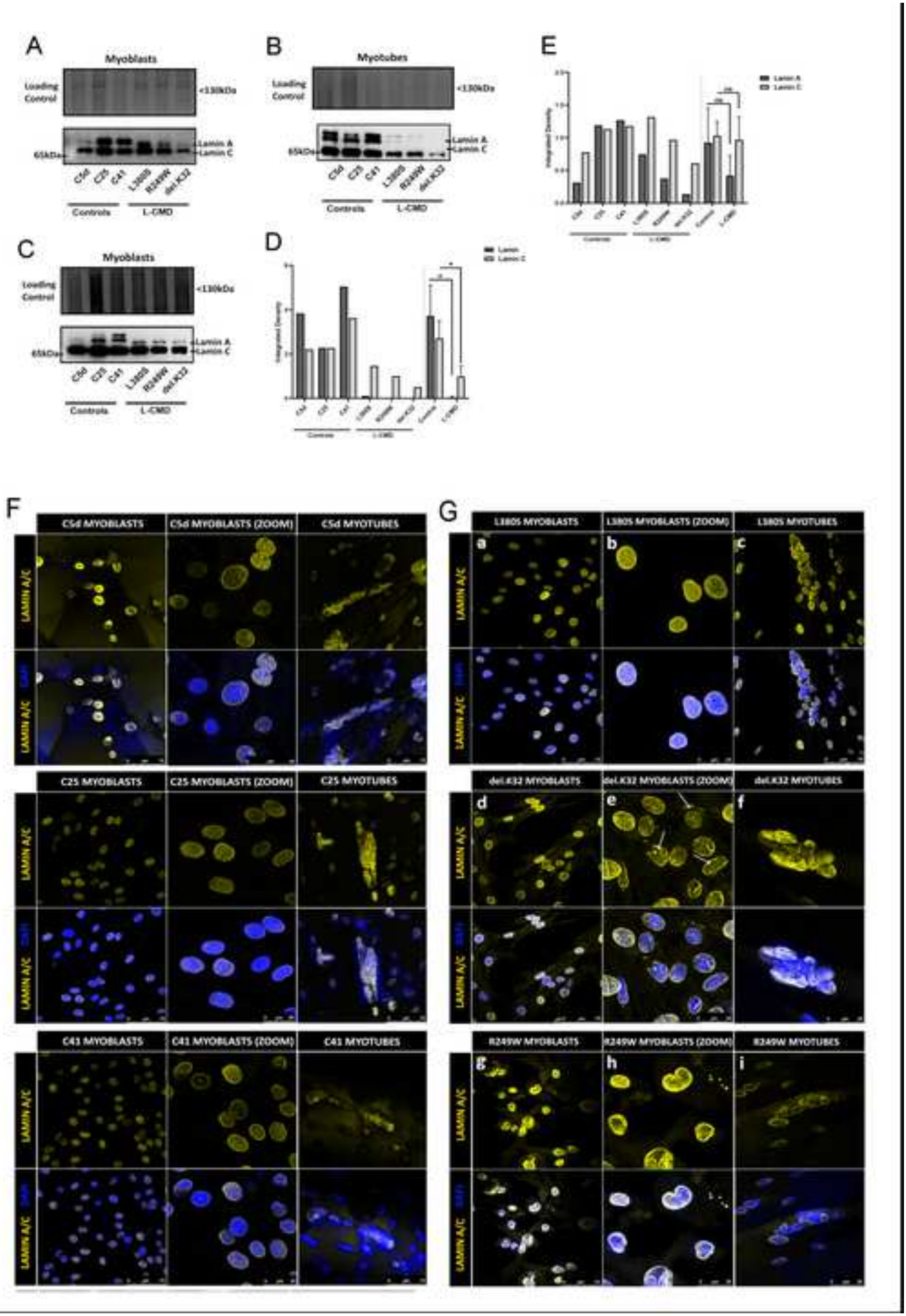

Figure 5 R

Click here to access/download;Figure;Figure 5 NEW 2024.tiff

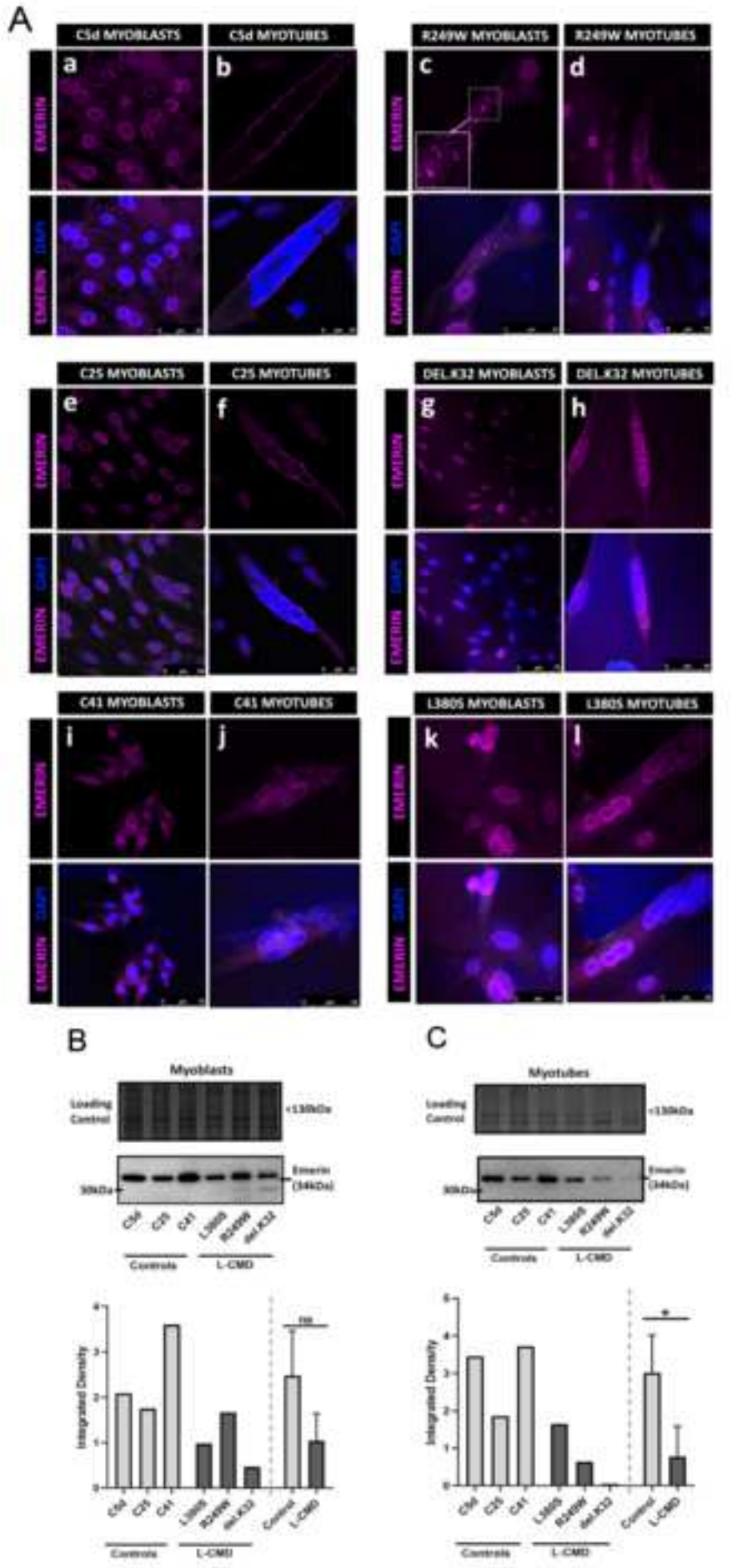

Figure 6 R

Click here to access/download;Figure;Figure 6 NEW 2024.tiff

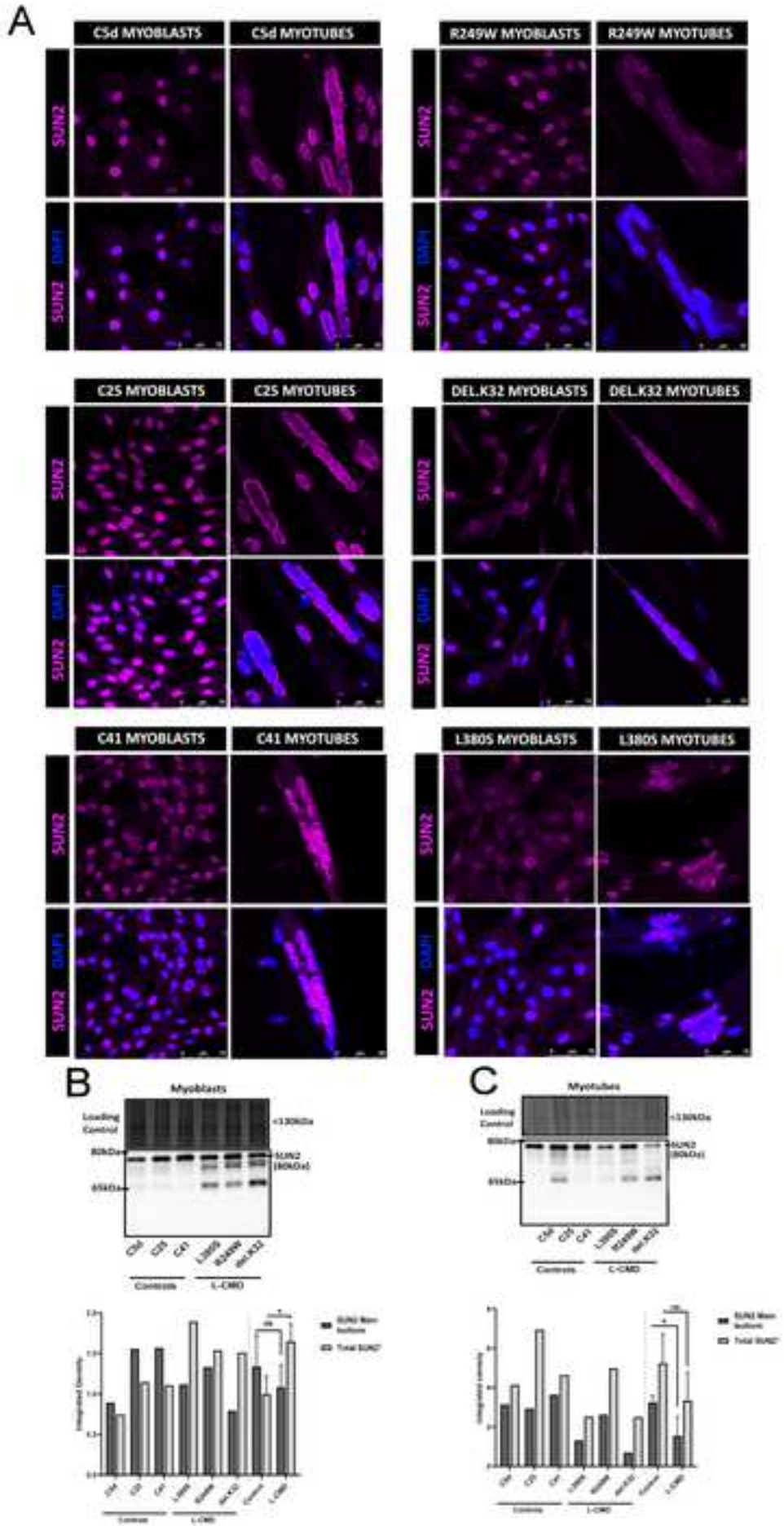

8 March 2024

Dear Professor Cohn

Manuscript Number: **NMD-D-24-00022**
Proteomic characterisation of human LMNA-related congenital muscular dystrophy muscle cells

Thank you for considering our manuscript for publication in Neuromuscular Disorders. We appreciate the time taken by the reviewers to review our manuscript.

Our detailed response to the points raised by Reviewers 1 and 2 are provided below. We have submitted a clean version of the revised manuscript and one with tracked changes for your consideration.

We confirm that neither the manuscript nor any parts of its content are currently under consideration or published in another journal.

All authors have approved the manuscript and agree with its submission to NMD.

We hope that this revised manuscript meets with your approval and look forward to hearing from you.

With kind regards,

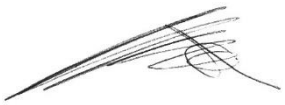

Professor Heidi Fuller

Dean of Education, Faculty of Medicine and Health Sciences
Senior Lecturer in Medical Science
Keele University, Keele, Staffordshire, UK ST5 5BG | https://www.keele.ac.uk/health/
Keele Deal Health Professional Development Unit: https://www.keele.ac.uk/health/pdu/

Laboratory research lead, Wolfson Centre for Inherited Neuromuscular Disease
TORCH Building, RJAH Orthopaedic Hospital, Oswestry, UK, SY10 7AG |
https://www.keele.ac.uk/pharmacy-bioengineering/ourpeople/heidifuller/

Reviewer #1: In this study, Emily Storey and colleagues conducted a proteomic characterization of LMNA-mutant muscle cells. The team analyzed three control cell lines and three others with different LMNA mutations associated with congenital muscular dystrophy. The results provide valuable insights into this rare disease, which currently lacks a cure. While the study is undoubtedly relevant to the field of Laminopathy and merits publication in Neuromuscular Disorders, a number of issues must be addressed before final approval.

Major Concerns:

1. "Cell Line Variation: The use of L-CMD cells with different LMNA mutations raises concerns. Since obtaining multiple cell lines for each mutation is challenging, a principal component analysis could help determine if the mutant clones behave similarly. If so, the authors could take them as biological replicates for the same disease. If not, they should be careful with their conclusions".

We appreciate the reviewer's comments and have ensured that we clearly state in the discussion that 'although the findings demonstrate a commonality between the L-CMD cell lines, intimating that impairment of LMNA has a common molecular effect, the actual mutations in each cell line were different.'

While it could be a useful addition, unfortunately, a reliable principle component analysis (PCA) of our proteomic dataset would not be possible, as there are certain criteria that our dataset does not meet. One main condition of PCA is a sufficient sampling adequacy, that is, a large enough sample size for PCA to generate a reliable result. Generally, at least 5 to 10 samples are required per variable. For our dataset, we only have 6 samples with over 10,000 proteins (variables) being identified. Another condition of PCA is for a linear relationship between all variables, although there are potential problems with correlations that are not high enough and correlations that are too high (Andy Field, Discovering Statistics using SPSS, 3rd Edition). Typically, the intercorrelation between variables need to be checked with any variable with lots of correlations below 0.3 being removed and similarly with any correlations with an $r > 0.8$. For 10,000 variables, or in this case 10,000 proteins, the correlation grid would comprise of 49,995,000 individual correlations.

2. "Generalization of Data: In my opinion, caution is needed when generalizing data for a specific LMNA mutation. In the discussion, the authors should avoid extrapolating results from a single mutant line to all cell lines harboring the same mutation".

We have added some further text to the conclusions section to clarify that in future it is important to study a greater number of L-CMD cell lines harbouring the same mutations as the cell lines used in this study, as well as other L-CMD mutations to determine whether the defects identified are conserved features of L-CMD. Text in this section has also been edited to remove reference to the identified defects as being "conserved across all L-CMD cell lines".

"3. Contradictory LMNA Protein Expression results: Discrepancies between western blot and immunofluorescence results regarding LMNA protein expression require clarification. Protocols ensuring total LMNA protein extraction from all subcellular regions are necessary to avoid possible partial protein extractions before western blot experiments".

There is discrepancy between western blot and immunofluorescence results of LMNA protein expression as IMF samples were not imaged using consistent laser intensity and therefore are not comparable to one another. This has been added into Results section 3.3. for clarification. 2x RIPA buffer was used for protein extraction for western blot samples which is sufficient to extract protein

from all subcellular regions and is recommended for extracting nuclear and membrane-bound proteins.

"4. Statistical Analysis: The absence of adjusted P-values in the statistical analysis it is not justified. Incorporating this adjustment could alter conclusions, particularly regarding LMNA protein expression."

We have updated the statistical section as follows to clearly show that no correction for multiple comparisons were applied so the reader is able to reach a reasonable conclusion as to the interpretation of the findings. Proteomic datasets generate 1000s of findings, if a Bonferroni adjustment had been applied to the 10,997 proteins identified in this study, approximately 550 proteins would be deemed significantly different just by chance - this correction would reduce Type I errors (false-positives) but would also increase Type II errors (false-negatives). As described by Perneger (1998), the Bonferroni method is concerned with the general null hypothesis (that all null hypotheses are true simultaneously) with the main weakness being that the interpretation of a finding depends on the number of other tests performed - the aim of mass spectrometry is to identify and measure individual proteins within the cell extracts, as a single entity.

Perneger TV. What's wrong with Bonferroni adjustments. BMJ. 1998 Apr 18;316(7139):1236-8. doi: 10.1136/bmj.316.7139.1236. PMID: 9553006; PMCID: PMC1112991.

"5. Protein Validation: Validation of significantly altered proteins in L-CMD myoblasts/myotubes is essential for confirming proteomic findings."

The validation of significantly altered proteins that were identified in the proteomic findings was outside the scope of this study due to time and resource constraints. However, this is something that we wish to follow up on in future work. Throughout the discussion and conclusion, it is mentioned that various proteomic findings require further validation in a future study.

Minor Concerns:
1. Introduction: I recommend adding the Orphanet ID of L-CMD (ORPHA:157973).
The Orphanet ID of L-CMD has been added into the opening line of the introduction.

2. References: I recommend to ensure consistent citation of reference 3 along with doi:10.1093/braincomms/fcab075, and include Van Tienen et al. (2018) in the references section.
The reference Yaou et al. (2021) (doi:10.1093/braincomms/fcab075) has been inserted to accompany reference 3. Van Tienen et al. (2018) has now also been included in the references.

3. Figure Details: Could the author provide an explanation for the higher bands in Figures 4A and C and quantify the nuclear membrane/nucleoplasm LMNA expression in Figures 4F and G.
In Results Section 3.3., paragraph 1, a small section has been inserted to speculate what the higher bands in the western blots in figure 4A, B and C could be. As explained in our response to Reviewer 1's major comment number 3, the immunos were not imaged with consistent laser intensity, therefore are not comparable or quantifiable. This is explained at the end of Section 3.3.

4. Figure Presentation: Consider increased magnification in Figure 5A for better visualization of nuclear phenotypes.
Figure 5A has been altered to show increased magnification and better visualization of the mislocalisation of emerin observed in the L-CMD R249W cell line.

5. Figure legends: include them.

We apologise for this omission. We have appended figure legends to the end of the main manuscript file.

6. Accessibility: I also recommend to make immunofluorescence images accessible to color-blind individuals by converting them to black and white while retaining color in merged panels.
Each of the immunofluorescence images have been changed to colours which are accessible to colour-blind individuals. The green immunofluorescence images have been converted to yellow, whilst the red immunofluorescence images have been converted to magenta. This is based on advice from the following article: https://www.ascb.org/science-news/how-to-make-scientific-figures-accessible-to-readers-with-color-blindness/.

7. Discussion: While comprehensive, and maybe too long, the discussion could benefit from comparing proteomic data with other LMNA transcriptomic or proteomic datasets.
While a systematic comparison of datasets is outside the scope of this study, we agree that it would be a useful piece of future work and have inserted a sentence into the Conclusions section to explain that it would be useful to compare the proteomic data with other published LMNA transcriptomic and proteomic datasets in a future study.

8. Materials and Methods: Specify that the CDK4 vector is a CDK4-R24C mutant.
This has been included in Materials and Methods Section 2.1. Cell culture.

Reviewer #2:

1. Figure legends seem to be missing.
As above, we have now included figure legends.

2. For ingenuity pathway analysis (IPA®), I wonder how to define "n", and why the number of "n" varied markedly for "molecular and cellular functions" analysis.
"n" simply represents the number of proteins that were associated with each molecular and cellular function term or canonical pathway. Some processes may be more enriched than others or may have a higher number of proteins associated with them. It is likely that there are a larger number of proteins associated with molecular and cellular functions in the L-CMD myotubes as a larger number of dysregulated proteins were identified in the L-CMD myotubes compared to in the L-CMD myoblasts.

3. I wonder if the authors could add the information about the domains that these three mutations are located and the binding partners that these three domains directly interact with.
We have inserted a paragraph into the discussion outlining the domains that are affected by the LMNA mutations and briefly explaining the possible affect of the mutations.

4. In L-CMD myotubes, but not myoblasts, emerin was significantly reduced compared to controls, however, it was mislocalized to the cytoplasm only in approximately one third of the L-CMD myoblasts examined that harboured the R249W mutation. I therefore wonder why the authors mainly discussed the effect caused by emerin mislocalization but not its reduction, unlike SUN2.
The effect of emerin reduction is mentioned in the same section of the discussion where the effect of emerin mislocalization is discussed, however this was previously not clearly linked to the observation that emerin was reduced in L-CMD myotubes compared to controls. A sentence has been inserted to remind the reader that an emerin reduction was observed in the L-CMD cell lines and to link to the discussion following about the effect of emerin reduction.

8 March 2024

Dear Professor Cohn

Manuscript Number: **NMD-D-24-00022**
Proteomic characterisation of human LMNA-related congenital muscular dystrophy muscle cells

Thank you for considering our manuscript for publication in Neuromuscular Disorders. We appreciate the time taken by the reviewers to review our manuscript.

Our detailed response to the points raised by Reviewers 1 and 2 are provided below. We have submitted a clean version of the revised manuscript and one with tracked changes for your consideration.

We confirm that neither the manuscript nor any parts of its content are currently under consideration or published in another journal.

All authors have approved the manuscript and agree with its submission to NMD.

We hope that this revised manuscript meets with your approval and look forward to hearing from you.

With kind regards,

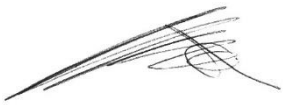

Professor Heidi Fuller

Dean of Education, Faculty of Medicine and Health Sciences
Senior Lecturer in Medical Science
Keele University, Keele, Staffordshire, UK ST5 5BG | https://www.keele.ac.uk/health/
Keele Deal Health Professional Development Unit: https://www.keele.ac.uk/health/pdu/

Laboratory research lead, Wolfson Centre for Inherited Neuromuscular Disease
TORCH Building, RJAH Orthopaedic Hospital, Oswestry, UK, SY10 7AG |
https://www.keele.ac.uk/pharmacy-bioengineering/ourpeople/heidifuller/

Reviewer #1: In this study, Emily Storey and colleagues conducted a proteomic characterization of LMNA-mutant muscle cells. The team analyzed three control cell lines and three others with different LMNA mutations associated with congenital muscular dystrophy. The results provide valuable insights into this rare disease, which currently lacks a cure. While the study is undoubtedly relevant to the field of Laminopathy and merits publication in Neuromuscular Disorders, a number of issues must be addressed before final approval.

Major Concerns:

1. "Cell Line Variation: The use of L-CMD cells with different LMNA mutations raises concerns. Since obtaining multiple cell lines for each mutation is challenging, a principal component analysis could help determine if the mutant clones behave similarly. If so, the authors could take them as biological replicates for the same disease. If not, they should be careful with their conclusions".

We appreciate the reviewer's comments and have ensured that we clearly state in the discussion that 'although the findings demonstrate a commonality between the L-CMD cell lines, intimating that impairment of LMNA has a common molecular effect, the actual mutations in each cell line were different.'

While it could be a useful addition, unfortunately, a reliable principle component analysis (PCA) of our proteomic dataset would not be possible, as there are certain criteria that our dataset does not meet. One main condition of PCA is a sufficient sampling adequacy, that is, a large enough sample size for PCA to generate a reliable result. Generally, at least 5 to 10 samples are required per variable. For our dataset, we only have 6 samples with over 10,000 proteins (variables) being identified. Another condition of PCA is for a linear relationship between all variables, although there are potential problems with correlations that are not high enough and correlations that are too high (Andy Field, Discovering Statistics using SPSS, 3rd Edition). Typically, the intercorrelation between variables need to be checked with any variable with lots of correlations below 0.3 being removed and similarly with any correlations with an $r > 0.8$. For 10,000 variables, or in this case 10,000 proteins, the correlation grid would comprise of 49,995,000 individual correlations.

2. "Generalization of Data: In my opinion, caution is needed when generalizing data for a specific LMNA mutation. In the discussion, the authors should avoid extrapolating results from a single mutant line to all cell lines harboring the same mutation".

We have added some further text to the conclusions section to clarify that in future it is important to study a greater number of L-CMD cell lines harbouring the same mutations as the cell lines used in this study, as well as other L-CMD mutations to determine whether the defects identified are conserved features of L-CMD. Text in this section has also been edited to remove reference to the identified defects as being "conserved across all L-CMD cell lines".

"3. Contradictory LMNA Protein Expression results: Discrepancies between western blot and immunofluorescence results regarding LMNA protein expression require clarification. Protocols ensuring total LMNA protein extraction from all subcellular regions are necessary to avoid possible partial protein extractions before western blot experiments".

There is discrepancy between western blot and immunofluorescence results of LMNA protein expression as IMF samples were not imaged using consistent laser intensity and therefore are not comparable to one another. This has been added into Results section 3.3. for clarification. 2x RIPA buffer was used for protein extraction for western blot samples which is sufficient to extract protein

from all subcellular regions and is recommended for extracting nuclear and membrane-bound proteins.

"4. Statistical Analysis: The absence of adjusted P-values in the statistical analysis it is not justified. Incorporating this adjustment could alter conclusions, particularly regarding LMNA protein expression."

We have updated the statistical section as follows to clearly show that no correction for multiple comparisons were applied so the reader is able to reach a reasonable conclusion as to the interpretation of the findings. Proteomic datasets generate 1000s of findings, if a Bonferroni adjustment had been applied to the 10,997 proteins identified in this study, approximately 550 proteins would be deemed significantly different just by chance - this correction would reduce Type I errors (false-positives) but would also increase Type II errors (false-negatives). As described by Perneger (1998), the Bonferroni method is concerned with the general null hypothesis (that all null hypotheses are true simultaneously) with the main weakness being that the interpretation of a finding depends on the number of other tests performed - the aim of mass spectrometry is to identify and measure individual proteins within the cell extracts, as a single entity.

Perneger TV. What's wrong with Bonferroni adjustments. BMJ. 1998 Apr 18;316(7139):1236-8. doi: 10.1136/bmj.316.7139.1236. PMID: 9553006; PMCID: PMC1112991.

"5. Protein Validation: Validation of significantly altered proteins in L-CMD myoblasts/myotubes is essential for confirming proteomic findings."

The validation of significantly altered proteins that were identified in the proteomic findings was outside the scope of this study due to time and resource constraints. However, this is something that we wish to follow up on in future work. Throughout the discussion and conclusion, it is mentioned that various proteomic findings require further validation in a future study.

Minor Concerns:
1. Introduction: I recommend adding the Orphanet ID of L-CMD (ORPHA:157973).
The Orphanet ID of L-CMD has been added into the opening line of the introduction.

2. References: I recommend to ensure consistent citation of reference 3 along with doi:10.1093/braincomms/fcab075, and include Van Tienen et al. (2018) in the references section.
The reference Yaou et al. (2021) (doi:10.1093/braincomms/fcab075) has been inserted to accompany reference 3. Van Tienen et al. (2018) has now also been included in the references.

3. Figure Details: Could the author provide an explanation for the higher bands in Figures 4A and C and quantify the nuclear membrane/nucleoplasm LMNA expression in Figures 4F and G.
In Results Section 3.3., paragraph 1, a small section has been inserted to speculate what the higher bands in the western blots in figure 4A, B and C could be. As explained in our response to Reviewer 1's major comment number 3, the immunos were not imaged with consistent laser intensity, therefore are not comparable or quantifiable. This is explained at the end of Section 3.3.

4. Figure Presentation: Consider increased magnification in Figure 5A for better visualization of nuclear phenotypes.
Figure 5A has been altered to show increased magnification and better visualization of the mislocalisation of emerin observed in the L-CMD R249W cell line.

5. Figure legends: include them.

We apologise for this omission. We have appended figure legends to the end of the main manuscript file.

6. Accessibility: I also recommend to make immunofluorescence images accessible to color-blind individuals by converting them to black and white while retaining color in merged panels.
Each of the immunofluorescence images have been changed to colours which are accessible to colour-blind individuals. The green immunofluorescence images have been converted to yellow, whilst the red immunofluorescence images have been converted to magenta. This is based on advice from the following article: https://www.ascb.org/science-news/how-to-make-scientific-figures-accessible-to-readers-with-color-blindness/.

7. Discussion: While comprehensive, and maybe too long, the discussion could benefit from comparing proteomic data with other LMNA transcriptomic or proteomic datasets.
While a systematic comparison of datasets is outside the scope of this study, we agree that it would be a useful piece of future work and have inserted a sentence into the Conclusions section to explain that it would be useful to compare the proteomic data with other published LMNA transcriptomic and proteomic datasets in a future study.

8. Materials and Methods: Specify that the CDK4 vector is a CDK4-R24C mutant.
This has been included in Materials and Methods Section 2.1. Cell culture.

Reviewer #2:

1. Figure legends seem to be missing.
As above, we have now included figure legends.

2. For ingenuity pathway analysis (IPA®), I wonder how to define "n", and why the number of "n" varied markedly for "molecular and cellular functions" analysis.
"n" simply represents the number of proteins that were associated with each molecular and cellular function term or canonical pathway. Some processes may be more enriched than others or may have a higher number of proteins associated with them. It is likely that there are a larger number of proteins associated with molecular and cellular functions in the L-CMD myotubes as a larger number of dysregulated proteins were identified in the L-CMD myotubes compared to in the L-CMD myoblasts.

3. I wonder if the authors could add the information about the domains that these three mutations are located and the binding partners that these three domains directly interact with.
We have inserted a paragraph into the discussion outlining the domains that are affected by the LMNA mutations and briefly explaining the possible affect of the mutations.

4. In L-CMD myotubes, but not myoblasts, emerin was significantly reduced compared to controls, however, it was mislocalized to the cytoplasm only in approximately one third of the L-CMD myoblasts examined that harboured the R249W mutation. I therefore wonder why the authors mainly discussed the effect caused by emerin mislocalization but not its reduction, unlike SUN2.
The effect of emerin reduction is mentioned in the same section of the discussion where the effect of emerin mislocalization is discussed, however this was previously not clearly linked to the observation that emerin was reduced in L-CMD myotubes compared to controls. A sentence has been inserted to remind the reader that an emerin reduction was observed in the L-CMD cell lines and to link to the discussion following about the effect of emerin reduction.